ACTIVATED DIFFUSION OF GASES IN MOLECULAR-SIEVE MATERIALS

P. L. WALKER, JR., L. G. AUSTIN, and S. P. NANDI

FUEL SCIENCE DEPARTMENT
THE PENNSYLVANIA STATE UNIVERSITY
UNIVERSITY PARK, PENNSYLVANIA

I. INTRODUCTION

Much has been written about diffusion of gases in and through porous solids. At least two good books are available on the subject (*1,2*). Diffusion of gases in solids can be conveniently bracketed into three

main types: bulk diffusion, Knudsen or molecular diffusion, and activated diffusion. In this chapter we shall be concerned mainly with activated diffusion, but a few brief comments on bulk and Knudsen diffusion are in order. The criterion as to whether bulk or Knudsen diffusion exists depends upon the magnitude of the gas mean free path relative to the pore diameter through which diffusion is occurring. If the mean free path is small relative to the pore diameter, the diffusing species will collide with each other far more often than with the pore walls, and bulk diffusion will exist. Kinetic theory gives the approximate formula of Eq. (1) for the bulk diffusion coefficient for a mixture of gas molecules of similar mass and molecular diameter (*3*):

$$D_B = \tfrac{1}{3}\bar{v}\lambda \tag{1}$$

where $\bar{v}$ is the average molecular velocity and λ is the mean free path.* Since from kinetic theory (*4*) $\bar{v} = (8k_BT/\pi m)^{1/2}$ and $\lambda = 0.707/\pi\sigma^2C_T$, where k_B is Boltzmann's constant, T is the temperature, m is the mass of a molecule or atom, σ is the kinetic diameter, and C_T is the total concentration,

$$D_B = \frac{1}{3}\left(\frac{8k_BT}{\pi m}\right)^{1/2}\left(\frac{0.707}{\pi\sigma^2C_T}\right) \tag{2}$$

Thus kinetic theory predicts that the bulk diffusion coefficient is inversely proportional to the gas pressure and directly proportional to the $\frac{3}{2}$ power of temperature. Evans and co-workers (*5*), who studied the steady-state interdiffusion of helium and argon at atmospheric pressure in a large-pore graphite, closely confirmed this temperature dependency.

If the mean free path is large relative to the pore diameter, the diffusing species will collide with a pore wall far more often than with each other, and Knudsen diffusion will be operative. The resistance to diffusion is due to the fact that, after collision with a pore wall, the molecule is just as apt to reverse its direction as it is to proceed in the direction of the previous flight. Kennard (*4*) showed from his studies of diffusion in fine capillaries at low pressures that this must be because each collision with the wall is actually a very brief period of adsorption in which the molecule loses its momentum to the solid surface. After this brief instant of adsorption, the molecule evaporates from the surface at a completely random angle. The Knudsen diffusion coefficient is given by Eq. (3),

* The authors have attempted to define all symbols when they first appear in the text.

$$D_k = \frac{2r}{3}\bar{v} = \frac{2r}{3}\left(\frac{8k_BT}{\pi m}\right)^{1/2} \tag{3}$$

where r is the pore radius. Thus the Knudsen diffusion coefficient should be directly proportional to the one-half power of temperature.

Wicke and Kallenbach (*6*) studied the steady-state interdiffusion of carbon dioxide and nitrogen at atmospheric pressure in an activated carbon from room temperature to 300°C. The diffusion coefficient varied with $T^{1.4}$. The activated carbon was composed of finely divided powder held together by a pitch binder. The authors propose a model where pores in which bulk diffusion occurs are connected by narrow openings in which gas transport occurs by Knudsen diffusion. On the basis of this model, a temperature dependency of diffusion between that given for bulk and Knudsen diffusion is predicted. Golovina (*7*) studied the steady-state interdiffusion of carbon dioxide and nitrogen at atmospheric pressures through a carbon membrane from room temperature to 600°C. The diffusion coefficient varied with $T^{1.34}$, again suggesting a mixture of bulk and Knudsen diffusion.

For most molecules, σ is of the order of 2 or 3×10^{-8} cm and C_T is of the order of 3×10^{19} multiplied by the pressure in atmospheres. A rough estimate of λ in centimeters is thus $10^{-5}/p$ (atm). In cracking catalysts and activated aluminas, pores primarily have a size between 30 and 200 A (*8*). In such materials, Knudsen diffusion will predominate up to gas pressures of at least 10 atm. The question of diffusion rate within porous catalysts and activated carbon is of prime importance, since it determines the extent of solid utilization for chemical reactions (*8*).

When the size of the diffusing species closely approaches the size of the aperture through which it passes, the physical interaction energy* between the species and aperture becomes important. This interaction energy may be considered essentially the sum of Lennard-Jones expressions for dispersive and repulsive interactions (*9*). When the aperture opening becomes sufficiently small relative to the size of the diffusing species, the repulsive interaction between them in the plane of the aperture becomes dominant; consequently, the diffusing species requires a certain activation energy to pass through the aperture. Thus at some point Knudsen diffusion changes over to activated diffusion. As we shall see later, in the activated diffusion regime small differences in size of

* In this chapter we shall be concerned with physical interaction of species with surfaces and not with chemical interaction or chemisorption.

the diffusing species can result in large differences in activation energy for diffusion through a particular aperture. Thus solids which have apertures of molecular size can exhibit large differences in their propensity for taking up molecules differing slightly in size. These solids exhibit a sieving effect of molecules depending upon their size and thus are called molecular-sieve materials.

In recent years, molecular-sieve materials have become of major commercial interest. By far the most important commercial molecular-sieve materials are the crystalline zeolitic aluminosilicates (*10*). Synthetic zeolites, which are produced commercially and commonly identified as 3A, 4A, 5A, 10X, and 13X, are grown hydrothermally from an alkaline mixture of silica and alumina (*10,11*). Single crystals of about 1 to 5 μ in size can be grown. Upon removal of the water of hydration at ca. 350°C, a network of empty cavities and apertures remain, which comprises about one-half the total volume of the crystals. A classic example of their molecular-sieve behavior is the ability of the 5A sieve to take up copious amounts of straight-chain paraffins and negligible amounts of branched-chain paraffins. The use of molecular sieves to separate straight- from branched-chain hydrocarbons has been of value to the petroleum industry in its efforts to increase the octane rating of gasolines and to the detergent industry in its efforts to produce biodegradable detergents. Recently, molecular-shape discriminating catalytic reactions have been demonstrated using zeolites (*12,13*). The normal hydrocarbons, which are accessible to the 5A zeolites, preferentially undergo cracking, dehydration, and hydrogenation reactions relative to the branched-chain hydrocarbons.

The fact that some naturally occurring and synthetic carbonaceous materials show molecular-sieve properties has been known for some time. Most ranks of coal show such properties. For example, they too show a much greater uptake of normal than branched hydrocarbons (*14*); however, their sorption* capacity is low compared to that of the zeolites. Synthetic molecular-sieve carbons can be produced upon the coking of selected thermosetting polymer or copolymer systems. As we shall see

* Workers have used the terms adsorption and absorption, more or less indiscriminately, to connote total uptake of gases and liquids on molecular-sieve materials. We have chosen to use the word sorption to indicate total uptake; adsorption, to indicate only surface uptake; and occlusion, to indicate volume uptake. In the experimental results which we shall be discussing, we generally do not know to what extent surface and/or volume uptake contribute to the total uptake, so we usually speak of sorption.

later, molecular-sieve carbons of high capacity and good selectivity can be produced from both polyvinylidene chloride and Saran. Molecular-sieve carbons can also be produced by the coating of activated carbons by thermosetting resins such as polyfurfuryl alcohol.

Carbonaceous molecular-sieve materials are not at present being produced commercially. However, interest is being shown in their use as a rough separation medium in conjunction with zeolite sieves and in their use where zeolite sieves are not suitable. For example, the cavities in the zeolite sieves collapse if heated much above 700°C (*10*). Some carbon sieves are stable up to 1400°C. Thus the possibility exists of operating separation processes at higher temperatures with carbon sieves. The type A zeolite sieves become increasingly unstable as the pH of the medium decreases below 5 (*10*). Carbon sieves are quite stable in strongly acidic solutions. Zeolite sieves very strongly and preferentially sorb water (*10*). In the case of a wet-gas stream, this can mean that the efficiency of the zeolite sieve for the separation of particular compounds will be decreased because of preferential uptake of water. Carbon sieves can be made more or less hydrophilic, depending upon the starting polymer system and heat-treatment conditions. In any case, carbon sieves exhibit much less hydrophilic character than the zeolites.

Activated diffusion of gases through metals and fused quartz has long been known to exist. Pioneering researches on hydrogen in palladium were made in 1866 (*15*); even earlier observations were made on the system hydrogen-iron (*16*). Diffusion of hydrogen in fused quartz has drawn much recent attention (*17,18*). Activated diffusion of molecules larger than nitrogen into metals and fused quartz is exceedingly slow; thus they are not useful in the important separation processes for hydrocarbons. Also, in most cases the sorption capacity is small. Therefore, activated diffusion of gases through metals and fused quartz will not be considered further in this review.

In this chapter, we first review some of the pertinent studies on zeolite and carbon molecular sieves, with particular attention to their sorptive properties. Next, we concern ourselves with the solution of the unsteady-state diffusion equation, used to calculate diffusion coefficients in porous materials. Significant experimental results on diffusion in zeolite and carbon molecular sieves will then be reviewed. Finally, theoretical calculations of the entropy and activation energy for activated diffusion in molecular-sieve materials will be considered. Theoretical values are compared with experimental values, where possible. This chapter pays considerable attention to zeolite molecular sieves (even though it is part

of a volume on the chemistry and physics of carbon) for two reasons: (1) structures of the crystalline zeolites are well known and permit meaningful comparisons of activated diffusion coefficients obtained experimentally and theoretically, and (2) a close comparison of sorption properties of zeolite and existing carbon molecular sieves places the possible commercial future of carbon sieves in a clearer perspective.

II. SELECTED REVIEW OF THE LITERATURE ON MOLECULAR-SIEVE MATERIALS

A vast literature exists on the structure of molecular-sieve materials and their sorption properties. It is not the purpose of this chapter to completely review this literature. Selected references will be discussed to demonstrate broadly the sorption characteristics of zeolite and carbon molecular sieves and to set the stage for results on activated diffusion to be considered later.

A. Zeolite Molecular Sieves

1. Structure. Natural zeolites (named from the Greek zeo, meaning to boil, and lithos, meaning stone, because when the crystals are gently heated they give off water vapor) got their name some two centuries ago (*19*). Mineralogists later distinguished 40 kinds of zeolites, each with its own crystal structure. The fundamental building block of any zeolite crystal is a tetrahedron of oxygen ions surrounding a smaller silicon or aluminum ion. Each of the oxygen ions has two negative charges; each silicon ion has four positive charges; each aluminium ion, three. Each silicon satisfies one-half the eight charges of the four oxygens which surround it. Each oxygen retains one negative charge, which enables it to combine with another silicon or aluminium ion and extend the crystal lattice in all directions. The aluminium ion, with one less positive charge than the silicon, can only satisfy three negative charges on the four oxygens which surround it. To produce a stable crystal structure, another positively charged cation must be added. These cations, called exchangeable ions, since they can be readily exchanged without destroying the zeolite structure (*20*), attach themselves loosely to the oxygens at the corners of the tetrahedra. This loose attachment plays an important part in determining the change of activation energy with size of diffusion species in a particular zeolite, as we shall see later.

In zeolites, the framework of silicon-oxygen and aluminium-oxygen tetrahedra forms a structure which is honeycombed with relatively large

cavities. The shape and size of the cavities and the size and number of apertures leading into the cavities depends upon the variety of zeolite. If the cavities are emptied of water by heating, the zeolites do not disintegrate in the process, as do most other water-bearing crystals. Chemists investigating this phenomenon in the 1920s noted that zeolites sorbed substances selectively and began to talk of zeolites as molecular sieves (*19*). In 1938, Barrer undertook his lengthy and continuing study of zeolite molecular sieves, showing their utility for separation of gases (*21–35*). In 1948, researchers at the Linde company set out to explore the commercial possibilities of zeolite sieves. Because of the relative rarity of natural zeolite crystals, they were compelled to seek ways to grow them artificially. By using a mixture of sodium and aluminium oxides and freshly prepared silica gel, they were able to grow hydrothermally many types of synthetic zeolite single crystals of over 1 μ in size, including a type A zeolite (*11*) which to date has no natural analog. This zeolite has cavities of a high capacity and apertures that can be adjusted to perform many useful separations. Later, a type X zeolite was grown (*36*), which also has a high capacity, but apertures somewhat larger in size than the type A zeolite.

Detailed, quantitative X-ray diffraction studies have been made on type A sieves to completely delineate their structure (*37,38*). The aluminosilicate framework of the type A zeolite is based on units which contain four AlO_4 and four SiO_4 tetrahedra in a rigid compact group (*37*). These units link together to form a ring of eight oxygen atoms in the center of each face of the unit cell on an irregular ring of six oxygen atoms at each corner of the threefold axis. In the center of the unit cell is a cavity 11.4 A in diameter, which is connected to six like cavities by the eight-membered rings which form restricted openings 4.2 A in diameter. In addition, the large cavity is connected to eight small cavities 6.6 A in diameter by the six-membered rings which produce openings 2.0 A in diameter. These latter cavities are not useful in molecular-sieve separation because of the very small aperture size leading into them.

Type 3A, 4A, and 5A zeolites are important commercially. The difference in their screening behavior is caused by differences in the exchangeable cation present. In the 4A sieve, the exchangeable cation is sodium. There are eight sodium ions (which take positions in or near the 4.2-A aperture openings and partially block them) for every six apertures between 11.4-A cavities. The free diameter of the 4.2-A apertures is thus reduced to ca. 3.5 A, as we shall see from molecular-probe studies. If the sodium in the 4A sieve is exchanged for calcium, a single calcium ion

replaces a pair of sodium ions. Now, with only four ions available for six apertures, two apertures per cavity are unobstructed and thus have a free diameter of 4.2 A. This is called the 5A sieve. If the sodium ion in the 4A sieve is exchanged for the larger potassium ion, a single potassium replaces a single sodium; there remain eight ions for six apertures. The free diameter of the 4.2 A apertures is reduced to ca. 3.2 A; but as we shall see later, this figure is apparently dependent on the particular diffusing species passing through the aperture. The potassium-bearing type A zeolite is called 3A.

Broussard and Shoemaker (*38*) and Barrer (*39*) recognized that the crystal structures of the Type A and X zeolites are both based on a cubo-octahedral structural unit, similar to that found in the mineral sodalite (*40*), as being the fundamental building block of both types of sieves. In the type A sieves, the sodalite units, each of which contains 24 (silicon, aluminium) ions interconnected with 36 oxygen ions, are arranged in a single cubic array, with each sodalite unit connected to its neighbor by four bridge oxygen ions. In the type X sieves, sodalite units are in tetrahedral coordination with each unit connected to its neighbor by six bridge oxygen ions. The type X structure is essentially similar to that of the naturally occurring faujasite (*35*). The apertures of importance in the type X sieves are composed of 12-membered oxygen rings. In the type 13X sieve, where sodium is the exchangeable cation, the aperture has a free diameter of 7.5 A in diameter (*38*), as given by X-ray diffraction studies.

2. Sorption Characteristics. Probably the most important use of zeolite molecular sieves, at the moment, is the removal of water from gas streams. Water is readily accessible to all type A and X zeolites and is held strongly and preferentially to most other sorbates. To measure the full capacity of the zeolites for other sorbates, it is absolutely essential that the zeolites be outgassed under high vacuum at 350 to 400°C (*41*).

Early sorption studies of Barrer (*21*) and Tiselius (*42*) were concerned primarily with water uptake on natural zeolites. The properties of zeolitic water have continued to be of interest, but quantitative and thermodynamic studies have been made difficult because of the chemical reactivity of water and irreversible side reactions. Consequently, the sorption properties of ammonia, another small polar molecule but a less reactive species than water, has been studied extensively in recent years. For example, Barrer and Gibbons (*35*) have studied the sorption of ammonia on type X sieves.

Emmett and Dewitt (*43*) were among the first to show the molecular-

ieve behavior of zeolites. Working with the natural zeolite chabazite [which has an aperture ca. 3.8 A in diameter, formed by a ring of eight oxygen atoms (*44*)] they found little sorption of nitrogen at −196°C, but significant sorption at −78°C. They attributed these results to activated diffusion. That is, in physical sorption it is thermodynamically necessary that the amount sorbed decreases with increasing adsorption temperature at equilibrium. However, if the sorption is very slow and has not reached equilibrium under particular sorption conditions, because of activated diffusion, increased sorbate uptake with increasing temperature can occur.

We now focus our attention primarily on sorption results on type A and X sieves, because of their commercial importance. These sieves all have large surface areas, on the order of 700 to 800 m^2/g, potentially available (*20*). The amount of this area actually accessible to particular sorbates depends upon their size relative to the size of the aperture openings in the zeolite. The 3A sieve, because of its small aperture opening, effectively excludes all organic compounds. At present, it is useful primarily for the drying of gases. Encapsulation and storage of permanent gases in the 3A sieve appears to have future commercial possibilities (*45*). The sieve is loaded by exposure to the gas at high pressures and elevated temperatures to overcome a substantial activation energy for diffusion and then cooled to room temperature before releasing the external gas pressure. Activated diffusion of permanent gases in this sieve will be considered later in the chapter.

Breck and co-workers have performed the most comprehensive sorption studies on the 4 and 5A sieves (*46*). As found by Emmett and Dewitt on chabazite, they also find that the sorption of nitrogen on the 4A sieve increases with temperature from −196 to ca. −78°C. Similar results are found for the sorption of carbon monoxide and argon (*10*), as is seen in Fig. 1. At temperatures above −78°C, equilibrium is apparently reached in the sorption time allowed, and the volume sorbed decreases with increasing temperature. In contrast, the volume of oxygen sorbed falls continuously over the entire temperature region studied. This is a vivid example of a molecular-sieve effect. The diffusion of oxygen is still sufficiently rapid at temperatures below −78°C so that equilibrium is attained. Kinetic diameters of oxygen, nitrogen, carbon monoxide, and argon, as calculated from viscosity data using the Lennard-Jones 6–12 potential energy expression, are 3.43, 3.68, 3.59, and 3.42 A, respectively (*47*). These diameters do not explain why the diffusion coefficient of oxygen into the 4A sieves is greater than that of argon. Of course, oxygen is not a spherical molecule; if a spherocylindrical

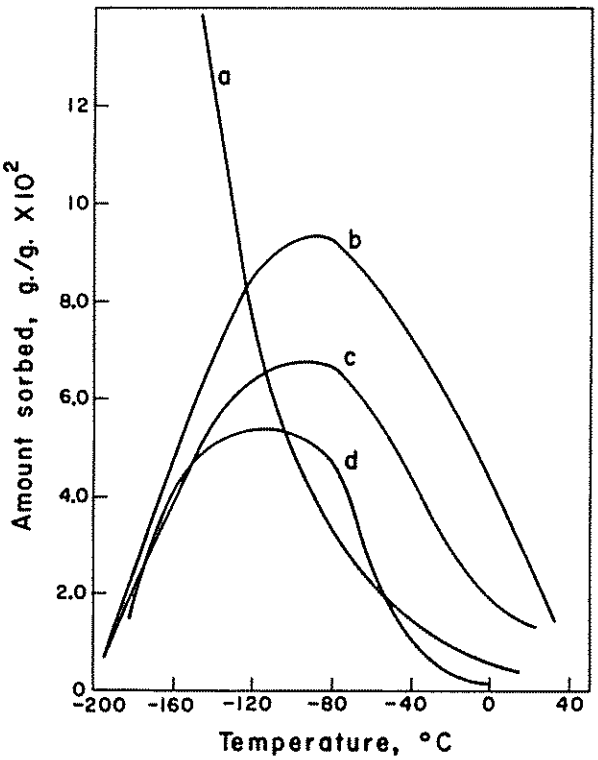

Fig. 1. Sorption isobars of gases on type 4A zeolite at 700 torr; (a) oxygen, (b) carbon monoxide, (c) nitrogen, and (d) argon. [From Thomas and Mays (*10*).]

shape is assumed (*48*), the width of the oxygen molecule would be less than the diameter of argon. This suggests that oxygen should have a smaller activation energy for diffusion through the 4A sieve than argon. In the 5A zeolite, no molecular-sieve effects of these molecules are observed. That is, the volume of gas adsorbed falls off monotonically with increasing temperature between −196 and 0°C in each case. Both the 4 and 5A sieves have large sorption capacities for carbon dioxide at −78°C. Surface areas calculated from sorption isotherm data,* using the BET equation, are 610 and 700 m^2/g (*49*).

* To calculate surface areas of the molecular-sieve materials from sorption data, the molecular area of the sorbing species has been assumed to be that which it would occupy on a free surface. Obviously, to some extent, this assumption will not be true. The deviation will depend upon the size and shape of the voids.

TABLE I

SORPTIVE CAPACITIES OF TYPE 4A AND 5A ZEOLITES (*46*) AT 25°C

Sorbate	Critical dimension, A	Pressure, torr	Sorption capacity, g/g	
			4A	5A
CO_2	3.3[a]	700	0.188	0.244
SO_2	3.6[a]	700	0.365	0.366
H_2S	3.6[a]	400	0.239	0.299
Methanol	—	90	0.189	0.232
1-Propanol	—	19	0.037	0.190
Ethane	—	700	0.074	0.087
Ethylene	3.9[a]	700	0.084	0.091
Propane	4.3[a]	600	0.017	0.130
Butene-1	—	400	0.029	0.154
n-Butane	4.3[a]	700	0.002	0.131
Cyclopropane	4.2[a]	700	0.00	0.125
Isobutane	5.0[a]	400	0.006	0.005
Benzene	3.7, 7.0[51]	90	0.003	0.002

[a] Kinetic diameter calculated from the minimum equilibrium cross-sectional diameter.

Sorptive capacities of types 4A and 5A zeolites for a series of adsorbates are summarized in Table I. The uptake of molecules with minimum kinetic dimensions less than ca. 4 A at 20°C is essentially the same on 4 and 5A sieves and is large. For straight-chain hydrocarbons having more than two carbon atoms, the uptake on the 4A sieve is small; uptake on the 5A sieve is large. Substantial sorption of normal paraffins up to at least C_{14} has been reported on the 5A sieve. On a volume basis, between 0.3 and 0.4 cc of liquid hydrocarbon is sorbed per cubic centimeter of zeolite. Negligible sorption of branched-chain hydrocarbons, which have minimum kinetic dimensions of at least 5 A, or aromatics, which have minimum kinetic dimensions of at least ca. 7 A, occurs on the 4 and 5A sieves. These results clearly show the feasibility of using the 5A sieve to separate straight-chain hydrocarbons from branched-chain hydrocarbons and aromatics.

The 10X sieve has a substantial capacity for molecules with minimum kinetic dimensions of at least ca. 7.7 A (*50*) [that is, $(C_2F_5)_2NC_3F_7$] but not greater than ca. 8.1 A (*50*) [that is, $(C_4H_9)_3N$]. Thus it can sorb many of the isoparaffins, aromatics, and hydroaromatics. The 13X sieve sorbs $(C_4H_9)_3N$ but not $(C_4F_9)_3N$, which has a minimum kinetic diameter of ca. 10.2 A (*50*). The 13X sieve has a high capacity for sorption of

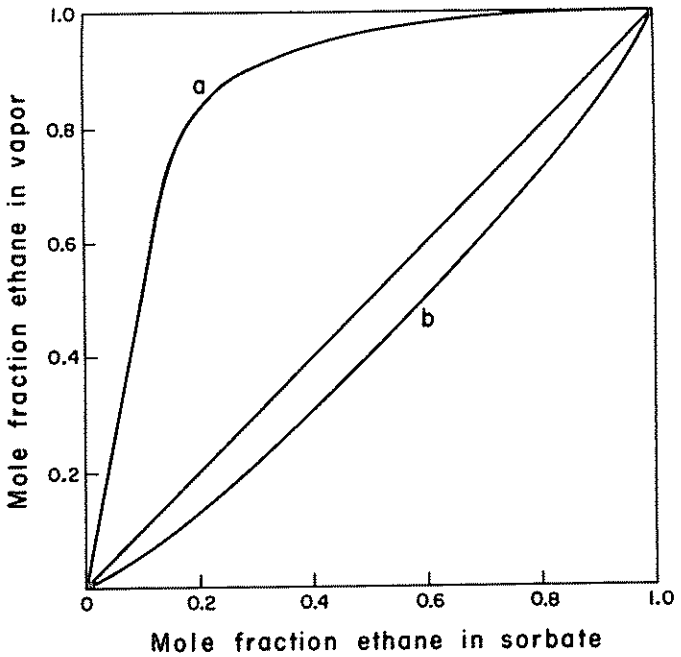

Fig. 2. Relative sorptivity of ethane-ethylene mixtures on (a) type 4A zeolite at 730 torr and 25°C, and (b) granular activated carbon at 760 torr and 25°C. [From Thomas and Mays (*10*).]

some aromatics with side chains, which are sorbed very slightly on the 10X sieve, such as 1,3,5-triethylbenzene (*10*).

A very important property of the zeolites, which is not based on the molecular-sieve effect, is their preferential sorption of polar, unsaturated, and aromatic compounds (*10*). The more polar or the more unsaturated the molecule, the more tightly it is held within the crystal. The sorptive forces in the zeolites are due primarily to the exchangeable cations exposed in the crystal sorption surface. These cations act as sites of strong, localized positive charge which electrostatically attract the negative end of polar or polarizable molecules. Figure 2 shows the very high selectivity which the 4A sieve has for ethylene in preference to ethane, when exposed to ethylene-ethane gas mixtures. It is recalled from Table I that the sorptive capacities of ethane and ethylene, when the 4A sieve is exposed to 700 torr of the pure hydrocarbons, are roughly equal. For comparison, Fig. 2 also shows the relative sorptivity of ethane-ethylene mixtures on a granular activated carbon. In this case,

ethane is sorbed slightly more preferentially than is ethylene. This would normally be expected, since ethane has a lower vapor pressure at 25°C than does ethylene. Polarity differences are also used to separate aromatic from saturated paraffins and hydroaromatic compounds. The type 13X sieve effectively separates benzene and toluene from paraffinic hydrocarbons and from cyclohexane and methylcyclohexane.

B. Carbon Molecular Sieves

There are two major types of carbon-molecular-sieve materials known at present—coals which occur naturally and polymer carbons which are produced artificially by the heating of polymers to produce a solid char or coke. The term carbon is used in the generic sense, since these molecular sieves contain other elements. In the case of coal, varying amounts of mineral matter are present. The mineral matter, which is primarily kaolinite, illite, and quartz, has a low surface area and does not exhibit molecular-sieve behavior; it will not be considered further. We shall be considering coals varying in rank from the so-called high-volatile-matter lignites (low-rank coal), through the bituminous coals, to the low-volatile-matter anthracites (high-rank coals). On a dry mineral-matter-free basis, these coals range in carbon content from ca. 60 to 94 per cent; other elements present are primarily oxygen, hydrogen, nitrogen, and sulfur (*52*). The synthetic polymer carbons are very low in metallic and metal oxide impurities but usually contain some oxygen and hydrogen and sometimes contain nitrogen, sulfur, and/or chlorine.

1. Structure. In direct contrast to the single-crystal zeolitic sieves, which we have been discussing, carbon molecular sieves are composed of varying amounts of multicrystalline and amorphous material. If carbon molecular sieves are heated to elevated temperatures (2700°C and higher), where substantial crystalline growth can occur, their fine-pore system disappears and their surface areas decrease to a very low value (*53,54*).

a. Coals. Hirsch, Cartz, and Diamond have studied in detail the structure of coals and coal macerals using X-ray diffraction (*55–59*). Macerals are the more or less homogeneous microscopic constituents of coal. Vitrain is the principal coal maceral, constituting in many cases from 70 to 90 per cent of the coal. Therefore, structural information on vitrains is very pertinent to the structure of the whole coal. Figure 3 presents X-ray diffraction patterns obtained by Cartz and Hirsch (*59*) for three typical vitrains of widely varying rank. The patterns can conveniently be divided into three parts. The scattering at high angles consists of

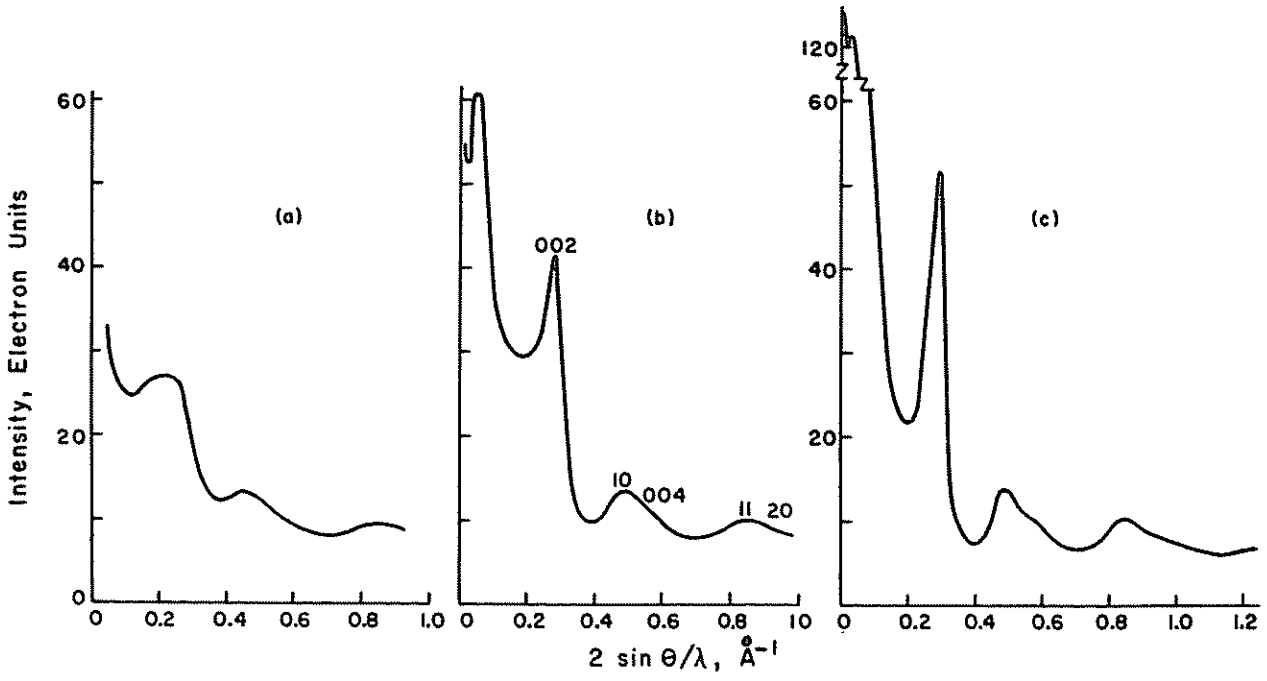

Fig. 3. X-ray diffraction patterns for three typical vitrains of (a) 78 per cent carbon, (b) 89 per cent carbon, and (c) 94 per cent carbon. [From Cartz and Hirsch (*59*).]

diffuse bands (*10,11,20*), which are interpreted in terms of the scattering from small condensed aromatic layers. The scattering at intermediate angles consists of a band (002) corresponding to a spacing of ca. 3.5 A. This band is considered to be due to the packing of aromatic layers parallel to one another. At low angles, intense diffuse scattering occurs which is caused by discontinuities in the structure (*60*). In coals, Compton (incoherent) scattering, owing to amorphous material, is also relatively strong at high angles, resulting in a background intensity higher than the intensity of the diffraction bands above the background (*61*). The diffraction patterns of all carbon-molecular-sieve materials are similar to those shown in Fig. 3. However, they differ from each other with respect to the breadth and position of each band and also the intensity of background scattering.

Analysis of the diffraction curves was made using the approach of Diamond (*58*), in which a linear combination of theoretical intensity curves from small aromatic layers of different sizes and from "amorphous" atoms is fitted to the experimental curves by the method of least squares. By means of a matrix transform, the distribution of layer diameters and proportion of amorphous material are derived.

Figures 4 to 6 summarize the results of Cartz and Hirsch (*59*) on the structure of vitrains of varying rank. The correlations in Figs. 4 and 5 are based on results for 18 different samples; in Fig. 6, on eight different samples. Figure 4 presents the change in average layer diameter with per cent carbon. Layer-size histograms are also available which show that there is a distribution in layer size from 5.0 to ca. 30 A. Figure 5 presents the change in amount of amorphous material present with per cent carbon. The amorphous material is considered to be due to substituted groups on the aromatic condensed-ring (layer) systems and may be identified with the aliphatic side chains, phenolic oxygen, and other substituted atoms known to be present in coal from infrared spectroscopy studies (*62*). Figure 6 presents the change in the average number of layers in a stack with per cent carbon. Histograms are also available which show that there is a distribution in extent of stacking. Below ca. 89 per cent carbon, ca. 40 per cent of the carbon occurs as single layers, the remainder (apart from the amorphous carbon) being in layers stacked parallel to each other in groups of 2, 3, etc. Above this range of carbon content, the fraction of single layers decreases to ca. 10 per cent at 94 per cent C. Thus, the packing of the layers improves with rank.

The main conclusions of Cartz and Hirsch on the structure of coal

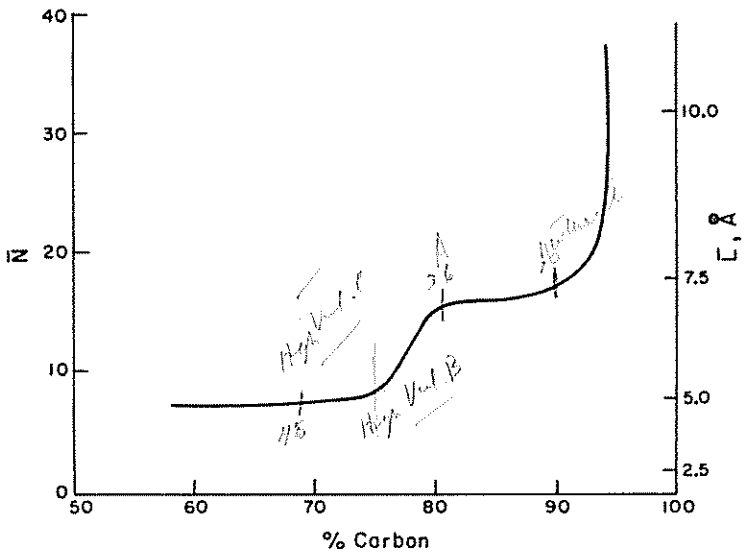

Fig. 4. Variation of the average layer diameter, $\bar{L}$, and the average number of atoms per layer, $\bar{N}$, with carbon content of vitrains. [From Cartz and Hirsch (*59*).]

can be summarized, as follows. Small condensed aromatic layers are the main building block of coal. These layers contain imperfections, but their nature is unknown. The presence of these imperfections makes it impossible to deduce an unambiguous structure for coal. Nevertheless considering all the evidence, it is concluded that the structural unit in bituminous coal consists of small condensed aromatic ring systems of probably one to three rings for low-rank vitrains and two to five rings for vitrains with 90 per cent C. These aromatic layers are linked to each other by direct carbon-carbon bonds and aliphatic groups (or possibly also by ether linkages) to form imperfect sheets, which are either buckled (through the presence of hydroaromatic groups) or in which adjacent aromatic ring systems are rotated relative to each other about an axis normal to the plane of the sheets (for example, as a result of the presence of five-membered rings). The diameter of the aromatic layers is about 7 to 8 A; the imperfect sheets are probably considerably larger. Thus for the vitrains with ca. 90 per cent, these sheets probably extend over ca. 20 A. These sheets are also considered to have side groups in the form of short aliphatic chains, hydroxyl, and quinone groups. Coals of lower rank (lignite) and higher rank (anthracite) are also thought to have this

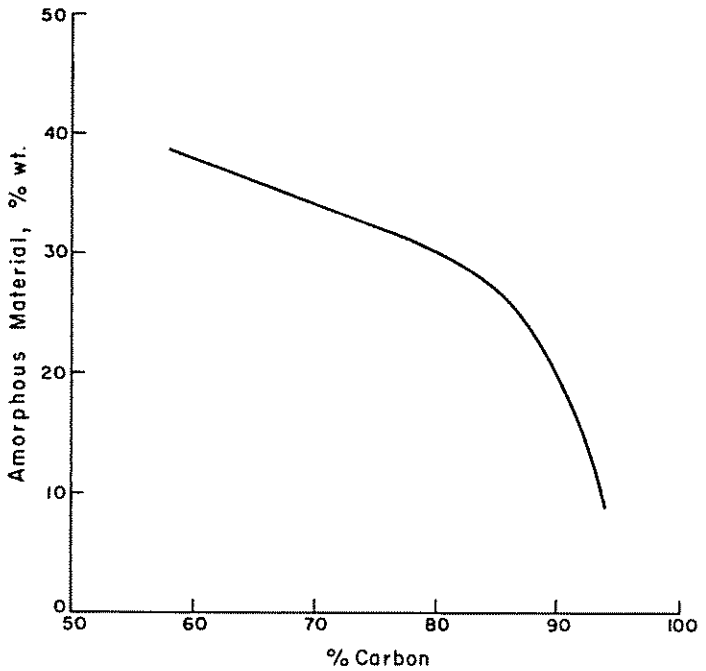

Fig. 5. Variation of the amorphous content with carbon content of vitrains. [From Cartz and Hirsch (*59*).]

eneral structure. Variations in the average height and width of the ayer groups and the amount of amorphous material with rank have been summarized in Figs. 5 and 6.

b. Polymer carbons. Molecular-sieve carbons have been produced by the charring of selected thermosetting polymers. To date, the approach to the production of these carbons has been primarily empirical. Little is understood about the relation between the original size and shape of the polymer units and the pore size and shape present in the carbon produced. Originally it was the hope of workers in this field (*63*) that carbons with uniform pore size would be inherited from the regular structure of polymer predecessors and that they would be able to predict final carbon structure on the basis of known pyrolysis reactions which polymer systems undergo. How this might be accomplished is uncertain, because few valence angles and distances survive thermal decomposition unchanged (*64*). Indeed, studies have indicated that original polymer configurations have only secondary importance. Instead, the course of

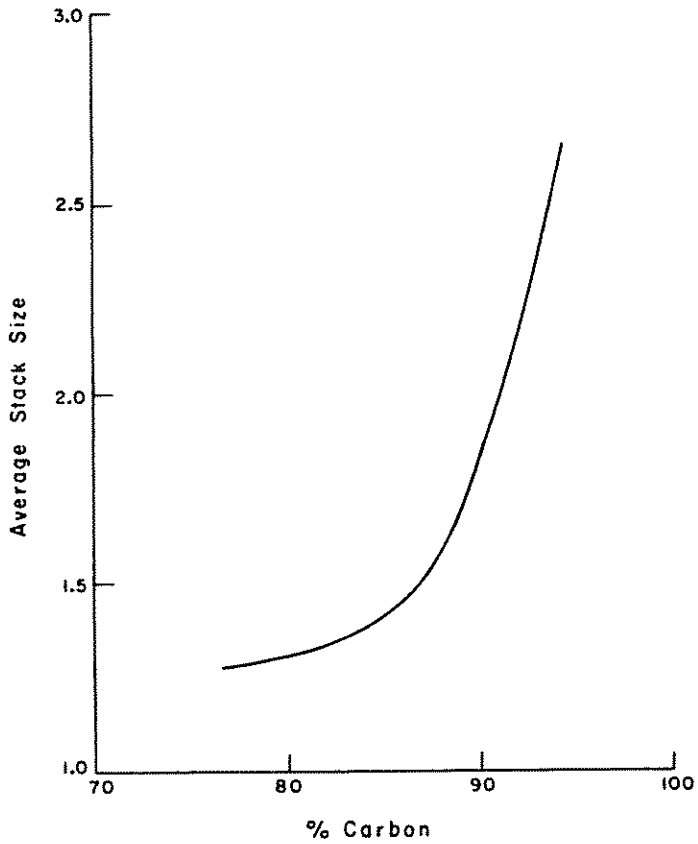

Fig. 6. Variation of the average number of layers in a stack with carbon content of vitrains. [From Cartz and Hirsch (*59*).]

carbonization (charring) is determined by the over-all energy requirements for formation of rigid carbon materials (*65*).

To date, far more studies have been conducted on the conversion of polyvinylidene chloride, $(C_2H_2Cl_2)_n$, and Saran* to molecular-sieve carbons than any other polymer systems. Consequently, much is known about their pyrolysis. When polyvinylidene chloride undergoes pyrolysis, it loses HCl stoichiometrically, leaving essentially pure carbon; that is,

$$(C_2H_2Cl_2)_n \rightarrow 2n\text{HCl} + 2n\text{C}$$

* Commercially available copolymer consisting of 80 to 90 per cent polyvinylidene chloride and various amounts of polyvinyl chloride, $(C_2H_3Cl)_n$, and plasticizer.

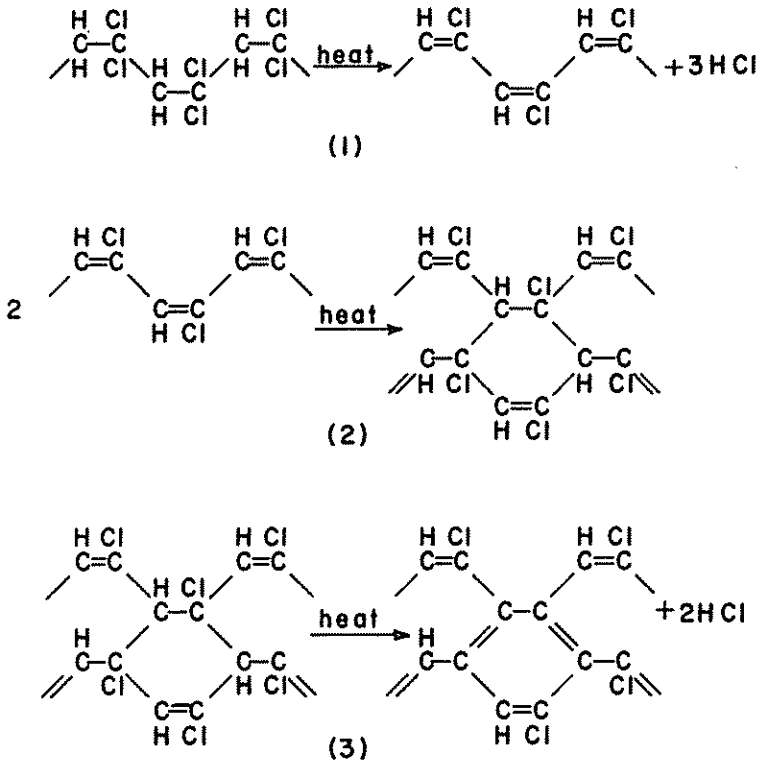

Fig. 7. Proposed mechanism for the pyrolysis of polyvinylidene chloride. [From Winslow et al. (*63*).]

Workers have studied the kinetics of HCl release during carbonization (*63,66*). They find that half of the HCl is readily lost below 200°C by a first-order reaction with an activation energy of ca. 30 kcal/mole. Further liberation of HCl requires progressively higher temperatures, until the process finally approaches completion at 600°C, producing a yield of carbon equal to 25 per cent of the starting polymer weight. A mechanism has been proposed for this conversion, as shown in Fig. 7. The first step is the loss of one HCl molecule per pair of carbon atoms, leading to the formation of a polymer chain.

It is concluded that further loss of HCl from a single chain is both chemically and sterically unlikely and that cross-linking of the chains by a Diels-Alder type of reaction, as shown in reaction (2) (Fig. 7), must occur before further HCl elimination takes place. Each cyclic

adduct produced in reaction (2) has additional hydrogens and chlorines in highly reactive tertiary positions. It is concluded that these immediately split out, by reaction (3), leaving thermally stable aromatic rings combined by polyene chains. Further cross-linking can occur either with other parts of the same chains, or with another adjacent chain. Examination of space models shows that the cross-linking reaction has a complicated sterochemistry, but it is tentatively concluded that it is probably third order in the concentration of C_2HCl units (*66*).

Upon pyrolysis, polyvinyl chloride loses essentially all its HCl at 225°C, leaving a residue still relatively rich in hydrogen (*63*). As a result, further heating yields large quantities of tar, with the residue remaining viscous up to about 450°C (*65*). Loss of hydrogen and hydrocarbons continues up to at least 800°C, yielding a carbon equal to ca. 15 per cent of the starting-polymer weight (*63*). Possible decomposition of part of the gas-phase hydrocarbons as they escape from the solid during the latter stages of carbonization could affect the ultimate pore structure of the carbon obtained. That is, carbon deposition could probably block the pore structure, leading to constrictions of various sizes.

Franklin (*65,67,68*) has studied the structure of carbons produced from polyvinylidene chloride and polyvinyl chloride upon carbonization to 1000°C and higher temperatures. As a result of quantitative measurements of the total X-ray scattering, it was shown that in the polyvinylidene chloride carbon prepared at 1000°C, 65 per cent of the carbon is in the form of graphite-like layers (condensed aromatic rings) 16 A in diameter and the remaining 35 per cent is in a form so disordered as to give only a gas-like distribution to the total X-ray scattering (amorphous material). Of the small graphite-like layers, ca. 45 per cent show no parallelism (single layers) and 55 per cent are grouped in parallel pairs with an interlayer spacing of 3.7 A. It was concluded, on the basis of the poor graphitizability of the carbon, that neighboring layers or layer packets are poorly aligned and strongly cross-linked by amorphous material. The low apparent density of the material, 1.59 g/cc, is also consistent with its poor layer alignment.

It was concluded that in the polyvinyl chloride carbon heated to 1000°C, 85 per cent of the carbon is in the form of graphite-like layers 18 A in diameter and the remaining 15 per cent is in an amorphous form. The graphite-like layers which show parallelism are grouped, on the average, in packets of between four and five. On the basis of the good graphitizability of this carbon and its relatively high density of 1.99 g/cc, it was concluded that its neighboring packets are well-aligned. Because

of the relatively small amount of amorphous material, the crystallites in this material are much less cross-linked than in the polyvinylidene carbon.

2. Sorption Characteristics. *a. Coals.* The surface area of coals was originally measured by means of heat of wetting with methanol at room temperature. Using a value of 0.1 cal/m^2 of internal surface for the heat of wetting obtained from methanol, surface areas ranging from 20 to 200 m^2/g were calculated for coals of different rank (*69,70*). The molecular-sieve behavior of coal became apparent later when surface areas of from only 1 to 10 m^2/g were calculated from sorption isotherms of nitrogen and argon at −196°C (*71–73*), using the BET equation (*74*). It was thought that the diffusion of nitrogen and argon into coals is sufficiently activated that at −196°C the fraction of internal surface area reached by the sorbate, for any reasonable equilibration time, is small. Recently, Nandi and Walker (*75*) have measured diffusion coefficients of nitrogen in coals of varying rank and have shown quantitatively that this reasoning is valid.

Other molecular-sieve characteristics of coals reminiscent of the zeolites have been found. Figure 8 shows the variation in uptake of nitrogen on a well-evacuated Welsh coking coal at a series of temperatures between −196 and 0°C for an equilibration time of 1 hr. As with the 4A-zeolite sieve, maximum sorption of nitrogen occurred at ca. −80°C (*76*). Anderson and co-workers (*14*), also studying the uptake of nitrogen on coals over a range of temperatures, confirmed the temperature dependency of sorption found by Maggs. They also found that the sorption capacity of the coals for nitrogen at −80°C was much lower than found previously with the zeolites. Reminiscent of the behavior of the 5A-zeolite sieve, Anderson and co-workers found sorption of normal butane to be considerably greater than that for isobutane on most coals at 0°C. These results are of little practical interest, however, since sorption was very slow, requiring up to 24 hr to approach equilibrium.

With the knowledge that coal is a molecular-sieve material, considerable work has been done to find the sorbate and sorption conditions under which the total surface area of coals can be most closely approximated. The two main requirements have been to work at sorption temperatures high enough to result in relatively rapid sorbate diffusion into the internal surface area (short equilibration time) and at sorption relative pressures high enough to permit calculation of surface areas from the BET equation. Conditions used, which have more or less closely satisfied

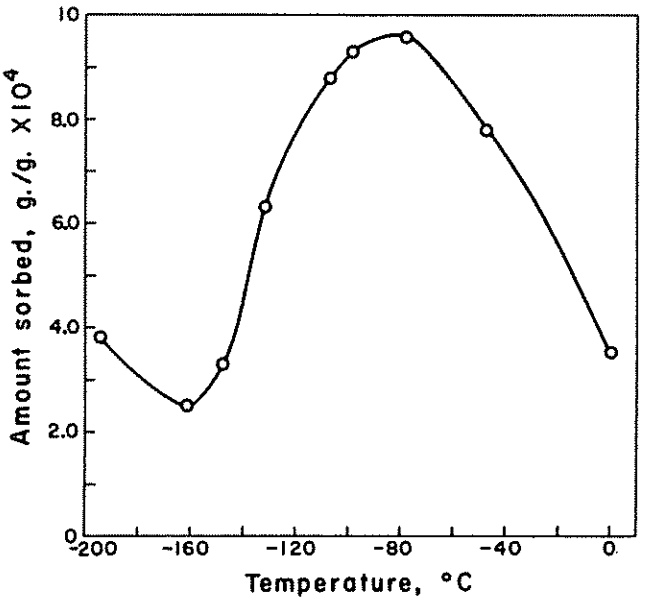

Fig. 8. Variation in uptake of nitrogen on a Welsh coking coal with temperature for an equilibration time of one hour. [From Maggs (*76*).]

the above requirements, are carbon dioxide at −78°C (*77–79*), krypton at −78°C (*80*), xenon at 0°C (*81*), and carbon dioxide at 25°C (*82*). The best system found to date appears to be carbon dioxide at 25°C. Table II summarizes typical surface-area results on a 200 × 325 mesh medium-volatile-matter bituminous coal, having a carbon content of 83.6 per cent on a dry mineral-matter-free basis. An equilibration time of ½ hr

TABLE II

SURFACE AREAS OF A MEDIUM-VM BITUMINOUS COAL AS MEASURED BY VARIOUS SORPTION SYSTEMS (*82*)

Adsorbate	Sorption temp, °C	Surface area, m²/g
N_2	−196	~1
Kr	−78	20
Xe	0	62
CO_2	−78	80
CO_2	25	104

was allowed for each sorption point on the isotherms, from which surface areas were calculated. Only for carbon dioxide at 25°C was equilibrium reached in this period of time. This system should satisfy closely the two main requirements listed above, since (1) carbon dioxide has a small kinetic dimension (ca. 3.3 A) and (2) carbon dioxide has a relatively high critical temperature (31.1°C). The latter property permits sorption measurements to be made at a relatively high temperature. To satisfy the requirement that isotherm data be measured up to sufficiently high relative pressures (ca. 0.2), sorption studies were conducted in an apparatus capable of operating up to at least 35 atm.

At least one attempt was made to improve the molecular-sieve properties of coal by activation (*83*). That is, coals have a significant fraction of their pore volume closed to helium. Reaction of coal with an oxidizing gas under appropriate conditions would be expected to open up closed-pore volume and also to enlarge the size of the already open pores. The result should be a carbon of larger capacity into which sorbate diffusion is more rapid. Oxidizing conditions are critical. Too high an oxidizing temperature results in collapse of part of the pore structure and an uneven activation of the remaining pores. Oxidation to a high burn-off, as is common in the production of activated carbon (ca. 50 to 70 per cent loss of carbon) is to be avoided, since the pores are enlarged too much and little molecular-sieve behavior is exhibited.

Oxidation of a high-volatile-matter anthracite in carbon dioxide has been studied (*83*). A small particle size (average particle diameter of 6 μ) was used in an effort to obtain good radial uniformity of particle activation. Optimum activation was produced by a burn-off of ca. 35 per cent at 840°C. Total sorption capacities of the raw anthracite, the anthracite devolatilized at 840°C in nitrogen to a weight loss of 9.0 per cent, and the oxidized anthracite to normal butane, isobutane, and neopentane were studied at 30°C. In addition, the total open-pore volumes of the samples were determined from mercury- and helium-density measurements. On the basis of the following minimum kinetic diameters—normal butane, 4.3 A (*50*), isobutane, 5.0 A (50), neopentane, 6.2 A (*50*), and helium, 2.5 A—pore-volume distributions of the anthracite samples are summarized in Fig. 9. In Table III the capacities of the activated anthracite for the hydrocarbons are compared with that of the 5A-zeolite sieve. Clearly, the 5A-zeolite is a superior sieve to the anthracite for separating normal butane from isobutane and normal butane from neopentane. Obviously, the 5A zeolite is not suited for separating isobutane from neopentane, whereas the activated anthracite does show a

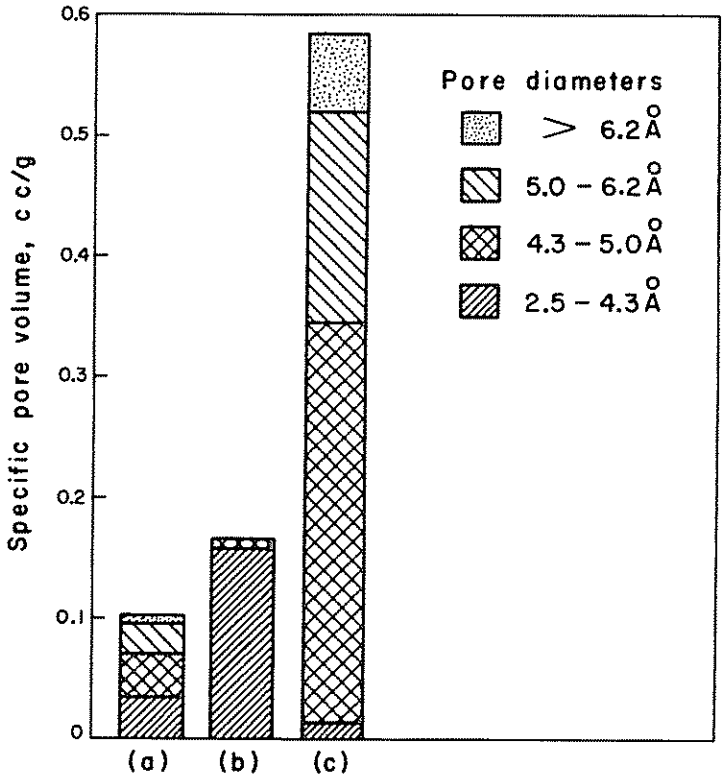

Fig. 9. Pore-volume distributions in (a) raw, (b) devolatilized, and (c) activated anthracites. [From Metcalfe et al. (*83*).]

reasonable capacity for isobutane and some sieve behavior for the isobutane-neopentane system.

It is not expected that molecular-sieve carbons can be produced from coals which show the critical sieving properties possessed by the zeolites. Nevertheless, because of the relatively low cost of molecular sieves produced from coal, they may have future applications for rough separations in conjunction with zeolites or polymer-based molecular sieves.

b. Polymer Carbons. As indicated earlier, polyvinylidene chloride and Saran have been the polymeric materials most frequently used to produce synthetic carbon molecular sieves. By process of elimination, their popularity appears reasonable. First, all thermoplastic polymers can be eliminated, since upon carbonization they yield cokes of medium to very

TABLE III

CAPACITY OF 5A-ZEOLITE SIEVE (*46*) AND ACTIVATED ANTHRACITE (*83*) FOR SELECTED HYDROCARBONS

	Equilibrium capacity, cc/g at 25–30°C		
	n-Butane	Isobutane	Neopentane
5A zeolite	0.218	0.008	Nil
Activated anthracite	0.56	0.24	0.06

good crystallite alignment possessing small internal surface areas. Second, many thermosetting polymers, upon being coked, yield chars characteristic of the 4A zeolite, whereas polyvinylidene chloride and Saran yield chars which have larger-sized micropores and show molecular-sieve properties useful for the separation of hydrocarbons. Third, the coking of polyvinylidene chloride and Saran results in a reasonably good yield of carbon—ca. 25 per cent.

The sorptive properties of Saran carbons appear to have been first investigated in some detail by Pierce and co-workers (*84*). The char produced upon carbonization to 600°C had a surface area, as calculated from ethyl chloride sorption at 0°C, of 720 m^2/g. Of prime interest was the observation that the hydrophobicity of the char could be altered markedly. The material as first prepared exhibited high water sorption at low relative pressures, which the authors attribute to the presence of a chloride complex in the surface. Following treatment with hydrogen at 600°C, low-pressure water sorption became quite small. Significant water sorption only commenced at a relative pressure of ca. 0.45. It was concluded that this is consistent with the removal of the chlorine complex as hydrogen chloride upon hydrogen treatment. Recently, Puri and Bansal (*85*) exposed charcoal to chlorine, resulting in the removal of hydrogen as hydrogen chloride and its partial replacement by chlorine. In direct conflict with Pierce and co-workers, they found that chlorine treatment drastically increased the hydrophobicity of the surface. Pierce and co-workers (*86*) showed in their later work that water uptake on carbon can be increased, following the formation of an oxygen complex on the surface, by exposure of the carbon to air at ca. 600°C. The fact that the hydrophobicity of carbon surfaces can be readily modified is of considerable importance, as it permits an alteration in the extent of preferential sorption of water versus other molecules on molecular-sieve carbons. This subject definitely warrants additional attention.

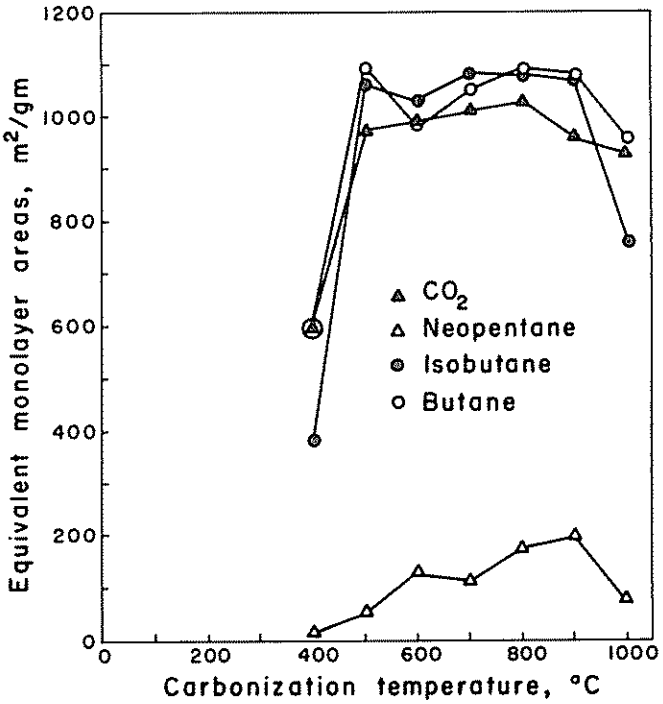

Fig. 10. Surface areas of Saran carbons heated to different carbonization temperatures. [From Lamond et al. (*89*).]

Further sorption studies on Saran molecular-sieve carbons have been numerous (*51,87–90*). Dacey and Thomas found that the 700°C char rapidly sorbed straight-chain hydrocarbons, like normal pentane, and flat molecules, like benzene, at room temperature (*87*). Sorption of neopentane was slower but could be made significant by using a finely ground powder. On the basis of benzene being sorbed more rapidly than neopentane, the authors concluded that the pores were slit-shaped, perhaps arising from the presence of condensed aromatic-like layers in the char. Kipling and Wilson (*51,88*) found that polyvinylidene chloride prepared at 700°C has close to the same capacity for neopentane and water at 20°C. They further found that the sorption of α-pinene (molecular diameter of ca. 8 A) is negligible.

Recently, Walker and co-workers have examined the possibility of modifying the molecular-sieve properties of Saran-type carbons by heating to temperatures up to 1500°C (*89*). Previously Dubinin showed

that at temperatures above 1000°C, sintering of the micropores in polyvinylidene chloride carbon occurs and the average pore size decreases (*90*). Carbons were produced from polyvinylidene chloride and Saran by carbonizing at a heating rate of 7.5°C/min up to 1000°C, followed by a heating rate of 15 to 30°C/min up to 1500°C. A soak time of 4 hr at maximum temperature was used. The extent of uptake of carbon dioxide (−78°C), butane, isobutane, and neopentane (all at 0°C) at a relative pressure of 0.5 was measured, using an equilibrium time of 1 hr. Surface areas were reported as "monolayer-area equivalent," following the suggestion of Barrer (*91*). Surface-area results are summarized in Figs. 10 and 11. The very high surface areas of the Saran carbons prepared above 500°C and the significant separation between isobutane and neopentane are noteworthy. The areas for the polyvinylidene chloride carbons go through a maximum of ca. 1300 m^2/g for a carbonization temperature of 1000°C. As evident from the large neopentane areas of the polyvinylidene chloride carbons prepared up to

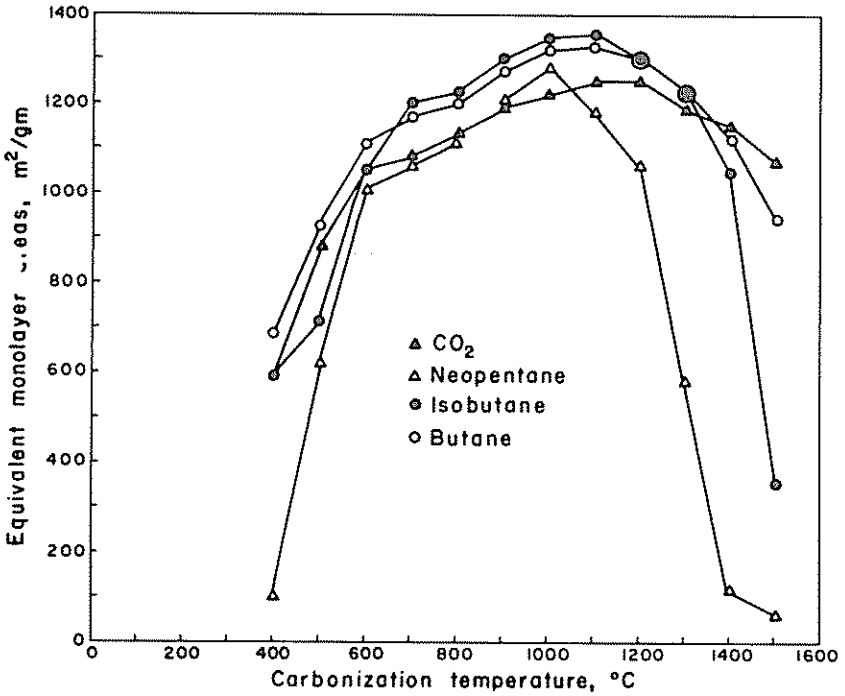

Fig. 11. Surface areas of polyvinylidene chloride carbons heated to different carbonization temperatures. [From Lamond et al. (*89*).]

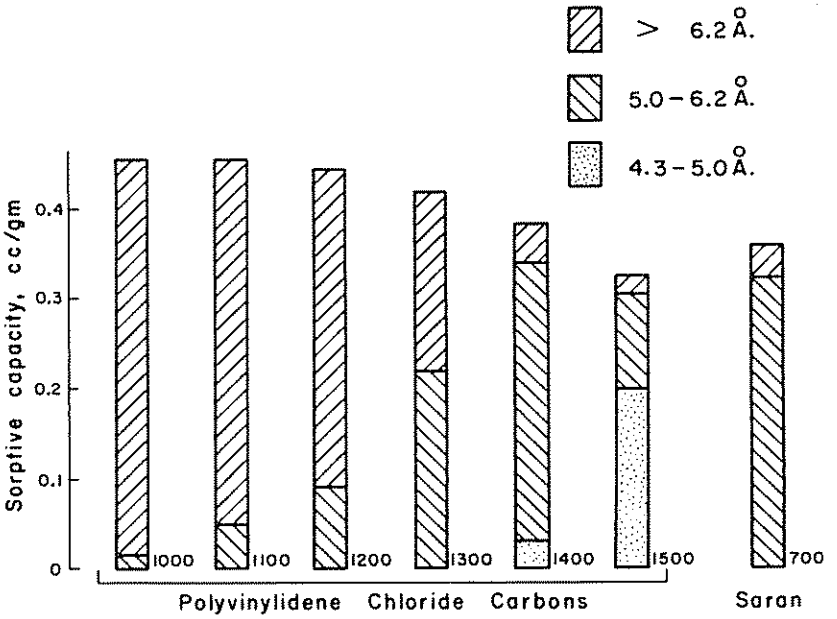
> 6.2 Å.
5.0 – 6.2 Å.
4.3 – 5.0 Å.
Sorptive capacity, cc/gm
0
0.1
0.2
0.3
0.4
1000
1100
1200
1300
1400
1500
700
Polyvinylidene Chloride Carbons
Saran

(a)

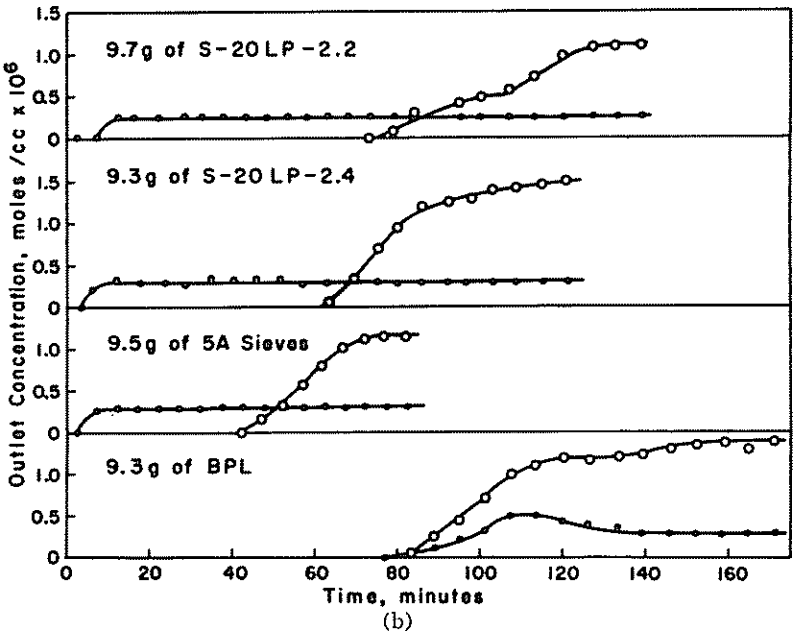
9.7g of S-20 LP-2.2
9.3g of S-20 LP-2.4
9.5g of 5A Sieves
9.3g of BPL
Outlet Concentration, moles /cc x 10⁶
0
0.5
1.0
1.5
0
20
40
60
80
100
120
140
160
Time, minutes

(b)

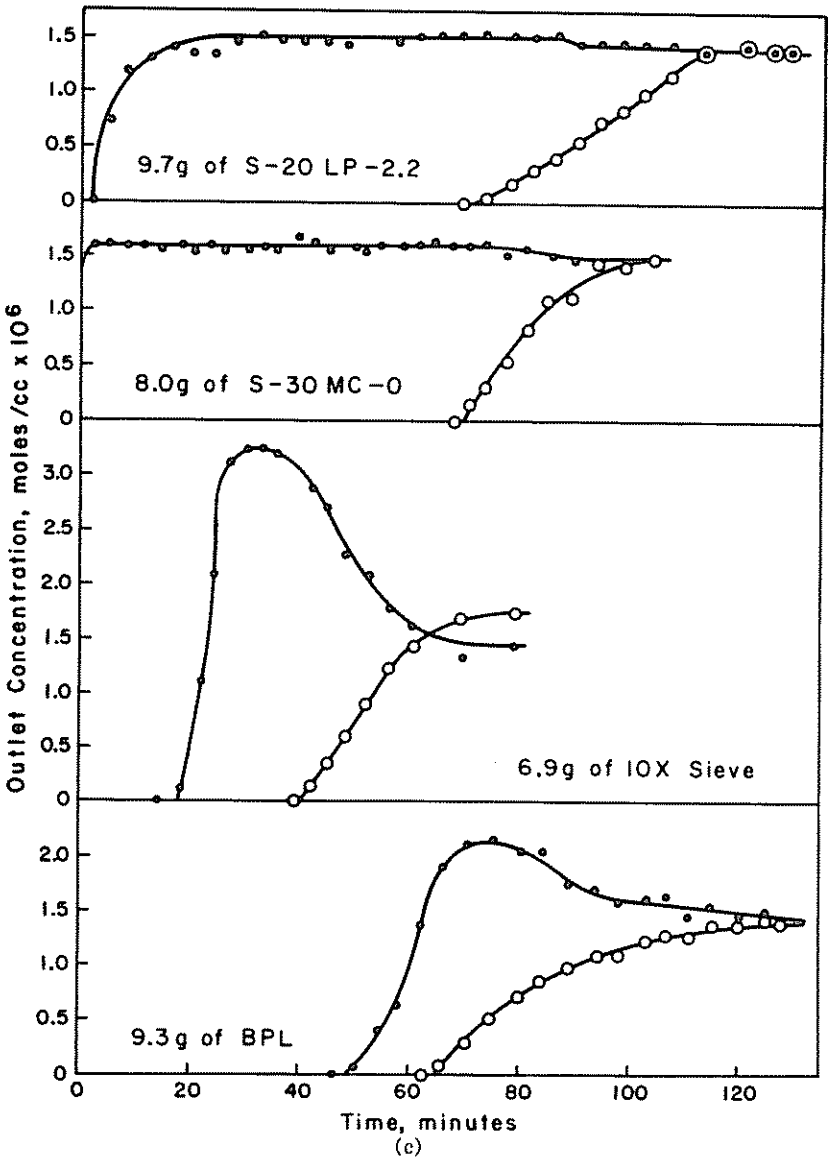

Fig. 12. (a) Pore-volume distributions in polyvinylidene chloride carbons and a selected Saran carbon. [From Lamond et al. (*89*).] (b) Dynamic adsorption of *n*-Heptane (○) and 2,2,4-trimethylpentane (●). [From Metcalfe (*93*).] (c) Dynamic adsorption of benzene (○) and cyclohexane (●). [From Metcalfe (*93*).]

1200°C, their pore size is somewhat larger than that of the Saran carbons. At heat-treatment temperatures above 1200°C, significant pore shrinkage occurs. Following heat treatment at 1500°C, neopentane sorption is negligible. Walker and co-workers conclude, from these latter results, that the internal surface area of polyvinylidene chloride carbons heated to 1200°C consist of cavities greater than 12 A in size connected by constrictions only slightly larger than 6.2 A. It is obvious that molecular-sieve carbons possessing varied properties can be prepared by the heating of polyvinylidene chloride to different maximum temperatures. The carbon prepared at 1400°C has molecular-sieve properties intermediate between the 5A and 10X zeolite sieves. The carbon prepared at 1500°C has properties approaching the 5A sieve; apparently a slightly higher heat-treatment temperature would produce a carbon showing a still greater separation potential for normal and isobutane. Heat treatment to still higher temperatures should produce a 4A-type carbon sieve.

The variation of pore volume, accessible to the various molecular probes, with heat-treatment temperature is depicted in Fig. 12(a) for the polyvinylidene chloride carbons and the 700°C Saran carbon. Sorption capacities are seen to be substantial.

Sorption of benzene and cyclohexane on the Saran carbons was found to be about 10 times as great as sorption of neopentane, again supporting the conclusion of slit-like pores in these carbons.

Walker and co-workers have also examined briefly the possibility of producing composite carbon molecular sieves (*92*). Activated carbons having no molecular-sieve properties for molecules at least less than 6.2 A in size, but having large surface areas, were coated with a thermosetting polymer, which upon carbonization yielded a molecular-sieve carbon. The object was to use the more expensive polymer carbon coating as a "gate." Molecules passing through the gate would be taken up on the high-capacity and relatively cheap activated carbon. The carbon coating was produced from phosphoric acid polymerized furfuryl alcohol. Static adsorption results showed that sieves could be produced having a large capacity for normal butane, a small capacity for isobutane, and a negligible capacity for neopentane. The sieves showed a greater capacity for benzene and cyclohexane than for neopentane, again showing the existence of slit-like pores.

Very recently, Metcalfe (*93*) has examined another approach at producing composite carbon molecular sieves and has characterized the sieves by dynamic adsorption studies. Results have been most encouraging. Saran was carbonized at a heating rate of 6 to 7°C/min up to 900°C,

held at 900°C for 4 hr, and then cooled. This char was used as the filler material in the fabrication of composite sieves. Binders used were a medium-melting-point coal-tar pitch, a lignite pitch, and methyl cellulose. The filler and binders, both ground to −100 mesh, were mixed at room temperature and then pressed into 3/16-in.-diameter pellets, also at room temperature. The pellets were heated at 5°C/min to 900°C in nitrogen and held at 900°C for 2 hr to carbonize the binder phase.

Static-adsorption results showed that coating of the carbonized Saran filler particles with the above binders, in most cases, decreased the adsorption capacity of the particles for hydrocarbons and altered their molecular-sieve behavior, as given previously in Fig. 10 and Ref. 89. Consequently, where necessary, the pellets were subsequently slightly activated in carbon dioxide at 800 to 850°C to open up closed pores in the binder carbon and permit ready access to the filler particles. The extent of activation was found to be critical, with the optimum amount varying with the particular binder used. Too little activation resulted in a pellet still having a low capacity and undesirable sieving properties; too high an activation resulted in a large capacity but in the loss of sieving behavior, undoubtedly because of the filler particles reacting with carbon dioxide and the enlarging of their pore size.

The pellets were evaluated as to their ability to separate hydrocarbons in a fixed-bed dynamic-adsorption apparatus. The hydrocarbons to be separated were entrained in the desired concentration in a helium-carrier stream. Following passage of the stream through the fixed bed of pellets, the concentrations of hydrocarbons remaining in the exit helium were measured using a gas chromatograph. Figures 12(b) and (c) summarize some of the interesting dynamic-adsorption results. The outlet concentrations of the hydrocarbons are plotted against the cumulative time which the gas stream has been passed through the fixed bed. The final outlet concentrations for the hydrocarbons closely approached their inlet values.

Figure 12(b) compares the utility of two composite carbon molecular sieves with a Linde 5A zeolite and a Pittsburgh Activated Carbon Company granular activated carbon BPL for the separation of *n*-heptane and 2,2,4-trimethylpentane (isooctane) at 34°C. Sieves S-20LP-2.2 and S-20LP-2.4 were both formed from 80 parts of Saran char and 20 parts of lignite pitch; the carbonized pellets being subsequently activated to 2.2 and 2.4 per cent burn-off, respectively, in carbon dioxide at 800°C. As expected, the BPL carbon shows no molecular sieving for these hydrocarbons; they both are completely held up in the bed for ca. 75 to 80 min

and then break through into the outlet gas stream. By contrast, the 5A sieve and the two composite carbon molecular sieves show excellent sieving ability. The isooctane breaks through the bed in ca. 3 to 7 min; the *n*-heptane does not break through until at least 40 min. Note that the two carbon sieves show as good a selectivity as the 5A sieve but in addition show a greater capacity for *n*-heptane.

Figure 12(c) compares the ability of two composite carbon molecular sieves with a Linde 10X sieve and activated carbon BPL for the separation of benzene and cyclohexane at 34°C. Sieve S-30MC-0 was formed from 70 parts of Saran char and 30 parts of methyl cellulose; no activation of the carbonized pellet was performed. The 10X sieve shows an interesting behavior to this system. For about 20 min both hydrocarbons are held up by the bed, with no sieving apparent. Cyclohexane then breaks through the bed and quickly reaches an outlet concentration above the inlet concentration (which is also the final outlet concentration). During this period, cyclohexane is being displaced from the bed by benzene, which results in the outlet concentration of cyclohexane being the sum of its inlet concentration plus displaced material. As considered earlier when discussing Fig. 2, this is a typical zeolite-sieve behavior; that is, there is preferential sorption of polar, unsaturated, and aromatic compounds. It is interesting that the BPL carbon shows a similar, but not as marked, behavior. It suggests that this carbon does have a slight adsorption preference for benzene. The behavior of the carbon sieves is in marked contrast to that of the 10X or BPL material. For both sieves, cyclohexane breaks through the column after short operation times, and the outlet concentration quickly reaches the inlet value; benzene only breaks through after about 70 min of operation. These carbon sieves exhibit an outstanding ability to separate cyclohexane from benzene.

The authors feel that molecular-sieve carbons produced from polymeric systems, in whole or in part, have commercial possibilities; but it is clear that much more research and development effort must be expended to bring about this reality.

III. THEORY OF UNSTEADY-STATE DIFFUSION IN MOLECULAR-SIEVE MATERIALS

A. Introduction

There are several different methods of measuring diffusion coefficients through porous solids (*2*). However, the low rates of diffusion in the

materials with which we are concerned necessitate the use of unsteady-state methods. Barrer (*1,26,32*) has considered several different systems for making unsteady-state measurements, each of which has its particular advantages and disadvantages. The method of Nelson and Walker (*94*) was used in this study; the experimental method is described later. In addition to certain experimental advantages, it has the advantage that it is not necessary for sorption of the gas in the solid to be of Henry's-law form to integrate the mass-transport equation. In essence, the method consists of equilibrating a known weight of solid with a fixed pressure of the gas under investigation. After equilibration, the gas pressure is suddenly reduced to a constant lower value (atmospheric pressure); the volume of gas released from the solid is measured as a function of time. Gas contained between particles of the solid or absorbed on the internal surfaces of the particles is rapidly equilibrated to the new pressure. Measurements of the gas released are made only on the slowly released sorbed gas. Because of the stepwise nature of the boundary conditions (constant pressure P_1 at $t < 0$, P_2 at $t > 0$) at the exterior of the particles, it is not necessary to assume Henry's law to hold, as is usually required for constant-volume systems (*26*).

B. Physical Models of the Mode of Mass Transport

Two distinct and extreme physical models might be applicable to the diffusional process. In the first physical model the gas held by the solid can be considered to be in an occluded state in which it does not behave as free gas following ideal-gas laws. The force fields associated with the Lennard-Jones potential energies are significant across the whole of the pore, owing to the small dimensions of the pores, so that an occluded gas molecule is not comparable to a free gas molecule. On the other hand, the molecule is not so firmly fixed in one position that it cannot diffuse through the system. It can move along a pore until it reaches a potential-energy barrier represented by a narrow ring of atoms through which it has to pass. This restriction and potential-energy barrier cause the diffusional process to be one of activated diffusion. It is reasonable to assume that the driving force for diffusion of occluded gas is $\partial C/\partial x$, where C is the concentration of occluded gas in units, for example, of gram-moles per cubic centimeter.

In the second physical model, the gas taken up by the solid might be considered present in two forms: (1) as relatively free molecules occupying the open porosity of the solid and (2) as relatively nonmobile molecules adsorbed in a layer on the internal walls of the solid. Diffusion will

then occur via the "free" gas molecules, which again will meet the potential-energy barriers of restrictions. However, the adsorbed* gas will desorb to maintain equilibrium, giving, in effect, a surface reservoir of gas. The relation between the concentration of diffusing molecules, C_1 say, and the total gas concentration C is

$$C = C_1\epsilon + f(C_1) \tag{4}$$

where ϵ is the open porosity within the particles of the solid, which is filled with gas of concentration C_1, and $f(C_1)$ is the adsorption isotherm. If C_s is the saturation amount in gram-moles per cubic centimeter and if the Langmuir isotherm for nondissociative adsorption applies, we have

$$C = C_1\epsilon + [KC_1/(1 + KC_1)]C_s \tag{5}$$

where K is the equilibrium constant of adsorption; that is, $C_1 + (1 - \theta) \rightleftharpoons \theta$. At relatively low pressures and high temperatures, KC_1 will be small; the Langmuir isotherm reduces to a Henry's-law form (amount adsorbed proportional to pressure) and

$$C_1 = C/(\epsilon + KC_s) \tag{6}$$

It is reasonable to suppose that for this physical model the driving force for diffusion is $\partial C_1/\partial x$, which is proportional to, but not equal to, $\partial C/\partial x$.

The first model, the occluded gas model, is more generally found to apply in investigations of materials with molecular-sieve properties. It must be recognized, however, that in the investigation of a material such as coal the second model must be considered as a possibility until it is proved not to apply. In porous carbon bodies with relatively large pores and high adsorption areas, the "free diffusion-adsorbed gas" model is likely to apply for transient diffusion measurements, with the possibility that some of the mass transfer occurs via mobility of the adsorbed gas, that is, by surface diffusion (*6*). Under circumstances where surface diffusion overweighs the mass transfer by diffusion of free gas molecules, we are again back to a system which behaves as, and falls within the definition of, the occluded gas system. Indeed, when a molecule diffuses across a surface, it will follow a path along a potential-energy trough; and it will have to overcome a series of symmetrical energy barriers, just as an occluded gas will. Thus there is little physical

* Note that the term *adsorbed* is used in this case. It is taken to mean the existence of a dynamic equilibrium between a sorbed surface layer and a relatively free gas within the pores of the solid.

difference between surface diffusion and our first model; when a surface is present in the form of pores of near molecular diameter, the two systems become physically identical. The activation energies are dependent on the three-dimensional potential-energy patterns produced by the interaction of the molecule with the arrangement of atoms of the solid. For pure surface diffusion, the activation energies depend on the atomic arrangement in the surface under the diffusing molecule, whereas for occluded gas diffusion the pattern depends on the arrangement of atoms completely around the diffusing-gas molecule.

C. Differential Equation of Mass Transport

Previous experience has shown that the unsteady-state diffusion process is insensitive to particle shape (*1*). Solutions for different idealized geometries give similar answers, except for small differences in the numerical value of the constants involved. Therefore, for any particle of roughly spherical shape, the spherical solution can be used, bearing in mind that the result obtained is not numerically correct in the absolute sense. Usually there are other factors which introduce more uncertainty in the absolute values than the particle shape. For example, unless the particle approximates to a single crystal of uniform properties, it is possible that a range of pore sizes exists. In many solids, the porosity can be divided into a microporosity and a macroporosity. True gaseous diffusion occurs relatively rapidly in the macropores; under steady-state conditions, the macroporosity will control the diffusivity through the solid. In unsteady-state measurements, the macropores can come rapidly to equilibrium with the external conditions. Therefore, the macropores split the total particle into a number of subunits; and it is these subunits from which the slower transient diffusion occurs. In a material such as coal, the effective radius of the diffusing subunit is a mean of the subunits present, where the value of this mean is not known. In the treatments given below, the sphere considered represents the subunit, which is not necessarily a complete particle.

Considering a spherical unit, a mean balance on a differential element of a shell of radius r gives, assuming Fick's law to apply,

$$\frac{1}{r^2}\frac{\partial}{\partial r}\left(r^2 D\frac{\partial C}{\partial r}\right) = \frac{\partial C}{\partial t} \tag{7}$$

Equation (7) applies to the occluded gas model, with C being the concentration of occluded gas per unit volume of space. In this system it is not necessary, at this time, to express concentration on the basis of

empty volume in the solid, since the occluded gas does not obey ideal-gas laws in this empty volume. On the other hand, for the second physical model the driving force for diffusion is $\partial C_1/\partial x$, where C_1 is the concentration in the open-pore volume. If we substitute for C_1 from (6), the mass balance now gives

$$\frac{1}{r^2}\frac{\partial}{\partial r}\left[r^2(D/(\epsilon - KC_s)\frac{\partial C}{\partial r}\right] = \frac{\partial C}{\partial t} \tag{8}$$

or

$$\frac{1}{r^2}\frac{\partial}{\partial r}\left(r^2\bar{D}\frac{\partial C}{\partial r}\right) = \frac{\partial C}{\partial t} \tag{9}$$

where $\bar{D} = D/(\epsilon + KC_s)$. Clearly the solution of (7) and (9) will be the same, although the meaning of the apparent diffusion coefficient $\bar{D}$ will be different from that of the true diffusion coefficient D.

The solutions for the boundary conditions imposed by the experimental technique considered here are well known (*95*) and are

$$\frac{V_t - V_0}{V_e - V_0} = 1 - \frac{6}{\pi^2}\sum_{n=1}^{\infty}\frac{1}{n^2}\exp\left(\frac{-Dn^2\pi^2 t}{r_0^2}\right) \tag{10}$$

$$= 6\left(\frac{Dt}{r_0^2}\right)^{1/2}\left[\pi^{-1/2} + 2\sum_{n=1}^{\infty}\text{ierfc}\,\frac{nr_0}{(Dt)^{1/2}}\right] - \frac{3Dt}{r_0^2} \tag{11}$$

$V_t - V_0$ is the volume of gas desorbed at time t, $V_e - V_0$ is the volume desorbed at infinite time, and r_0 is the equivalent spherical radius of the diffusing unit. The series of (10) converges well for large values of $D^{1/2}t^{1/2}/r_0$, whereas the series in (11) converges rapidly for small values of $D^{1/2}t^{1/2}/r_0$.

D. Computational Methods

For small values of $D^{1/2}t^{1/2}/r_0$, (11) reduces to

$$\frac{V_t - V_0}{V_e - V_0} \simeq \frac{6}{\pi^{1/2}}(D^{1/2}/r_0)t^{1/2} \tag{12}$$

If measurements are made of the unsteady-state diffusion of gas into a previously evacuated solid, $V_0 = 0$. The raw experimental data consists of V_t values as a function of time. V_e is estimated from an adsorption isotherm or long-time diffusion measurements. $D^{1/2}/r_0$ is then obtained, most simply as the slope of the plot of V_t/V_e versus $t^{1/2}$. However, the reduction to (12) is not very precise over a wide range of time. Further,

reliable values of V_e cannot be obtained without extending the diffusion experiment over very long periods of time. In addition, the initial time measurements are difficult to obtain accurately, since the system must settle down after changing the pressure. It is advantageous to use a wider time range of the experimental results, which can be done as follows.

Differentiating (11) with respect to $t^{1/2}$ gives

$$\frac{dV_t}{dt^{1/2}} = \frac{6D^{1/2}}{r_0}(V_e - V_0)H\left(\frac{D^{1/2}t^{1/2}}{r_0}\right) \tag{13}$$

where

$$H\left(\frac{D^{1/2}t^{1/2}}{r_0}\right) = \pi^{-1/2} - \frac{D^{1/2}t^{1/2}}{r_0} + \sum_{n=1}^{\infty} \frac{2}{\pi^{1/2}} \exp\left[-\left(\frac{nr_0}{D^{1/2}t^{1/2}}\right)^2\right] \tag{14}$$

It is shown (*95*) that the terms of the summation in (14) are negligible up to $D^{1/2}t^{1/2}/r_0 = 0.4$, which corresponds to 87 per cent completion of the diffusion process. Therefore, $D^{1/2}/r_0$ and $V_e - V_0$ can be obtained by a plot of $dV_t/dt^{1/2}$ versus $t^{1/2}$, by noting the slope S and the intercept I, which are related by $D^{1/2}/r_0 = -S/I\pi^{1/2}$ and $(V_e - V_0) = I\pi^{1/2}/(6D^{1/2}/r_0)$. This technique has the advantage that results are obtained using experimental data from the most valid region (placing no reliance on very short or very long times), while at the same time the validity of the assumptions made in deriving the equations are tested by a fit of the results to the predicted straight line. The use of this method has been demonstrated by Nelson and Walker (*94*) for the diffusion of nitrogen in the 3A zeolite.

The method principally used in the results reported here has also been described by Nelson and Walker (*94*). Considering (10), we see that three unknowns are involved: V_0, V_e, and $D^{1/2}/r_0$. These unknowns can be obtained by the solution of the three equations representing three points on the curve, V_1, V_2, V_3, as follows:

$$\begin{aligned} V_1 - V_0 &= (V_e - V_0)f_1 \\ V_2 - V_0 &= (V_e - V_0)f_2 \\ V_3 - V_0 &= (V_e - V_0)f_3 \end{aligned}$$

where f_i is used to denote the function

$$f_i = 1 - \frac{6}{\pi^2}\sum_{1}^{\infty} \frac{1}{n^2} \exp\left(-\frac{Dn^2\pi^2 t_i}{r_0^2}\right)$$

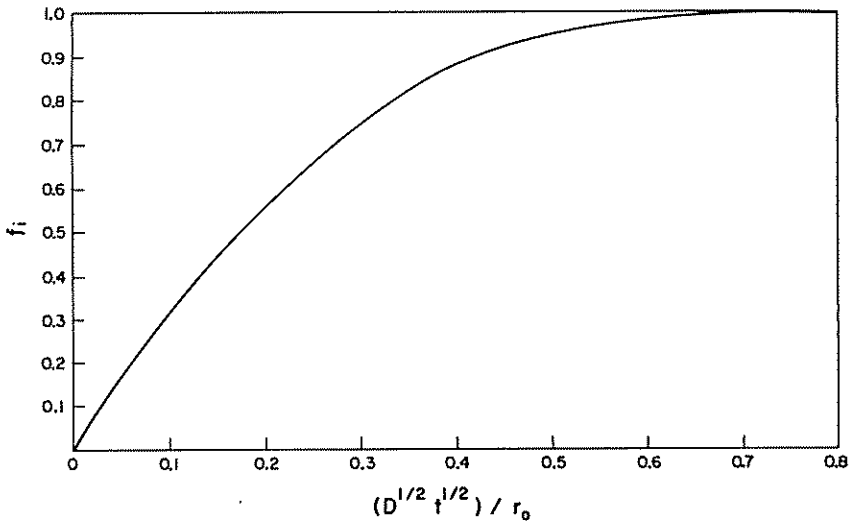

Fig. 13. Solution to differential equation (7), which gives Fick's second law. [From Crank (*96*).]

Eliminating V_0 and V_e between the equations gives

$$\frac{f_1V_3 + f_2V_1 + f_3V_2}{f_1V_2 + f_2V_3 + f_3V_1} = 1$$

This can be solved for $D^{1/2}/r_0$ by a method of successive approximations The procedure adopted was to assume values of $D^{1/2}/r_0$ successively and to converge on the required value of $D^{1/2}/r_0$ systematically. The appropriate values of V_e and V_0 were then obtained by back-substitution.* A satisfactory value of $D^{1/2}/r_0$ can be arrived at by hand calculation after three or four trials; successive values of f_i were obtained from Fig. 13, which gives (10) in graphical form.

E. Temperature Dependence of Activated-Diffusion Coefficients

The significance of the measured value of the activated-diffusion coefficients (either D or $\bar{D}$) can readily be formulated by using the

* As will be seen more clearly in Section IV, the volume values obtained by the Nelson and Walker method are relative values which correspond to an arbitrary point of reference on the volume-measuring scale. Since, in any one experimental run, the volume values all correspond to the same reference point, differences in volume, such as $V_e - V_0$, are absolute values.

methods of absolute rate theory (*96,97*). Let us consider first the possible meanings of the true diffusion coefficient D. Consider a molecule which passes from a potential-energy valley to the top of a potential-energy barrier existing because of a ring of atoms of small radius. If the increase in energy is sufficient to give an activated-diffusional process, the molecules in the valleys can be considered in equilibrium with the "activated" molecules on the saddles. Two limiting physical cases might apply. In the first case, a number of molecules exist in each potential-energy valley (or cavity), because the cavity is large compared to the size of the diffusing molecule and the relative pressure of the gas is substantial. In the second case, only one (or no) molecule exists in each cavity, either because the cavity size approximates the size of the molecule or because the relative pressure of the diffusing gas is very low.

Examining the first case, the probability of a molecule being in the ring, in the activated state, depends on the concentration of nonadsorbed molecules. Considering a unit cross-sectional area of the solid, the number of constrictive rings (hereafter called holes) per square centimeter is fixed. Assuming that a hole is of molecular dimensions, so that a maximum of one activated complex per hole is permitted, we can express the number of holes as a concentration of holes in gram-moles per square centimeter, N say. Let $\theta^\ddagger$ be the fraction of these holes occupied by activated molecules. Then, for an appreciable activation energy, the equilibrium is

$$(1 - \theta^\ddagger)N + C \rightleftharpoons \theta^\ddagger N \tag{15}$$

where C is the concentration of diffusing molecules in units of, say, gram-moles per cubic centimeter. The rate of passage of molecules through the holes is given by rate $= k\theta^\ddagger N$. Since $\theta^\ddagger$ is small, the value of $\theta^\ddagger N$ can be replaced from the equilibrium relation $\theta^\ddagger N/N(C/C_0) = \exp(-\Delta F_0^\ddagger/RT)$ with C_0 being the standard state of concentration.

Then

$$\text{rate} = k(C/C_0)N \exp(-\Delta F_0^\ddagger/RT) \tag{16}$$

where the units of k are sec^{-1} and C/C_0 is, of course, dimensionless. The units of rate are thus gram-moles per square centimeter per second. If the concentrations on each side of the barrier are C_1 and C_2, the net rate of reaction is

$$\begin{aligned} \nu &= k(C_1/C_0)N \exp(-\Delta F_0^\ddagger/RT) - k(C_2/C_0)N \exp(-\Delta F_0^\ddagger/RT) \\ &= \Delta(C/C_0)kN \exp(-\Delta F_0^\ddagger/RT) \end{aligned}$$

If the distance between the saddle points is δ, $\Delta(C/C_0)/\delta = d(C/C_0)/dx$. Then, since δ is small,

$$\nu = k \frac{\delta N}{C_0} \exp(-\Delta F_0^{\ddagger}/RT) \frac{dC}{dx} \tag{17}$$

If we compare (17) with Fick's law, it is apparent that

$$D = (k\ \delta N/C_0) \exp(-\Delta F_0^{\ddagger}/RT) \tag{18}$$

In the usual way, the free energy of the weak decay vibration (or the translation across the top of the energy barrier) can be factorized and combined with the frequency k to give

$$D = (k_B T\ \delta N/hC_0) \exp(\Delta S_0^{\ddagger}/R) \exp(-\Delta H_0^{\ddagger}/RT) \tag{19}$$

where h is Planck's constant, or

$$D = D_0 \exp(-\Delta H_0^{\ddagger}/RT) \tag{20}$$

$\Delta S_0^{\ddagger}$ is the truncated entropy of activation (with the entropy of vibration or translation along the axis of the potential energy barrier removed).* Providing δ, N, and C_0 are in consistent units, the units of D_0 are independent of the standard state chosen. However, the numerical magnitude of $\Delta S_0^{\ddagger}$ depends on the standard state chosen for C_0, since if C_0 is taken as 1 molecule/cc, N must be in units of molecules per square centimeter; if C_0 is taken as 1 g-mole/cc, N will be in gram-moles per square centimeter. (For a regular crystalline array, N in holes/cm^2 is $1/\delta^2$).

Examining the second limiting physical case, we see that the probability of an activated molecule being in a hole is fixed when an adjacent cavity is occupied and zero when it is not. Higher concentrations of diffusing material give bigger diffusion rates, because more cavities are occupied and not because the probability of passage through a given occupied hole goes up with concentration. This is obviously a different physical picture than that for which a given cavity has an increasing

* It will be noted that $\Delta F_0^{\ddagger}$ is the standard-state free energy of activation at temperature T; therefore, $\Delta S_0^{\ddagger}$ and $\Delta H_0^{\ddagger}$ are the corresponding values of entropy and enthalpy at T. If $\Delta H_0^{\ddagger}$ is the ground-state enthalpy of activation, it is convenient to define a parameter Φ by $\Phi = S_0 - (H_0 - H_0^0)/T$ or $\Delta\Phi^{\ddagger} = \Delta S_0^{\ddagger} - (\Delta H_0^{\ddagger} - \Delta H_0^{0\ddagger})/T$. Then $\Delta F_0^{\ddagger} = \Delta H_0^{0\ddagger} + T\,\Delta\Phi^{\ddagger}$. $\Delta H_0^{0\ddagger}$ is independent of temperature and corresponds approximately to the energy of activation obtained from an Arrhenius plot. It can be shown that $\exp(\Delta\Phi^{\ddagger}/R)$ is the ratio of the reduced partition functions of the products (activated complex in this case) over those of the reactants. In theoretical calculations in Section V, we shall use the parameter Φ instead of entropy.

concentration within it as the concentration of gas goes up. The one cavity–one molecule model applies for the diffusion of interstitial atoms in a solid—hydrogen in palladium, for example. It also applies where the partial pressure of the diffusing species is very low, as we shall see later.

The equilibrium between cavities and holes across a unit cross-sectional area is

$$M \rightleftharpoons N^{\ddagger} \tag{21}$$

M is the number of occupied cavities per square centimeter and can be put in the units of gram-moles per square centimeter; $N^{\ddagger}$ is the number of occupied holes in the same units. The rate is given by rate $= kN^{\ddagger}$ and the equilibrium relation by $\gamma N^{\ddagger}/M = \exp(-\Delta F_0^{\ddagger}/RT)$. γ is the number of holes per cavity divided by the number in the diffusion plane. The molecule in the cavity is in equilibrium with activated complexes in any of the holes around the cavity; if the concentration of occupied holes is N', $\gamma N^{\ddagger} = N' \rightleftharpoons M$. For example, in Fig. 14, the number of

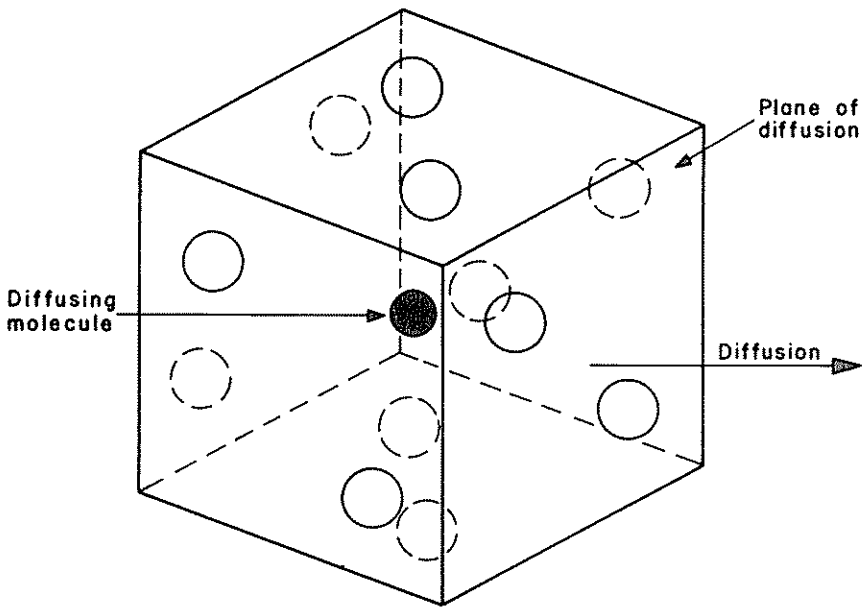

Fig. 14. A six-sided cavity having two holes (or apertures) per side through which diffusing molecules can pass.

holes per cavity is 12 and the number in the diffusion plane is 2; therefore, γ is 6. The treatment, as before, then yields

$$\nu = (k)(\delta/\gamma) \exp(-\Delta F_0^{\ddagger}/RT)(dM/dx) \tag{22}$$

Assuming that the number of molecules in the holes is small compared to those in the cavity, we can convert M to conventional units of concentration from the relation $M = \delta C$, giving

$$\nu = (k_B T/h\gamma)\delta^2 \exp(-\Delta F_0^{\ddagger}/RT)(dC/dx) \tag{23}$$

and

$$D = (k_B T/h\gamma)(\delta^2) \exp(\Delta S_0^{\ddagger}/R) \exp(-\Delta H_0^{\ddagger}/RT) \tag{24}$$

D can then be expressed in the same form as (20). It should be noted that the entropy of activation again has the entropy of vibration (or translation) along the decay axis removed, but its numerical magnitude is now independent of any gas-concentration standard state. The same form as (24) can be obtained from (19) if the standard state of gas concentration is chosen to be equivalent to 1 molecule per cavity, for then, N in holes/cm^2 = $1/\delta^2$, C_0 is $1/\delta^3$ molecules/cc, and $N/C_0 = \delta$ (assuming one hole in the diffusing plane per cavity).

Since the mathematical form of the two limiting physical cases, (19) and (24), is identical, in each case an activation energy and D_0 can be determined from an Arrhenius plot of log D versus $1/T$. If the structure of the solid is of known geometry, so that δ or δ and N is known, the entropy of activation can be determined from the value of D_0.

On the other hand, if the free diffusion-adsorbed gas model is applicable, it is recalled that $\bar{D} = D/(\epsilon + KC_s)$, where K has consistent units of cubic centimeter per gram-mole. The temperature dependence of K is given by

$$\begin{aligned} KC_s &= (C_s/C_0) \exp(-\Delta F_0/RT) \\ &= (C_s/C_0) \exp(\Delta S_0/R) \exp(-\Delta H_0/RT) \end{aligned} \tag{25}$$

Again, the value of the entropy of adsorption is dependent on the standard state chosen. $-\Delta H_0$ can be replaced with q, the heat of adsorption, to give

$$\bar{D} = \frac{D_0 \exp(-\Delta H_0^{\ddagger}/RT)}{\epsilon + (C_s/C_0) \exp(\Delta S_0/R) \exp(q/RT)} \tag{26}$$

It is clear that a plot of log $\bar{D}$ versus $1/T$ will not be linear over a wide temperature range, which gives one method of distinguishing between

models 1 and 2. At low temperatures, where the quantity adsorbed is high, the porosity term will be negligible, giving

$$D \simeq \frac{D_0 \exp(-\Delta S_0/R) \exp[-(\Delta H_0^{\ddagger} + q)/RT]}{(C_s/C_0)} \tag{27}$$

At higher temperatures,

$$D \simeq (D_0/\epsilon) \exp(-\Delta H_0^{\ddagger}/RT) \tag{28}$$

Therefore, as the temperature is increased, the slope of the Arrhenius plot should become smaller in magnitude.

F. Rate Equations with Net Attraction at the Center of the Aperture Plane

We have first considered the situation in which the free diameter of the ring of atoms in the aperture plane was sufficiently small to produce a net repulsive interaction energy for the passage of a molecule. As we shall see later in the case of the passage of rare gas atoms through the aperture plane of the 5A zeolite, the free diameter is sufficiently large to result in a net attractive interaction. This situation can be considered briefly.

Consider a situation as shown in Fig. 15, where the atom is diffusing along the path *abcd*. Using the normal concepts of absolute rate theory,

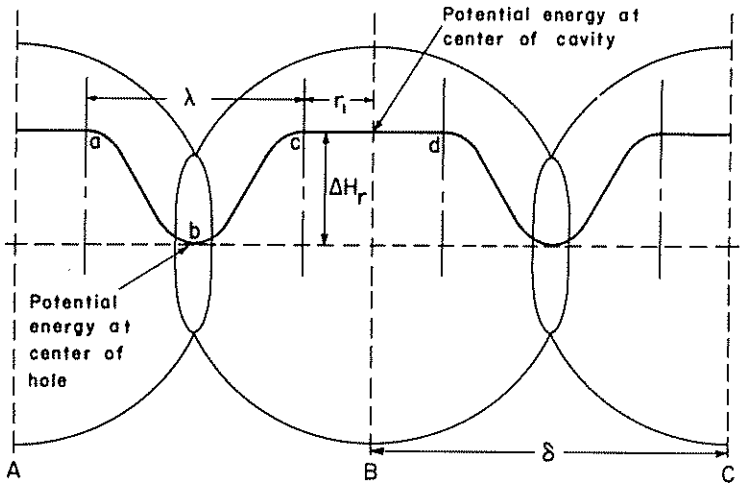

Fig. 15. Idealized potential-energy diagram for species diffusing through a zeolite. Species has a net attractive interaction at center of aperture plane.

we may assume that atoms at b are in equilibrium with those at a and c, with the slow step in the diffusion being the passage across the energy plateau cd. Let θ be the fraction of holes in the diffusing plane which are occupied (or, put another way, θ is the probability of a hole being occupied). Taking a standard state of 1 atom per cavity, the concentration of atoms can be taken as C atoms per cavity. Then assuming a unit activity coefficient

$$\theta = 2C(1 - \theta) \exp (\Delta F_r^{\ddagger}/RT) \tag{29}$$

The total concentration in the two half cavities between A and B is $C_1 = 2C + \theta$ atoms per cavity. The rate of diffusion across cd is given by

$$\text{rate} = C\bar{u}/2r_1 \tag{30}$$

where $\bar{u}$ is the mean velocity of travel of the atom along cd. In the usual way $\bar{u} = (k_BT/2\pi m)^{1/2}$. If θ is small compared to C, then $C_1 \approx 2C$, and the net rate of diffusion is

$$\nu = (C_1 - C_2)(k_BT/2\pi m)^{1/2}/2r_1 \tag{31}$$

where C_2 is the concentration in the two half-cavities BC, in atoms per cavity. For a regular array of δ spacing, the number of cavities per cubic centimeter is $1/\delta^3$ and the number of holes per square centimeter is $1/\delta^2$. Then

$$\nu = \Delta C(k_BT/2\pi m)^{1/2}\delta/4r_1 \tag{32}$$

where ν is in gram-moles per square centimeter-second and ΔC in gram-moles per cubic centimeter. As before, $\Delta C/\delta$ can be replaced by dC/c and

$$\nu = (k_BT/2\pi m)^{1/2}(\delta^2/4r_1)\, dC/dx \tag{33}$$

Clearly this is a nonactivated diffusion, and it will give results comparable to the Knudsen diffusion equation. Physically, the assumptions involved in its derivation imply that an atom at a is accelerated to b and decelerated from b to c, so that the mean velocity over a to c is large compared with that over the passage from c to d.

On the other hand, if θ is large compared to C, $C_1 \approx \theta$ and (31), (32), and (33) must be put as

$$\text{rate} = (\theta/2) \exp (-\Delta F_r^{\ddagger}/RT)(k_BT/2\pi m)^{1/2}/2r_1 \tag{34}$$

The net rate of transfer is

$$\nu = \Delta\theta \exp (-\Delta F_r^{\ddagger}/RT)(k_BT/2\pi m)^{1/2}/4r_1 \tag{35}$$

if the entropy of the translational degree of freedom along cd, $[(2\pi mk_BT/h^2)^{1/2}/2r_1]$, is factorized from $\Delta F_r^{\ddagger}$ to leave ΔF_r, we obtain

$$\nu = \Delta\theta \exp(-\Delta F_r/RT)(k_BT/h) \tag{36}$$

Expressing ν in gram-moles per square centimeter-second and $\Delta\theta = \Delta C$ in gram-moles per cubic centimeter, and replacing $\Delta C/\delta$ with dC/dx, we have

$$\nu = (k_BT/h)\delta^2 \exp(-\Delta F_r/RT)\, dC/dx \tag{37}$$

In this case activated diffusion results.

It is important, therefore, to be able to compare the values of $2C$ and θ. An overestimate of θ is obtained if $1 - \theta$ in (29) is taken as 1, that is,

$$\theta \simeq 2C \exp(\Delta F_r^{\ddagger}/RT) \tag{38}$$

or

$$\begin{aligned} \theta/2C &\leqslant \exp(\Delta F_r^{\ddagger}/RT) \\ &\leqslant (Q_\theta/Q_C) \exp(\Delta H_r^{\ddagger}/RT) \end{aligned} \tag{39}$$

where Q_θ and Q_C are partition functions of θ and C. Q_C can be taken as

$$Q_C = (2\pi mk_BT/h^2)^{3/2}(4/3)r_1^3 \tag{40}$$

since a standard state of 1 molecule per cavity has been used. For Q_θ, the vibrational partition functions across the radius of the hole can be taken as 1, leaving only the vibrational component along abc. This can e estimated from the equation for Q_ν' given in Section V.

G. Heats of Sorption

Another method of potentially differentiating between the occluded gas model and the free gas-adsorbed gas model is to determine (1) the heat of sorption for comparison with the activation energy of diffusion and (2) the form of the sorption isotherm. It should be remembered that the derivation of (26) is based on the assumption that the amount of adsorbed gas is proportional to the free gas concentration [see the derivation of (6)]. If this is not true over the pressure range investigated, model 2 would not lead to a constant effective diffusion coefficient, nor would a linear Arrhenius plot be obtained. If model 1 applies, it will apply independent of the form of the sorption isotherm.

Consider sorption which follows a Langmuir isotherm such that

$$K_p p(1 - \theta)C_s = \theta C_s \tag{41}$$

The gram-moles of gas released in going from an equilibrium pressure of p_0 to a new equilibrium pressure of p_a (where p_a is atmospheric pressure for our system) is, for 1 cm^3 of sample,

$$C_0 - C_a = C_s\left(\frac{Kp_0}{1 + Kp_0} - \frac{Kp_a}{1 + Kp_a}\right) + \frac{\epsilon(p_0 - p_a)}{RT} \tag{42}$$

The term with the porosity ϵ represents the free gas volume and assumes the ideal-gas law to apply to the gas in this space. (The suffix p has been dropped from K_p for convenience in algebraic manipulation.) The amount of gas released is related to the volume of gas (measured at p_a and T_a) released from the sample of weight W by $C_0 - C_a = \rho p_a(V_e - V_0)/WRT_a$, where ρ is the density of the solid. Therefore,

$$\frac{(V_e - V_0)p_a}{(W/\rho)(RT_a)} = \frac{(p_0 - p_a)C_sK}{(1 + Kp_0)(1 + Kp_a)} + (p_0 - p_a)\frac{\epsilon}{RT_a} \tag{43}$$

When sorption is appreciable and the porosity ϵ is small (or if the one molecule per cavity concept applies), the second term on the right side of (42) can be neglected and

$$\frac{W(RT_a/p_a)(p_0 - p_a)}{V_e - V_0} = \frac{1 + Kp_a}{(C_s/\rho)K}(1 + Kp_0) \tag{44}$$

where C_s/ρ is the saturation sorption per gram of material. The terms on the left side are known, and a plot of this versus p_0 should give a straight line (since p_a is approximately constant for all runs). This, then, is a test for Langmuir sorption. When the isotherm reduces to a Henry's-law form, Kp_0 is small compared to one. The left side of (44) is then constant for a given temperature. For Henry's law applying for experimental conditions where $p_0 - p_a$ is kept constant but the temperature of diffusion is varied, we find

$$(V_e - V_0) \propto K \propto \exp(q/RT) \tag{45}$$

A plot of log $(V_e - V_0)$ versus $1/T$ gives the heat of sorption from the slope. On the other hand, if the solid is nearly saturated (higher pressures, lower temperatures, bigger q), Kp_0 is much greater than 1. Equation (44) then reduces to

$$\frac{V_e - V_0}{W(RT_a/p_a)(p_0 - p_a)} = \frac{(C_s/\rho)}{Kp_0p_a} \tag{46}$$

and, for fixed values of p_0 and p_a,

$$(V_e - V_0) \propto 1/K \propto \exp(-q/RT) \tag{47}$$

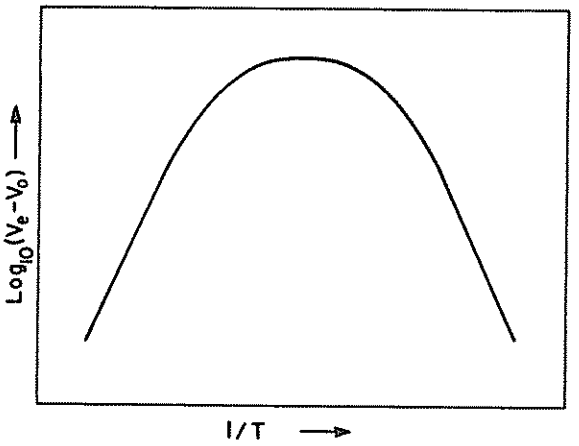

Fig. 16. Possible van't Hoff plots of V_e–V_0 values, as determined from unsteady-state diffusion measurements over a wide range of temperatures.

Thus $V_e - V_0$ will increase with increasing temperature. The complete van't Hoff plot must obviously give a curve, as shown in Fig. 16. When p_a and p_0 are close in value, the maximum value of $V_e - V_0$ is reached when $Kp \sim 1$ and

$$(V_e - V_0)_{max} = \frac{W(C_s/\rho)(RT_a/p_a)(p_0 - p_a)}{4p_a} \tag{48}$$

It must be emphasized that the experimental technique used here was developed for the measurement of diffusion coefficients and is not really suitable for the determination of isotherms or heats of sorption, since it operates over a pressure range of about 1.5 down to 1 atm. However, (44) is useful because it enables a test to be made for Langmuir or Henry's-law sorption. In the results to be discussed, it was sometimes found that sorption followed Henry's law but that the van't Hoff plots, log $(V_e - V_0)$ versus $1/T$, were not linear. However, diffusion coefficients were constant with varying pressure, and Arrhenius plots of activated diffusion were linear over a wide temperature range. It can be concluded, therefore, that model 1 applied, since linear Arrhenius plots would only be obtained for the second model if Henry's law applied with a constant van't Hoff slope. If a nonlinear Arrhenius plot of activated diffusion is obtained (for all the systems we studied, linear plots have been obtained), it does not necessarily prove that the first model is not applicable, since it is possible that the activation energy of diffusion could change with

the concentration of occluded gas, especially as the heat of sorption appears to change with concentration of sorbed gas.

IV. EXPERIMENTAL DIFFUSION COEFFICIENTS IN ZEOLITES AND CARBON MOLECULAR SIEVES

In this section, we first summarize previous measurements of activated diffusion coefficients in zeolites and carbon molecular sieves. We then consider our activated diffusion results in the type A zeolites and coals.

A. Summary of Previous Results

1. Zeolites. Table IV summarizes pertinent previous activated diffusion results in zeolites. Tiselius (*42,98*) was apparently the first person to measure activation energies* for diffusion of species in zeolites. Of particular interest were his studies of water diffusion in heulandite. Heulandite is a platy zeolite composed of two-dimensional lattice layers. Tiselius found diffusion of water to show a minimum rate and a maximum E normal to the layers or the (00ℓ) planes.

Barrer and co-workers have studied extensively the kinetics of diffusion of gases in the natural and synthetic zeolites. Barrer and Ibbitson (*99*) studied the diffusion of a series of normal hydrocarbons of increasing chain length in chabazite. They found that, during the initial stages of sorption, the results could be approximated by the parabolic diffusion law, $(V_t - V_0)/(V_e - V_0) = kt^{1/2}$ [which is similar to our (12)]. They further found that Arrhenius plots of $\log k$ versus $1/T$ decreased in slope at higher temperatures. This latter finding suggests that the free diffusion-adsorbed gas model was, at least in part, influencing the results, as we discussed in Section III. The authors realize this and consequently refer to their results as apparent activation energies or E_a. The fact that Barrer and Ibbitson report an increasing E_a with increasing chain length of the normal hydrocarbons is consistent with $\bar{D} \sim \exp[-(\Delta H_0^{\ddagger} + q)/RT]$, as given in (27). The heat of adsorption q increases with increasing molecular weight of the normal hydrocarbons.

Later Barrer and Brook (*32*) reported additional E_a values for hydrocarbon diffusion in chabazite, determined as described above. Again the E_a for n-butane diffusion is greater than that for propane. Of particular interest are E_a values for dimethylamine and methylene dichloride compared to that of propane, since these molecules are of comparable size and shape but have decreasing polarity in the order

* For brevity, we let E represent activation energy.

given. Polarity in the sorbate substantially influences the E for diffusion, both by increasing the potential-energy maximum in the aperture and decreasing the potential-energy minimum in the cavity.

Barrer (*26*) studied the diffusion of gases in different mordenites and levynites. By appropriately considering effects of the distribution of the sorbate between the gas phase and the adsorbed phase on the kinetics, true E values were calculated. Barrer showed the marked extent to which E for diffusion is dependent upon the particular cation present in the mordenite structure. The best estimate of the free diameter of the eight-membered oxygen ring in mordenite should be 3.9 A, as given by Barrer and Peterson (*102*), who studied the structure of the hydrogen (cation) form. Barrer showed, in the case of K-mordenite and levynite, the pronounced effect of the size of the gas on its E for diffusion. As the kinetic diameter of the gases increased from 2.9 A (for hydrogen) to 3.6 A (for krypton), the E for diffusion in K-mordenite increased progressively from 2.5 to 10.0 kcal/mole. In levynite, as the kinetic diameter of the gases increased from 2.8 (for neon) to 3.6 A, the E increased from 2.6 to 12.0 kcal/mole.

Habgood (*41*) studied the diffusion of nitrogen and methane in 4A zeolite powder and pellets. Diffusion coefficients for the pellets were found to be considerably lower than for the powder, which he attributed to the presence of some amorphous nonsorbing binder (which holds the pellets together) sealing off part of the zeolite surface through which sorption occurs. In general, the diffusion coefficient increased with creasing sorbate concentration. At zero concentration, E values for ..iffusion of nitrogen and methane were estimated to be 4.0 and 7.4 kcal/mole.

Nelson and Walker (*94*) and Nelson (*105*) studied the diffusion of selected gases in the type A zeolites, using the apparatus to be described in the next section. Methods used for calculating diffusion coefficients were described in Section III. For the propane-5A system, diffusion measurements were made following the charging of the zeolite to a number of different pressures above atmospheric (735 torr). Figure 17 presents portions of isotherms for the volume of propane released versus the initial charging pressure. It is seen that, at each sorption temperature, the isotherm closely obeys Henry's law. Values of the diffusion parameter, $D^{1/2}/r_0$, were independent of propane-loading pressure over the entire temperature range studied. Negligible curvature of the Arrhenius plots of the diffusion parameter was found for all the gases studied. The sharp increase in E for the diffusion of propane is consistent

TABLE IV

ACTIVATED DIFFUSION RESULTS ON ZEOLITES

Investigators	Zeolite	Diffusing species	Temp range, °C	Activation energy, kcal/mole	Aperture minimum free diameter, A
Tiselius (*42,98*)	Heulandite(201)	Water	20–75	5.4	
	Heulandite(001)	Water	20–75	9.1	
	Analcite	Ammonia	About 302	11.5	2.3–2.4(100)
Emmett and DeWitt (*43*)	Chabazite (65% dehydrated)	Nitrogen	−195−−183	3.6	
Barrer and Ibbitson (*99*)	Analcite	HCl	45–175	13.8	2.3–2.4(100)
	Analcite	Propane	18–135	6.8	
	Chabazite	Propane	23–225	4.5	3.7, 3.9(101)
	Chabazite	*n*-Butane	23–156	8.9	
	Chabazite	*n*-Pentane	224–295	7.1	
	Chabazite	*n*-Heptane	182–300	11.1	
Barrer and Brook (*32*)	Chabazite	Propane	150–200	3.1	
	Chabazite	*n*-Butane	150–200	7.3	
	Chabazite	Methylene dichloride	0–50	6.4	
	Chabazite	Dimethylamine	0–100	~17	
Barrer (*26*)	Li-mordenite	Krypton	About −78	7.6	<3.9(102)
	Li-mordenite	Argon	About −78	7.3	
	NH_4-mordenite	Krypton	−78–0	9.0	
	NH_4-mordenite	Argon	−185−−78	7.0	
	Na-mordenite	Krypton	−78–20	11.0	
	Na-mordenite	Argon	About 20	9.3	
	K-mordenite	Krypton	About −78	10.0	

	K-mordenite	Argon	About −78	8.4	
	K-mordenite	Nitrogen	About −78	4.8	
	K-mordenite	Oxygen	About −78	4.4	
	K-mordenite	Hydrogen	About −78	2.5	
	Levynite	Krypton	About −78	12.0	3.2, 5.1(101)
	Levynite	Argon	About −78	9.4	
	Levynite	Neon	About −78	2.6	
Habgood (*41*)	4A	Nitrogen	−79–0	4.0	3.5(37)
	4A	Methane	−79–0	7.4	
Nelson and Walker (*94*)	5A	Propane	28–360	0.54	4.2(37)
	4A	Propane	302–370	8.7	3.5(37)
	4A	Ethane	103–254	3.0	
	3A	Argon	280–400	14.0	3.2(50)
	3A	Nitrogen	293–363	16.2	
Carr (*105*)	Sodalite	Krypton	250–400	~30	2.2–2.4(104)
	Sodalite	Argon	250–400	~22	

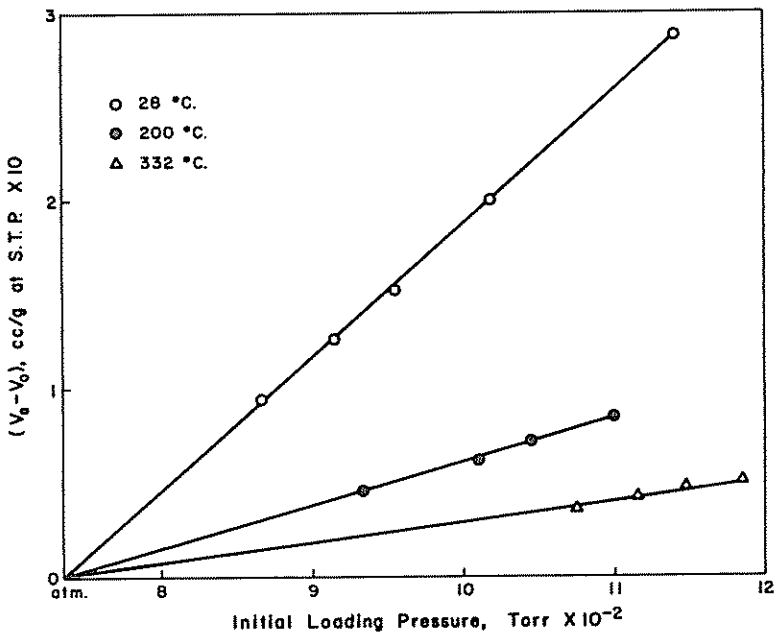

Fig. 17. Portions of isotherms for propane sorption on type 5A zeolite. V_e–V_0 values calculated from unsteady-state diffusion results.

with the sharp decrease in its uptake in going from the 5A to the 4A zeolite, as presented in Table I. Further, the marked decrease in E fo. the diffusion of ethane in the 4A sieve, relative to propane, is consistent with the substantial ethane uptake on the 4A sieve, as also shown in Table I.

Recently Carr (*103*) studied the encapsulation of argon and krypton in sodalite at temperatures up to 450°C and pressures up to 850 atm. Following encapsulation, he studied the diffusion of the gases out of sodalite at various temperatures. It is noted from Table IV that activation energies for diffusion of the rare gases are high, which means that argon and krypton can be held in sodalite at room temperature for very long periods of time.

2. Carbon Molecular Sieves. To the authors' knowledge, only one series of measurements of the E for diffusion has been made in a carbon molecular-sieve material, other than coal. Dacey and Thomas (*87*) measured the rates of sorption of a number of hydrocarbons on carbon

produced by heating polyvinylidene chloride to 700°C. They plotted amount sorbed versus the square root of time and calculated rates from the slopes of the plots. Values of E were then estimated from Arrhenius plots of these rates. As the authors recognize, this approach can only be justified when the equilibrium sorption is independent of temperature; as is evident from (12). As far as possible, all kinetic measurements were made at pressures above that required to reach the saturation value of sorption. However, the authors do note that in some cases increasing the relative pressure (in the pressure range where they thought they had saturation) at constant temperature increased the slope of their plots. This places their activation-energy values open to some suspicion. In fact, neopentane was found to have a smaller E (4.5 kcal/mole) than n-heptane (7.7 kcal/mole), which is inconsistent with the smaller minimum kinetic diameter for n-heptane.

Table V summarizes previous activated-diffusion results on coal.

TABLE V

ACTIVATED DIFFUSION RESULTS ON COALS

Investigators	Carbon content of coal, % (d.a.f.)	Diffusing species	Temp. range, °C	Diffusion coefficient, cm^2/sec	Activation energy, kcal/mole
Zwietering et al. (*106*)	88.6	Methane	−115–−140	$(0.6–4.8)10^{-15}$	3.9
Ioy (*107*)	93.7	Methane	−78–30	$(0.08–3.9)10^{-12}$	4.3
Pruss (*108*)	86.9	Argon	−78–30	$(3.2–8.0)10^{-9}$	1.5
Bolt and Innes (*109*)	83.1–94.0	Carbon dioxide	38	$(3.5–9.2)10^{-8}$	—
Sevenster (*110*)	Unknown	Water	25–60	$(4.8–6.4)10^{-13}$	2.1–2.8

Zwietering and co-workers (*106*) studied the sorption kinetics of methane, held at a pressure of 267 torr, at temperatures between −115 and −140°C. To calculate diffusion coefficients, they used a simplified version of (12). Since the samples were degassed prior to sorption measurements, V_0 was taken as zero. The authors assumed that the domains in which activated diffusion occurs are spherical and, therefore set r_0 equal to $3V/S$, where V and S are the volume and area of the sphere. They then used the equation

$$V_t/V_e = 2S(Dt)^{1/2}/V\pi^{1/2} \tag{49}$$

The authors further assumed that S is the surface area measured by nitrogen adsorption at 77°K and V is the reciprocal of the helium density measured at room temperature. Since the nitrogen area measured at 77°K represents the macropore area of the coal (as we show in Table II), it is clear that the authors envision activated diffusion to be occurring over domain sizes, which are considerably less than the particle size. A 25°C sorption isotherm for methane on the coal up to pressures of 500 atm was available; above 150 atm the isotherm flattened out at a saturation value. By using the Clausius-Clapeyron equation and a heat of sorption for methane of 5 kcal/mole, it was calculated that 150 atm at 25°C is equivalent to a pressure of about 70 torr at the maximum diffusion temperature (−140°C). Therefore, V_e was taken as the saturation value measured at 25°C over the temperature range used in the diffusion measurements. Obviously, the absolute values of diffusion coefficient given by Zwietering and co-workers are very dependent upon the methods used to estimate S, V, and V_e. It is not necessary to know S and V (because they do not change with temperature) to calculate an E for diffusion.

Joy (*107*) estimated diffusion coefficients for methane in an anthracite using an approach analogous to that of Zwietering and co-workers.

Pruss (*108*) measured the kinetics of argon sorption in a low-ash bituminous coal. To calculate the diffusion coefficient, he assumed that only the first term of the summation in (10) was important and that r_0 equalled the particle radius. This latter assumption probably accounts for the value of D being orders of magnitude greater than that found by Zwietering and co-workers and by Joy.

Bolt and Innes (*109*) studied the diffusion of carbon dioxide at 38°C from twelve 48 × 65 mesh coals ranging in rank from anthracite to subbituminous. They used an approach analogous to that of Pruss (*108*) to calculate diffusion coefficients. No trend of diffusion coefficient with rank was found. Values ranged from 3.5×10^{-8} cm²/sec for a coal of 77 per cent carbon to 9.2×10^{-8} cm²/sec for a coal of 79 per cent carbon.

Sevenster (*110*) studied the diffusion of water into three −60-mesh bituminous coals. He calculated diffusion coefficients using an approach analogous to that used by Zwietering and co-workers.

All these studies show that the coefficients of diffusion of gases in coals are small and that the diffusion is activated. At room temperature, the diffusion coefficients of the smaller gas molecules certainly have an upper limit of ca. 10^{-7} cm²/sec, with possibly the value being as small as 10^{-12} to 10^{-16} cm²/sec, depending upon the correct value for r_0.

B. Present Results

1. Experimental. *a. Apparatus.* At temperatures above ca. 300°C, difficulties are encountered in measuring rates of unsteady-state diffusion. The total volume of gas which can be loaded into the open-pore structure of a given sample is small, when thermal conditions are unfavorable to sorption. Further, the problem of temperature control frequently cannot be conveniently overcome by the use of a thermostatically controlled bath. For a system which includes a furnace operating at a high temperature, some other means of avoiding errors from temperature fluctuations must be sought. To overcome these difficulties, a differential experimental system was selected, as shown in Fig. 18. In principle, the procedure consisted of charging the sample under investigation up to some pressure in excess of atmospheric and then measuring the unsteady-state release of gas after sudden reduction of the pressure back to atmospheric.

With the exception of the volumeter, the main section of the apparatus

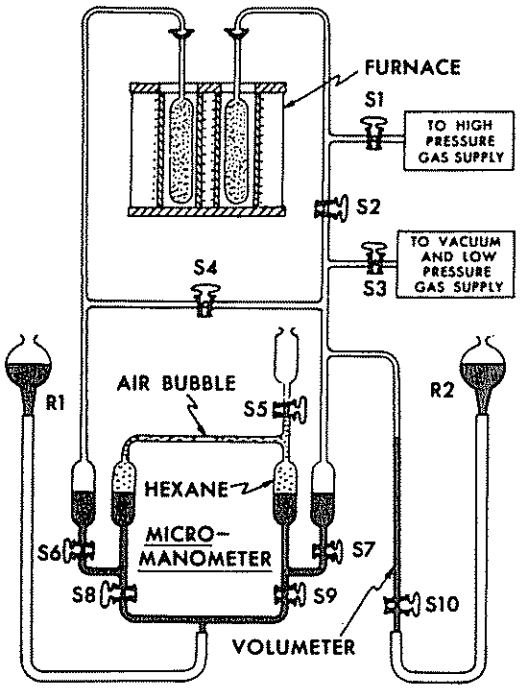

Fig. 18. Unsteady-state diffusion apparatus.

was constructed symmetrically. Two quartz sample tubes were used, each connected to the remainder of the apparatus by ball-and-socket joints. Both sample tubes contained an equal weight of the sample. The one shown at the left of Fig. 18 was used to impose a reference pressure (atmospheric) on the left side of the micromanometer, while the right-hand tube was subjected to a pressure of about 500 torr above atmospheric at the start of a run.

The micromanometer used was of the type described by Young and Taylor (*111*), the operation of which was based on the movement of a bubble of air trapped in a small-bore capillary tube connecting two U-tube reservoirs, containing a low-boiling intermediate fluid and mercury. Hexane was used as the intermediate fluid. The stop cock in contact with this liquid was lubricated with a paste made from glycerine and dextrin. The air bubble could be introduced by manipulating stopcocks and the mercury reservoir R_1.

Two volumeters (one of which is shown in Fig. 18) were calibrated with mercury. One volumeter, of 1.5-mm bore, was used for the major part of the investigation. It had a capacity of 2.2 cc and was calibrated to 0.01 cc. The other volumeter was of a 1-mm bore. It was calibrated to 0.005 cc, with a total capacity of 1.0 cc. The smaller volumeter was used for runs where the gas release was small. The apparatus could be connected to a vacuum assembly of a rotary oil pump and mercury diffusion pump through stopcock *S*3. The experimental gas at atmospheric pressure also could be introduced through *S*3. Diffusing gases were taken from cylinders which could be connected to the system through a two-stage regulator. Gas at higher pressure could be introduced to the sample tube on the right side through *S*1.

The micromanometer section of the apparatus was kept in a water bath at 28°C. The remainder of the apparatus, with the exception of the sample tubes (which were kept in the furnace) and the volumeter, was lagged with glass wool and aluminum foil to minimize temperature fluctuations caused by any air current in the room. With this arrangement small volumes of gases could be measured accurately.

The furnace held two identical silica tubes, $1\frac{1}{2}$ in. in diameter and 6 in. in length, into which the sample tubes were suspended vertically. Thermocouples were placed between the sample tube and the silica tube. The power input to the furnace was regulated by a Leeds-Northrup Series 60, D.T.A. control using a chromel-alumel thermocouple as the sensing element. With the power input to the furnace adjusted by a Variac, the furnace could be maintained at any desired temperature from

room temperature to 900°C. The output of a thermocouple, placed in the right-side furnace tube, was measured by a precision potentiometer to obtain the temperature of the furnace.

b. Procedure. Equal weights of sample were placed in the quartz sample holders. The weight of samples taken was ca. 25 g for the synthetic zeolites and high-temperature heat-treated coals and 5 to 10 g for the raw coals. The weight of sample to be used was dictated by the amount of gas that would be released within 100 sec of the start of the run. If the gas release was found to be more than 1.5 cc or less than 0.1 cc in 100 sec, then less or more sample, respectively, was taken. After filling the sample tubes, a plug of glass wool was placed at the neck of the sample tube to prevent any powder from coming into the other parts of the apparatus during evacuation or sudden release of pressure. The sample tube was then sealed into the apparatus with vacuum wax.

With the sample in place and stopcocks *S*1, *S*6, and *S*7 closed and *S*4 and *S*2 open, *S*3 was opened to the vacuum system. After 10 min the power to the furnace was switched on and the sample was heated at the rate of 2°C/min to the required degassing temperature, depending on the nature of the sample. For anthracites and heat-treated anthracites a degassing temperature of 450°C was selected. An important criterion in selecting a degassing temperature was that it should be higher than the highest temperature-of-diffusion measurement; otherwise gases or vapors that did not escape during the degassing could come out during diffusion measurements at higher temperature. This requirement fixed the lower limit of degassing temperatures. The upper limit was fixed by the stability of the sample under consideration. From previous studies it was shown that anthracites do not undergo any appreciable change at 450°C. For the type A zeolites, a degassing temperature of 400°C was used for all runs except with carbon dioxide, in which case a temperature of 600°C was selected. It was reported that the type A zeolites were stable up to 600°C, when heated in the absence of water vapor (*46*). For bituminous coals, degassing temperatures in the range 130 to 200°C were used depending on the coal rank. The degassing time for type A zeolites, anthracites, and heat-treated anthracites was 24 hr; for the remainder of the coals, a degassing time of 12 hr was used.

After degassing, the sample was allowed to cool to the lowest temperature at which diffusion measurements were possible, still under vacuum. At this time *S*3 was closed and *S*1 opened to the diffusing gas until the pressure in the apparatus was atmospheric, after which *S*2 was closed and *S*3 opened to atmospheric pressure. The right-side sample tube was

then brought to a pressure of about 500 torr above atmospheric through $S1$, while the rest of the apparatus continued to be exposed to the diffusing gas at atmospheric pressure. Attempts were made to maintain the same charging pressure in a series of runs at different temperatures with the same sample. Only in cases where the effects of pressure on diffusion were measured were the charging pressures varied at a particular temperature. After exposing the sample to the diffusing gas, 24 hr was allowed for equilibration for anthracites, heat-treated anthracites, and the synthetic zeolite. For other samples, 12-hr equilibration time was allowed. These times were found to give reproducible values.

Before the start of the run, the micromanometer was adjusted by manipulating different stopcocks and mercury reservoir R_1 to place the air bubble in a convenient position inside the capillary tube. The cross-wire of a cathetometer was focused on one end of the air bubble, and stopcocks $S6$ and $S7$ were then closed. The mercury level in the volumeter was then brought to a zero reading by opening $S10$ and adjusting the reservoir R_2. At the start of the run $S1$ was closed, $S2$ opened very quickly, and the elapse of time recorded immediately. The excess gas in the free space escaped very rapidly through $S3$, and the pressure in both sample tubes became equal. The system was then isolated by closing $S3$. Stopcocks $S6$ and $S7$ were now opened and $S4$ closed. The air bubble would begin to move, because of the evolution of gas from the right-side sample tube. The bubble was displaced by lowering the reservoir R_2. The time and volume readings were noted at which the bubble regained its equilibrium position, as determined by the cross-wire of the cathetometer. The process of lowering R_2 and allowing the bubble to regain its position was repeated throughout the run.

After a run at the lowest practical temperature was completed in the manner described, the temperature of the furnace was increased by 10 to 50°C (depending on the type of the sample) in the presence of the diffusing gas. After the attainment of temperature, $S2$ was closed, $S1$ opened, the right sample tube charged with diffusing gas at higher pressure, and the system allowed to come to equilibrium. Again the sequence of operations described in the previous paragraph was repeated. In this way a series of runs at different temperatures was made. The procedure when the effect of pressure on diffusion was studied was similar, only in this case the charging pressure was the variable from run to run. When the same solid was used to measure the diffusion of different gases, the sample was degassed after the runs with a particular gas were completed.

c. Method of Computation. The method of computation was described in Section III. The diffusion parameter $D^{1/2}/r_0$ was calculated using the experimental data obtained, as described above, and the total solution to (10). To the authors' knowledge, this is the first time that the complete unsteady-state-diffusion equation has been used to obtain the diffusion parameter for sorption in a molecular-sieve material.

2. Diffusion Results on Type A Zeolites. Earlier diffusion results obtained by Nelson and Walker on type A zeolites (*94*), using this apparatus and computational procedures, have just been described. They performed measurements on the propane-4A zeolite system. In

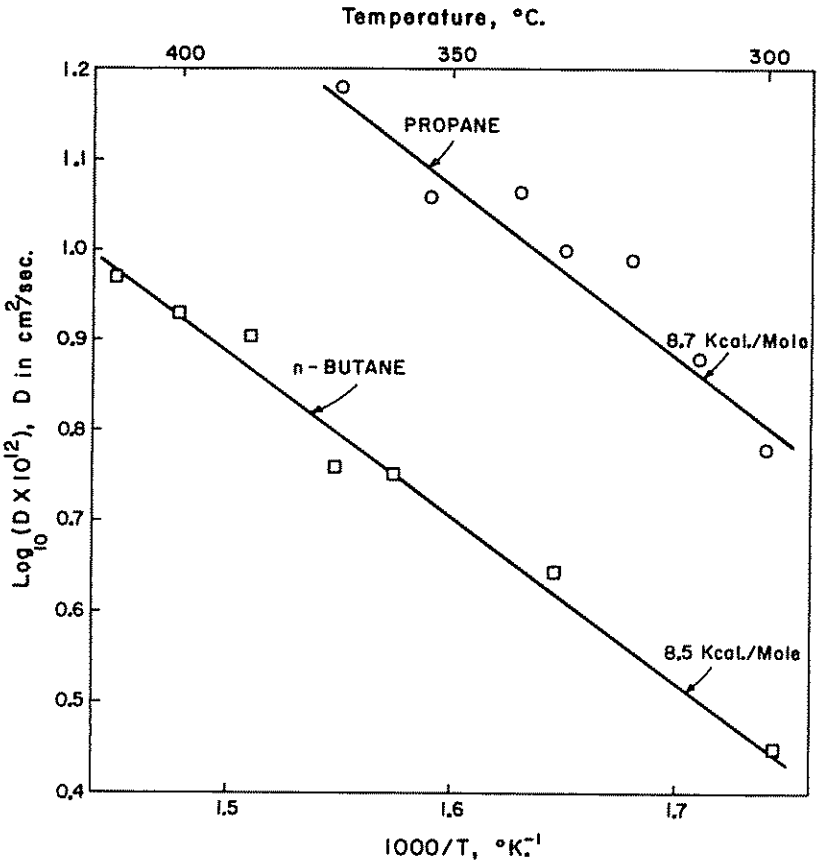

Fig. 19. Arrhenius plots of diffusion coefficients for propane and *n*-butane in type 4A zeolite.

Fig. 19, these results are compared with results on the n-butane–4A zeolite system. To convert the diffusion parameter $D^{1/2}/r_0$ to D, a value of 2.0×10^{-4} cm is taken for r_0. That is, as discussed earlier, the type A zeolite particles are single crystals about 1 to 5 μ in diameter. The diffusion coefficients are: $D_{\text{propane}} = 12.4 \times 10^{-9} \exp(-8.7/RT)$ and $D_{n\text{-butane}} = 4.2 \times 10^{-9} \exp(-8.5/RT)$. It is noted that the values of E are essentially equal; this fact will be considered in Section V.

TABLE VI

DIFFUSION COEFFICIENTS FOR GASES IN 3A ZEOLITES

Gas	Kinetic diameter, A (*47*)	D_0, cm²/sec	E, kcal/mole
Neon	2.79	4.5×10^{-8}	7.0
Argon	3.42	3.7×10^{-8}	12.6
Krypton	3.61	60.3×10^{-8}	16.4
Xenon	4.06	124×10^{-8}	19.2
Hydrogen	2.92	4.5×10^{-6}	9.9
Carbon dioxide	3.99	4.0×10^{-11}	4.3
Nitrogen (*94*)	3.68	1.0×10^{-5}	16.2

Diffusion of a number of gases was studied in the 3A zeolite. On the basis of the previous finding of Nelson (*105*) that the diffusion parameter for propane in 5A zeolite was independent of loading pressure, this variable was generally not investigated in this study, since values of $V_e - V_0$ were much less, for comparable temperatures and loading pressures, than were found for propane. The one exception was carbon dioxide, which will be discussed. Figure 20 presents Arrhenius plots for the diffusion coefficients. Table VI summarizes the diffusion data. Diffusion measurements were also made for helium. However, the rate was so rapid that measurements were of poor accuracy for runs above 47°C. In the narrow temperature range 34 to 47°C, the diffusion did not appear to be activated. As expected, the E for the diffusion of the rare gases increases progressively with increase in kinetic diameter. These results will be considered in detail in Section V.

Diffusion of carbon monoxide and oxygen from the 3A zeolite was also studied. These results were markedly different than those found for the gases reported in Table VI. Over the temperature range 200 to 432°C, the diffusion of oxygen showed no temperature dependency, having a D of $1.96 \pm 0.16 \times 10^{-12}$ cm²/sec for measurements at six temperatures. Over the temperature range 178 to 432°C, the diffusion

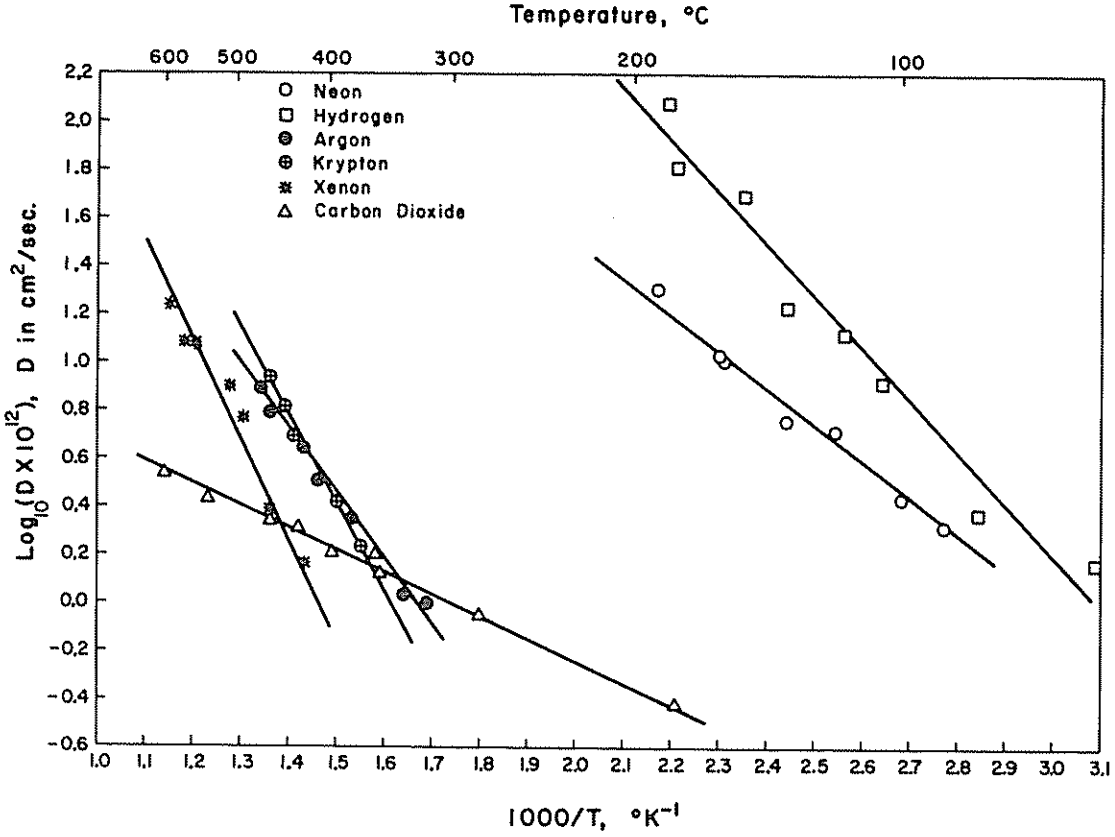

Fig. 20. Arrhenius plots of diffusion coefficients for gases in type 3A zeolite.

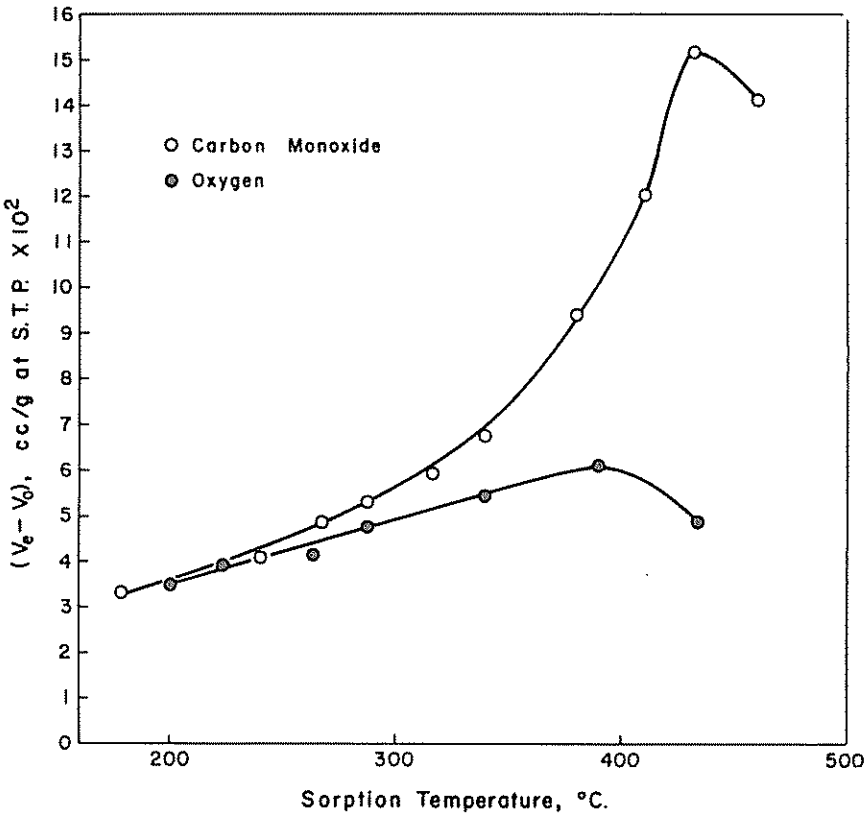

Fig. 21. Change in V_e–V_0 with temperature for a loading pressure of 1190 torr for carbon monoxide and oxygen sorption on type 3A zeolite.

of carbon monoxide also showed no temperature dependency, having a D of $2.03 \pm 0.20 \times 10^{-12}$ cm²/sec for measurements at 10 temperatures. Of interest was the fact that $V_e - V_0$ values for both gases increased with increasing temperature at a constant loading pressure of 1190 torr, over the above temperature ranges. These results are plotted in Fig. 21. It is seen that $V_e - V_0$ for both gases decreases as the temperature is increased above 432°C. The maximum in the $V_e - V_0$ versus temperature plots is characteristic of chemisorption isobars (*111a–113*), strongly suggesting that we are no longer dealing primarily with physical sorption for these two systems for studies much above room temperatures. For the runs at temperatures below 432°C, it is concluded that chemical

sorption equilibrium was not attained, prior to commencing diffusion measurements.

3. Diffusion Results on Coals. Diffusion of gases from 200 × 325 mesh samples of coals varying in rank from anthracite to high volatile bituminous has been studied. Analyses of the coals are listed in Table VII. Results will be given for the diffusion parameter $D^{1/2}/r_0$. Values of D will not be given, since r_0 values for the coals are not known.

a. Effect of Loading Pressure on Diffusion Parameter. Selected runs were made to study the effect of loading pressure on $D^{1/2}/r_0$. Argon diffusion from Upper Kittanning coal at 40°C was studied at six loading pressures between 880 and 1220 torr. The diffusion parameter for these runs was 0.03032 ± 0.00008 $sec^{-1/2}$, the spread of values being well within experimental error. Nitrogen diffusion from Loree anthracite at 27°C was studied at five loading pressures between 860 and 1200 torr. Again no significant effect of loading pressure on the diffusion parameter was found. For both gases, plots of $V_e - V_0$ versus loading pressure

TABLE VII

ANALYSES OF COALS

Coal	State	Composition on as-received basis, wt. %					Volatile matter, % (d.a.f.)	Carbon, % (d.a.f.)
		H_2O	Ash	C	H	S		
St. Nicholas	Pa.	1.6	9.1	84.2	2.37	0.51	4.5	94.0
Loree	Pa.	4.0	7.1	82.7	2.80	0.80	5.4	93.0
Dorrance	Pa.	0.7	9.9	82.9	2.54	0.73	5.8	92.5
Trevorton	Pa.	0.5	9.7	—	—	1.05	9.0	91.0
Upper Kittanning	Pa.	0.5	9.5	80.4	4.22	1.46	18.0	89.1
Kelley	Pa.	0.7	4.7	82.9	5.70	—	27.2	87.8
Pratt	Ala.	0.8	7.9	78.8	4.75	1.60	29.2	86.0
Upper Freeport	Pa.	0.4	7.9	79.8	5.03	1.59	33.0	87.0
Pittsburgh	Pa.	1.4	6.6	76.2	5.41	2.22	39.5	82.9
Pittsburgh 8	Ohio	1.5	16.4	65.5	4.87	4.51	42.4	79.5
No. 6	Ill.	1.9	7.6	66.1	5.50	2.75	45.4	73.0

were linear. Carbon dioxide diffusion from Loree anthracite and Kelley coal was studied as a function of loading pressure. For the Loree anthracite, $D^{1/2}/r_0$ decreased progressively from 0.0146 to 0.0122 $sec^{-1/2}$ at 27°C, as the loading pressure was varied from 850 to 1220 torr. For the Kelley coal, $D^{1/2}/r_0$ decreased progressively from 0.0197 to 0.0185 $sec^{-1/2}$ at 42°C, as the loading pressure was increased from 790 to 1240 torr; and

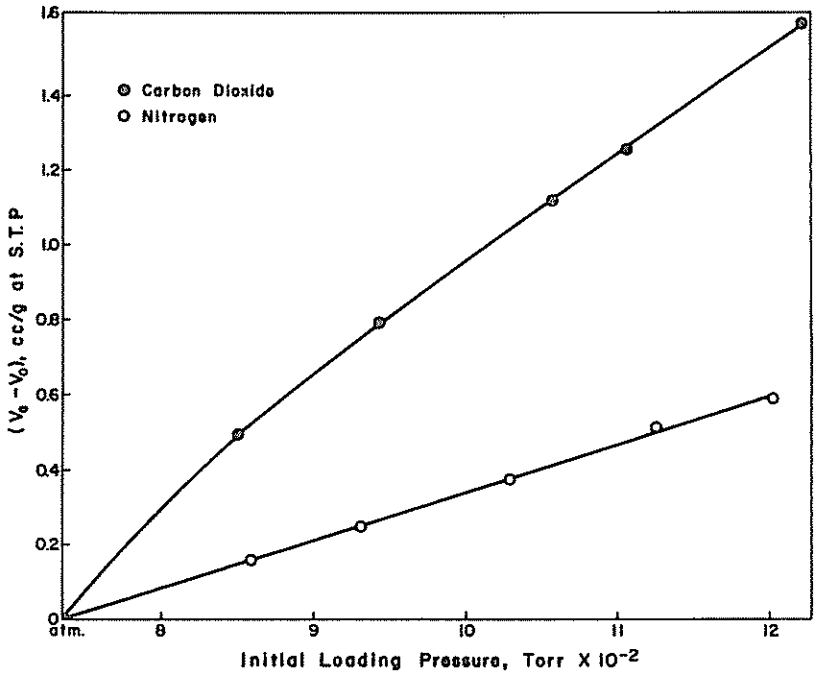

Fig. 22. Portions of isotherms for carbon dioxide and nitrogen sorption on Loree anthracite. V_e–V_0 values calculated from unsteady-state diffusion results.

from 0.0299 to 0.0293 at 78°C, as the loading pressure was increased from 830 to 1250 torr. At 116°C, an increase in loading pressure from 83 to 1230 torr produced no significant change in $D^{1/2}/r_0$. As expected, at comparable loading conditions, sorption of carbon dioxide was much greater than either argon or nitrogen. Figure 22 presents sorption results for carbon dioxide and nitrogen on Loree anthracite at 27°C. The carbon dioxide isotherm does not obey Henry's law in this pressure range.

b. Diffusion of Nitrogen and Carbon Dioxide from Coals. As discussed in Section II, the surface area of a coal calculated from a nitrogen sorption isotherm at 77°K represents only a small fraction of its total surface area. This has been attributed to limitations imposed by activated diffusion. On the other hand, the surface areas calculated from carbon dioxide isotherms at 195 and 298°K are large and are thought to represent more closely the total surface area of coal. To confirm the role of activated diffusion, diffusion parameters were measured for nitrogen and carbon dioxide in four coals with carbon content varying from 82.9

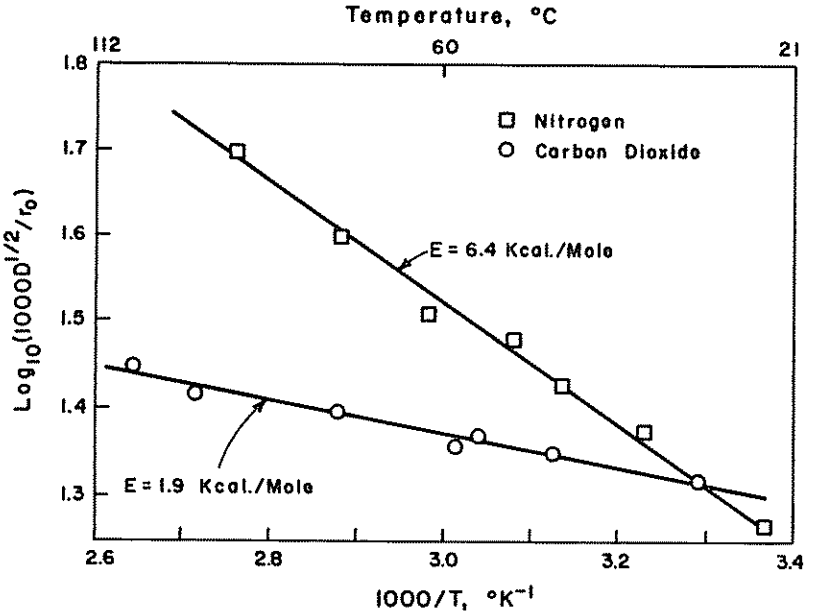

Fig. 23. Arrhenius plots of diffusion coefficients for nitrogen and carbon dioxide in Pratt bituminous coal.

(Pittsburgh) to 94.0 per cent (St. Nicholas) (*74*). For each coal the activation energy for diffusion of nitrogen was higher than for carbon dioxide. For each coal the diffusion parameter for nitrogen was greater than that for carbon dioxide above ca. 30°C. Figure 23 shows the Arrhenius plots for Pratt coal. The diffusion parameters equal 4.2 exp $(-3.2/RT)$ and 0.098 exp $(-0.95/RT)$ $sec^{-1/2}$ for nitrogen and carbon dioxide, respectively.

Values of $D^{1/2}/r_0$ under typical sorption conditions for Pratt coal are listed in Table VIII. To a first approximation, these results can be used in conjunction with the general solution of the unsteady-state-diffusion equation (Fig. 13) to calculate the fraction of the micropore volume of Pratt coal filled for particular diffusion times. With 30 min as a convenient diffusion time, values of the parameter $D^{1/2}t^{1/2}/r_0$ and $(V_t - V_0)/(V_e - V_0)$ are listed in Table VIII. It is seen that essentially all the micropore volume should be reached by CO_2 at 195 and 298°K in 30 min. On the other hand, a negligible fraction of the micropore volume is reached by nitrogen at 77°K in 30 min. Any reasonable increase in diffusion time of nitrogen at 77°K will produce an insignificant increase in

TABLE VIII
PORE VOLUME ACCESSIBLE TO PRATT COAL UNDER PARTICULAR DIFFUSION CONDITIONS

Parameter	N_2 at 77°K	CO_2 at 195°K	CO_2 at 298°K
$D^{1/2}/r_0$, $sec^{-1/2}$	2.9×10^{-9}	8.1×10^{-3}	2.0×10^{-2}
$D^{1/2}t^{1/2}/r_0$	1.2×10^{-7}	0.35	0.85
$(V_t - V_0)/(V_e - V_0)$	Nil	0.83	~1.0

volume filled. Thus from these diffusion results it is clear why nitrogen surface areas for coals, calculated from adsorption data at 77°K, are very low.

c. Diffusion of Argon from Coals. Diffusion of argon from coals listed in Table VII was studied over the temperature range from ca. 25 to 100°C. The diffusion, in each case, was found to be activated. Typical plots are shown in Fig. 24. In Fig. 25, E values for argon diffusion are

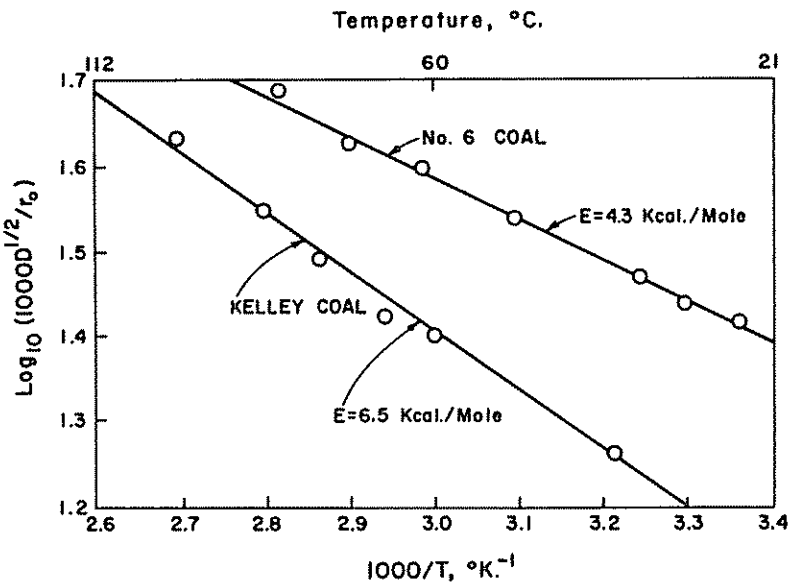

Fig. 24. Arrhenius plots of diffusion coefficients for argon in Kelley and No. 6 bituminous coals.

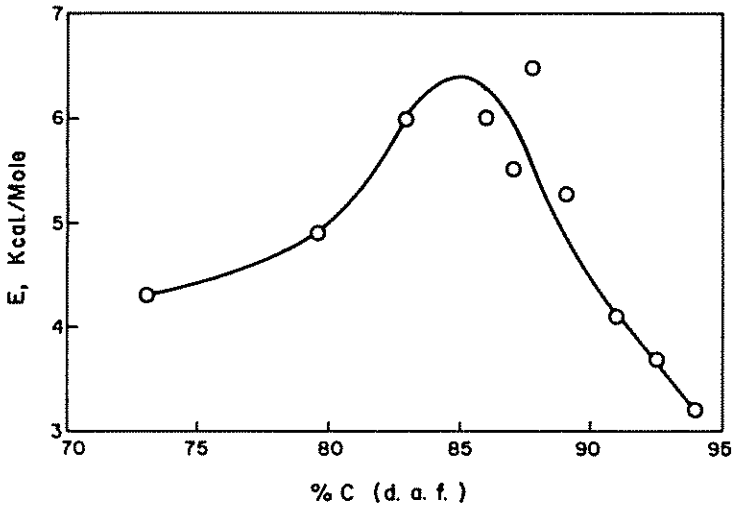

Fig. 25. Relation between activation energy for diffusion of argon in coals and their carbon content.

plotted against carbon content of the coals. A volcano-shaped curve is obtained with its peak at ca. 86 per cent carbon (d.a.f.). Curves of helium density (*52*), heat of wetting (*70*), and butane (*114*) sorption versus coal rank show minima at ca. 85 to 90 per cent carbon content. These results are consistent with the correlation between E for diffusion and coal rank found here. A maximum in E between 85 and 90 per cent carbon indicates that the average size of the micropores goes through a minimum at this point. This would result in the internal microporosity in coals of this carbon content being most inaccessible to displacement and sorbing fluids.

d. Diffusion of Gases from Heat-Treated Anthracites. In Section II the sintering of micropores in Saran and polyvinylidene chloride carbons at elevated temperatures was shown to exist from molecular-probe studies. Sintering can also be observed by the increase in E for diffusion of a molecule through a carbon, which has seen increasing heat treatment temperatures. Figure 26 presents Arrhenius plots for the diffusion of argon from Dorrance anthracite heated between 600 and 900°C. Samples were heated to maximum temperature at 5°C/min and soaked for 2 hr. A progressive increase in E for diffusion with increase in heat treatment temperature is clearly seen. Sufficient sintering occurs that the BET surface areas, measured by carbon dioxide sorption at −78°C, falls

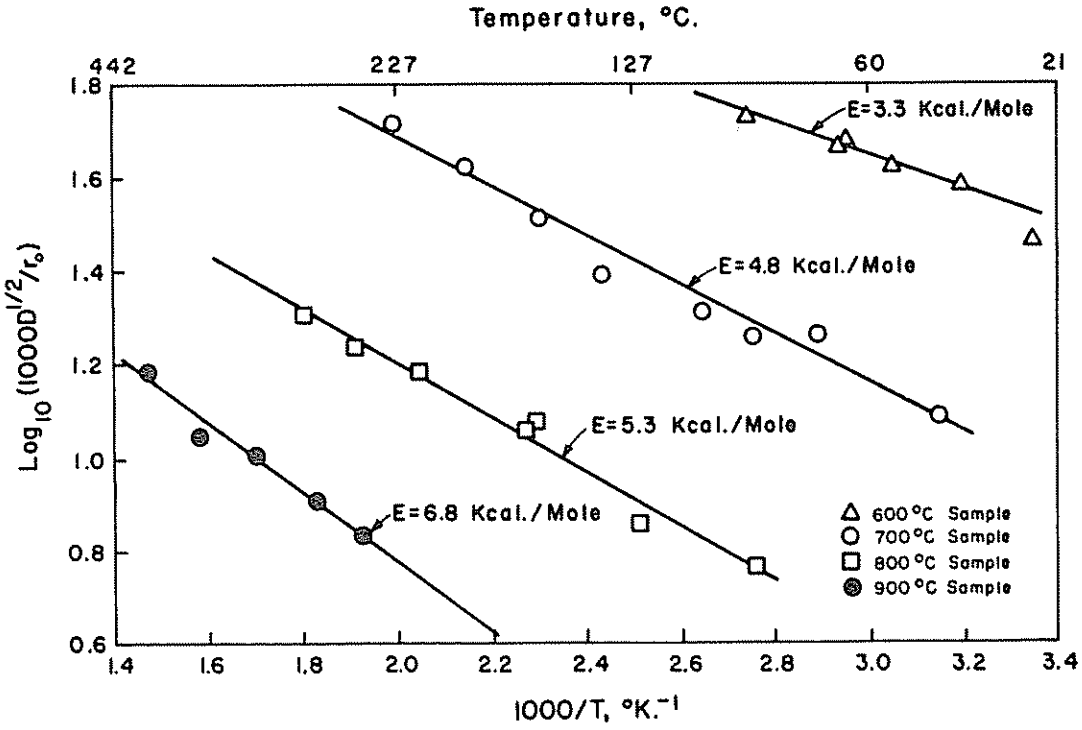

Fig. 26. Arrhenius plots of diffusion coefficients for argon in heat-treated Dorrance anthracite.

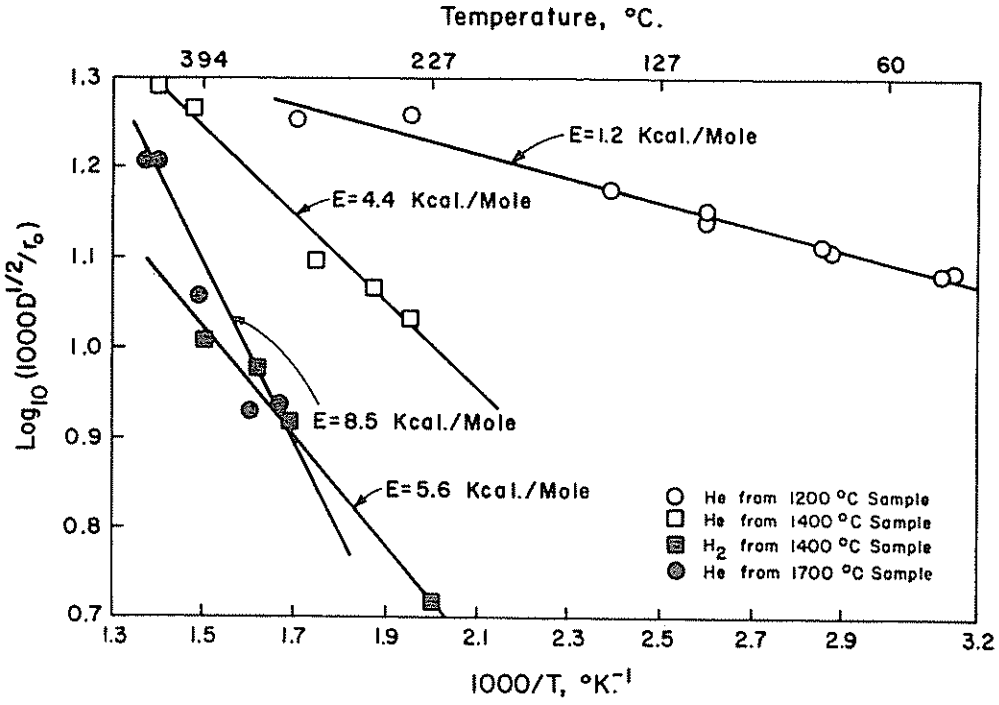

Fig. 27. Arrhenius plots of diffusion coefficients for helium and hydrogen in heat-treated St. Nicholas anthracite.

from 250 m^2/g for the 600°C heat-treated sample to 26 m^2/g for the sample heat-treated to 900°C.

Sintering occurs to such an extent at temperatures above about 1000°C that only the smallest species diffuse in anthracite at a measurable rate. Figure 27 presents Arrhenius plots for the diffusion of helium and hydrogen from St. Nicholas anthracite heated between 1200 and 1700°C. Note the sharp increase in E for helium diffusion with increasing heat treatment temperatures. Since helium has a kinetic diameter of 2.58 A (*47*), it is expected that activated diffusion would not commence until the pores closely approach this size. For example, it is recalled that helium did not show activated diffusion in the 3A zeolite.

Because of the large activation energies found for diffusion of gases from anthracites heated above 1200°C, it might be thought that they would be useful for the encapsulation of gases. However, their micropore volumes decrease sharply following heat treatment above 1200°C. For example, $V_e - V_0$ falls to less than 0.02 cc of helium (at STP)/g for initial loading pressures of ca. 1200 torr at ca. 200°C.

V. THEORETICAL CALCULATIONS OF ACTIVATED DIFFUSION IN TYPE A ZEOLITES

A. Activation Energies of Diffusion

1. Introduction. To estimate, theoretically, activation energies for diffusion in molecular-sieve materials, it is first necessary to calculate the potential energy of interaction between the different species and the crystal at all locations in the crystal. In the case of the type A zeolites, it is necessary to calculate the interaction between the diffusing species and the atoms in the surface of the cavity and also the interaction between the diffusion species and the atoms in the aperture connecting the cavities. As we shall see, once we have these potential-energy diagrams, an estimation of activation energies for diffusion through the zeolites can be made.

As discussed by Barrer and Stuart (*34*), the interaction ϕ between a diffusing species and a crystal is made up of four terms:

$$\phi = \phi_D + \phi_R + \phi_P + \phi_Q \tag{50}$$

where the terms represent the dispersion, repulsion, polarization, and quadrupole interactions, respectively. The diffusing species, which we shall be considering, have no quadrupole moment; hence, ϕ_Q will be

zero. Further, the polarization interaction for our systems will be small compared to the dispersion interaction (*9,37*); as an approximation it will be neglected. As is customary, the potential energy of interaction at distance r between the centers of an interacting pair may now be considered the sum of a Lennard-Jones (6–12) potential for the dispersive and repulsive energies

$$\phi(r) = (-A/r^6) + (B/r^{12}) \tag{51}$$

where A and B are constants. A is calculated from

$$A = \tfrac{3}{2}\alpha_1\alpha_2[E_1E_2/(E_1 + E_2)] \tag{52}$$

where the α's are polarizabilities and the E's are characteristic energies (ionization potentials were used) of the interacting species (*115*). B equals $Ar_0^6/2$, where r_0 is the equilibrium separation of the interacting species, or the distance corresponding to the maximum net energy of attraction.*

Potential-energy calculations have been made for the rare gases, propane, and *n*-butane in the type A zeolites. Table IX summarizes values for the parameters used to calculate the interaction energy according to (51). For estimating equilibrium distances r_0, the hard-sphere approximation was used, giving

$$r_0 = \tfrac{1}{2}(r_1 + r_0') \tag{53}$$

where r_1 is the van der Waals diameter of the oxygen or potassium ion in the zeolite framework and r_0' is the equilibrium distance between the centers of two diffusing molecules. Values of r_1, taken for oxygen and potassium, are 2.80 and 2.66 A, respectively. Values of r_0' were estimated from the Lennard-Jones (6–12) potential expression, $r_0' = 2^{1/6}\sigma$, where σ

* Unfortunately, theoretical calculations of interaction energies between a diffusing species and a crystal based on the above approach are not in a very satisfactory state of affairs at the moment, because of uncertainty as to what equation to use to calculate the constant A and what values to take for polarization of the atoms composing the solid lattice. We have taken the London expression (*116*) to calculate A in favor of the Kirkwood-Muller (*117*) or Slater-Kirkwood expressions (*118*). Barrer and Ruzicka (*115*) have shown that the London A constants for the inert gases increase less with increasing atomic weight than the A constants calculated from the other two expressions. Thus the spread of activation energies for diffusion of the inert gases calculated from the London expression will be less than the spread calculated from the other two expressions. It will be seen later that the London expression predicts a spread of activation energies more in line with experimental results for the type A zeolite than do the other two expressions. This is the main justification we give for its use.

TABLE IX

VALUES OF PARAMETERS USED TO CALCULATE INTERACTION POTENTIAL ENERGIES IN THE TYPE A ZEOLITES

Species	$\alpha \times 10^{25}$, cc/molecule	Ionization energy, eV	r_0, A		$A \times 10^{44}$, cal cm^6/mole	
			Gas-O^{2-}	Gas-K^+	Gas-O^{2-}	Gas-K^+
He	2.16[47]	24.5[119]	2.85	2.70	25.4	8.64
Ne	3.95[47]	21.6[119]	2.93	2.93	44.3	14.7
Ar	16.4[47]	15.8[119]	3.31	3.25	160	50.0
Kr	24.8[47]	14.0[119]	3.43	3.36	230	69.9
Xe	40.3[47]	12.1[119]	3.68	3.61	347	103
O^{2-}	39.0[34]	13.6[35]	—	—	—	—
K^+	8.4[34]	31.6[35]	—	—	—	—
Propane	62.9[47]	11.2[120]	4.24	—	539	—
n-Butane	84[47]	10.8[120]	4.20	—	714	—

is the kinetic diameter, which we have referred to previously. Values of σ were taken from Hirschfelder *et al.* (*47*).

2. Rare-Gas Diffusion in Type A Zeolites. *a. Potential Energies in Zeolite Cavity.* Potential-energy diagrams for rare gases diffusing radially from the center of a cavity toward the solid cavity surface can be considered. The potentials $\phi_D + \phi_R$ for the interaction of a gas with the surface of the spherical cavity in the type A zeolite may in principle be estimated by summing all the interactions between the gas and the lattice oxygen ions. The aluminum and silicon ions will also make a small contribution to the over-all interaction energy, but this will be neglected as a first approximation. The summation is a tedious process and may be approximated by an integration. The cavities in the type A zeolites have a free diameter of 11.4 A (*37*); and, consequently, the center-to-center distance between two diametrically opposite oxygen atoms is 14.2 A (diameter of oxygen atom in the zeolite structure is taken as 2.8 A). There are 72 oxygen atoms on the surface of the cavity; for the calculation it has been assumed that the oxygens are uniformly distributed over the surface. The integration, given in the Appendix, produces the following energy expression:

$$\phi(a) = \frac{N}{2}\left\{-\frac{A}{R^6}\frac{1}{4a}\left[\frac{1}{(1-a)^4} - \frac{1}{(1+a)^4}\right] + \frac{B}{R^{12}}\frac{1}{10a}\left[\frac{1}{(1-a)^{10}} - \frac{1}{(1+a)^{10}}\right]\right\} \quad (54)$$

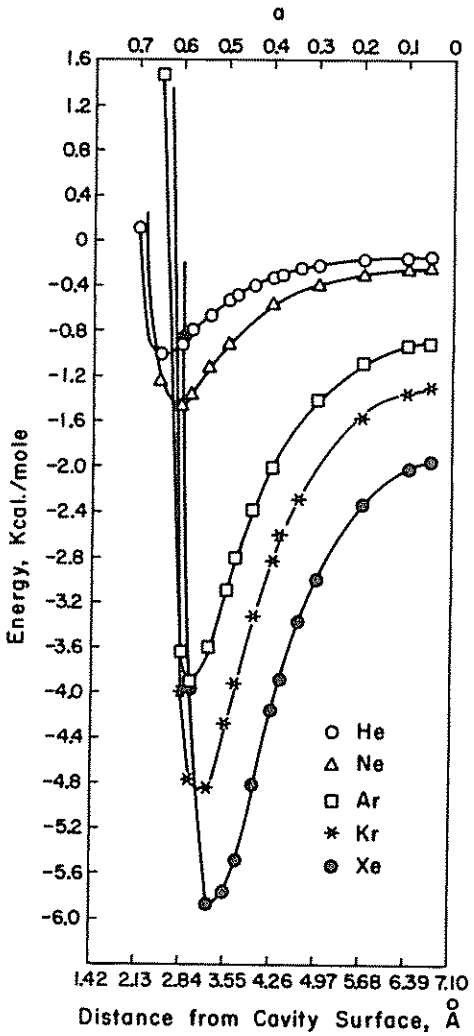

Fig. 28. Potential-energy plots for the rare gases interacting with the surface of a cavity in a type A zeolite.

where $R = 7.1$ A, $N = 72$ oxygen atoms, and $a =$ the fractional distance between the center of a cavity and the center of an oxygen atom in the cavity surface (which also would be the fractional distance between the center of the cavity and the plane running through the eight oxygen atoms forming apertures into and from the cavities).

Figure 28 presents potential-energy plots for the rare gases in the cavity of a type A zeolite, as calculated from (54). The minima in these plots should correspond closely to the heats of sorption of the rare gases on the type A zeolites at very low coverages. Surprisingly, the authors have found no experimental heats of sorption data of rare gases on the type A zeolites. As the rare gases approach the cavity surface more closely than their equilibrium position, their potential energy increases very sharply, with the repulsive interaction dominating, as expected. Of course, as we shall see shortly, when the diffusing species approaches the perimeter of a cavity at a point where an aperture is located, the

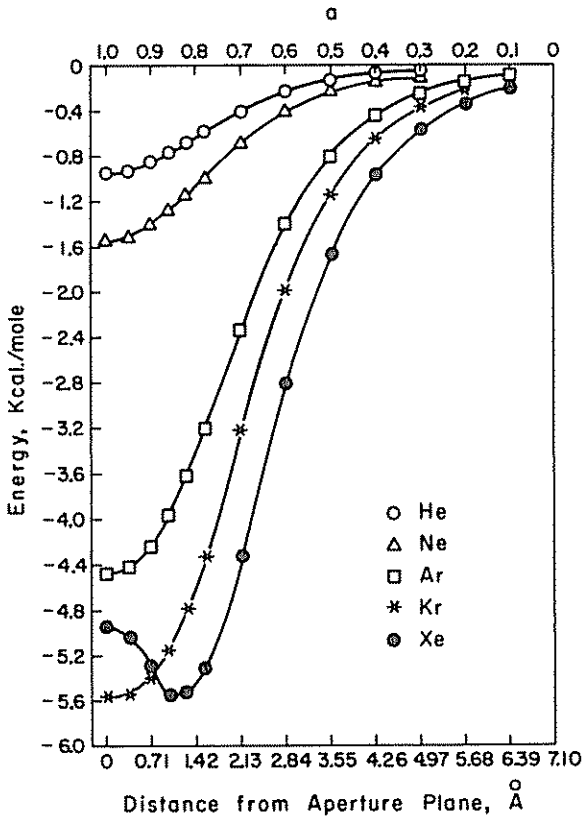

Fig. 29. Potential-energy plots for the rare gases interacting with an aperture, formed by eight oxygens, in type 5A zeolite, as the gases approach at right angles to the plane of the aperture along its centerline.

potential-energy patterns (close to the perimeter) will be much different than those shown in Fig. 28.

b. Potential Energies for Approach to Aperture Plane in 5A Zeolite. Potential-energy diagrams for rare gases diffusing radially from the center of a cavity to the center of an aperture plane in the 5A zeolite can be considered. This calculation will be divided into two parts. First, energies will be calculated for the interaction of the rare gases with the oxygens forming the aperture ring. Second, energies will be calculated for the interaction of the rare gases with the cavity, with the oxygens forming the aperture removed. These two sets of energy diagrams will then be added together to give the potential energy for the gases diffusing radially from the center of the cavity to the center of the aperture plane.

The interaction energy of the rare gases with the aperture in the type A zeolites, for a path of travel at right angles to the plane of the aperture and along its center line, has been calculated by the method of summation. As discussed in Section II, the aperture of interest is formed by a circular ring of eight oxygens and has a free diameter of 4.2 A. The centers of two diametrically opposite oxygen atoms in the ring would be 4.2 + 2.8, or 7.0 A, apart. Figure 29 presents the potential-energy plots. In fact, they represent the situation for only the 5A zeolite, which has two of its apertures per cavity unblocked by exchangeable cations. For each gas there is a net attractive interaction in the center of the aperture plane.

The interaction of a gas with the cavity surface when the gas approaches the center of an aperture plane was approximated by integration. With the eight oxygens which form the aperture removed, 64 oxygen atoms are left on the surface of the cavity. These oxygens were assumed to be distributed uniformly over the remainder of the surface. The integration, given in the Appendix, produces the following energy expression:

$$\phi(a) = \frac{N'}{2}\left\{-\frac{A}{R^6}\frac{1}{4a}\left[\frac{1}{(1+a^2-1.23a)^2}-\frac{1}{(1+a)^4}\right] + \frac{B}{R^{12}}\frac{1}{10a}\left[\frac{1}{(1+a^2-1.23a)^5}-\frac{1}{(1+a)^{10}}\right]\right\} \quad (55)$$

where $R = 7.1$ A, and $N' = 64$. Figure 30 presents the potential-energy plots, calculated from (55).

The potential energies shown in Figs. 29 and 30 are now added together to give the total interaction energies, which are shown in Fig. 31.

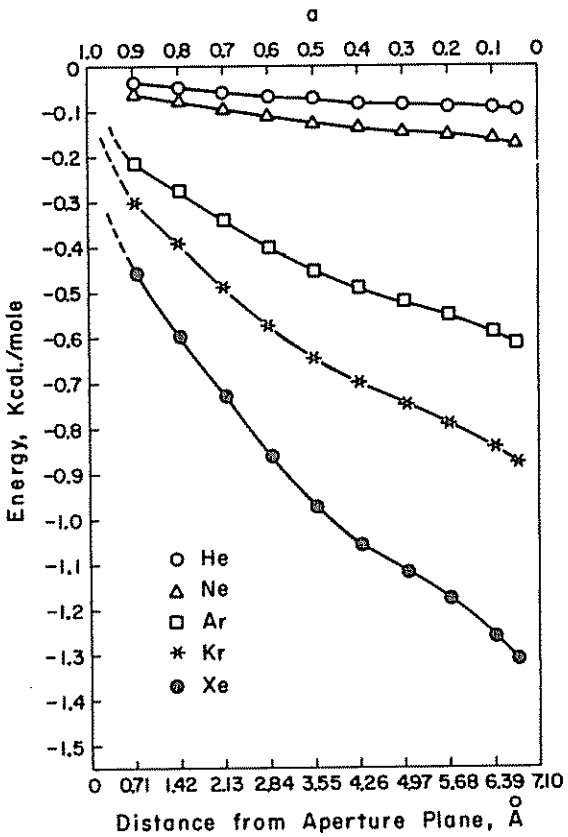

Fig. 30. Potential-energy plots for the rare gases interacting with the surface of a cavity, as the gases approach at right angles to the plane of the aperture along its centerline. The eight oxygens forming the aperture are removed for this calculation (see Fig. B1).

c. Activation Energies in 5A Zeolite. By superposition of Figs. 28 and 31 (as shown in Fig. 32 for xenon), we are able to suggest a possible route that the rare gases may take as they travel through the zeolite structure. Molecules, upon leaving an aperture, can travel radially toward the center of the cavity until they reach the potential-energy profile given by the interaction of molecules with the cavity surface (point *S*, Fig. 32). The molecules can then fall into the potential-energy minimum given by such interaction (point *B*, Fig. 32) and stay in this minimum as they travel parallel to the cavity surface. Eventually, they

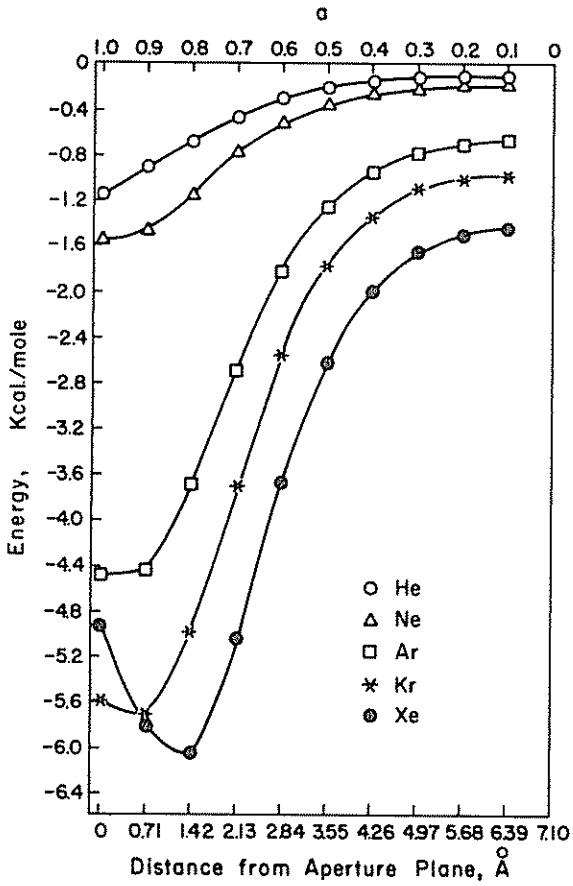

Fig. 31. Potential-energy plots for the rare gases interacting with an aperture and the surface of a cavity in type 5A zeolite, as the gases approach at right angles to the plane of the aperture along its centerline. The potential energies in this figure are the sum of those in Figs. 29 and 30.

reach the potential-energy profile of the other unblocked aperture in the wall of the 5A cavity through which they can leave the cavity and enter an adjacent cavity. The maximum energy required to travel this route can be estimated from Fig. 32. For xenon, this energy equals $|-6.0| - |-3.5|$, or ca. 2.5 kcal/mole. Experimentally, we have found that diffusion of the rare gases through the 5A zeolite is nonactivated.

If, instead of the molecule traveling in a strictly radial direction as it

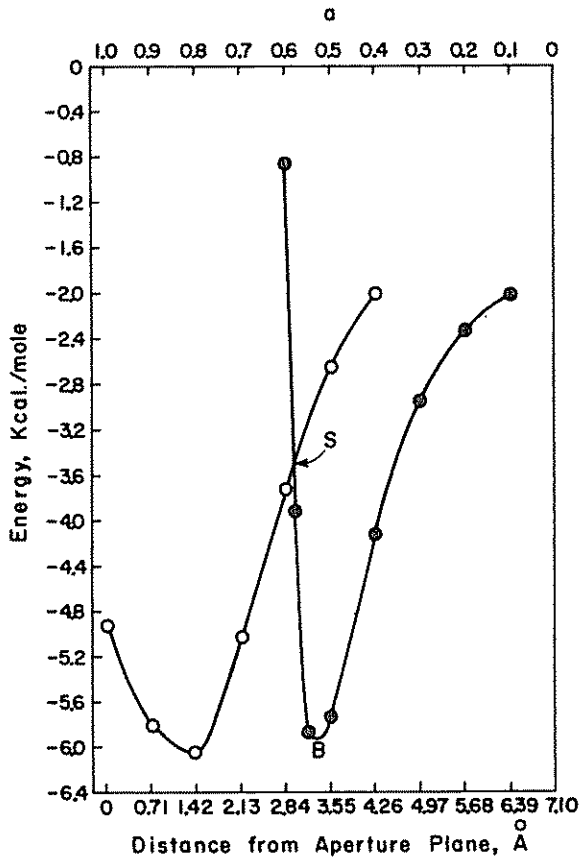

Fig. 32. Potential-energy plots of xenon in type 5A zeolite taken from Figs. 28 and 31. By superposition of these plots, a possible path of travel of xenon in the cavity is suggested.

leaves the aperture, it was to bend gradually along the wall of the cavity, its potential energy would not rise as sharply as shown in Fig. 31. As a consequence, the potential energy at the saddle point (S) would have a higher negative value than that shown in Fig. 32, which would decrease the energy requirement for diffusion through the 5A-zeolite structure and bring the value more in line with the negligible E found experimentally.

d. Likely Position of Rare Gases in the 5A-Zeolite Cavity. On the basis of the potential-energy diagram shown in Fig. 31, a molecule would not

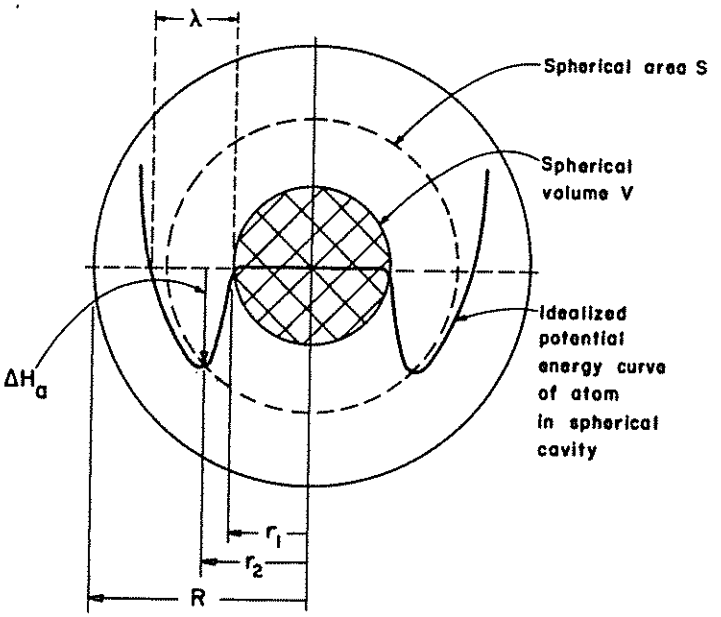

Fig. 33. Idealized potential-energy curve of an atom in the spherical cavity of a type A zeolite.

normally be expected to leave an aperture and pass directly across the center of a cavity to another aperture. This is particularly true in the case of diffusion of the rare gases in the 5A zeolites, where diffusion is relatively rapid and, consequently, measurements are made at close to room temperature. The situation for diffusion in the 3A zeolite may be different, because measurements need to be made at much higher temperatures, to obtain a rate of diffusion sufficiently large to be measurable.

Before concerning ourselves with theoretical calculations of activation energies for diffusion in the 3A zeolites, it is, consequently, necessary to know whether the concentration (of atoms in the cavities) used in Fick's diffusion refers to atoms in volume V (see Fig. 33) or to atoms adsorbed in area S. The relative number of atoms in these positions clearly depends on the standard-state free energy of adsorption, ΔF_a, from the center of the cavity to the trough. ΔF_a depends, in turn, on ΔH_a and $\Delta \Phi_a$. Let the fraction of the total spherical area S which is occupied by molecules lying within the potential energy trough be θ. Then,

$$(C/C_0)(1 - \theta) = \theta \exp (\Delta F_a/RT) \qquad (56)$$

where C is the concentration of atoms in the spherical volume V and C_0 is the standard state for this concentration (activity coefficients being assumed to be one). At low concentrations, where Henry's law applies, θ can be assumed to be small and

$$\theta C_0/C = \exp(-\Delta F_a/RT) \tag{57}$$

If a standard state of 1 atom per cavity is used, the number of adsorbed atoms per cavity will be $\theta(4\pi r_2^2/A_a)$, where A_a is the area occupied by the atom. Thus the relative concentrations are

$$\theta(4\pi r_2^2/A_a)/C = (4\pi r_2^2/A_a)\exp(\Delta\Phi_a/R)\exp(-\Delta H_a/RT) \tag{58}$$

Of, if the ratio of concentrations is denoted by ζ,

$$\zeta = (4\pi r_2^2/A_a)(Q_2Q_\nu/Q_3)\exp(-\Delta H_a/RT) \tag{59}$$

where Q_2 is the partition function of two degrees of translational freedom in the spherical area S for the adsorbed atom; Q_ν is the vibrational partition function of the adsorbed atom, perpendicular to the spherical shell; and Q_3 is the partition function of the nonadsorbed atom, with three degrees of translational freedom. These partition functions can be approximated as follows (*96*):

$$Q_3 = (2\pi mk_BT/h^2)^{3/2}V \tag{60}$$

From Fig. 33, V is taken as $\frac{4}{3}\pi r_1^3$. Also

$$Q_2 = (2\pi mk_BT/h^2)S \tag{61}$$

where S is the spherical area shown in Fig. 33, that is, $4\pi r_2^2$. The value of Q_ν can be approximated as follows. Let ν be the frequency of vibration perpendicular to the spherical shell and assume that the vibration is simple harmonic with a maximum displacement energy of ΔH. Then

$$\nu = (\Delta H/2m\lambda^2)^{1/2} \tag{62}$$

where ΔH is in ergs and $\lambda/2$ is the maximum displacement of the vibration. For ΔH in calories per gram-atom,

$$\nu = [(\Delta H)(J)(10^7)/2N_Am\lambda^2]^{1/2} \tag{63}$$

where N_A is Avogadro's number and J is 4.185. ΔH may be equated with $-\Delta H_a$ and λ with the distance marked as such in Fig. 33. The partition function of a simple harmonic oscillation is

$$Q_\nu = [1 - \exp(-h\nu/k_BT)]^{-1} \tag{64}$$

Thus Q_ν can be determined from (63) and (64). A_a can be estimated by using the usual close-packing approximation, giving $A_a \approx 3.46r^2$, r being the equilibrium atomic radius of the atom or $r_0'/2$.

Values of the parameters required to estimate ζ's for the rare gases are listed in Table X. Values for r_1 have been taken somewhat arbitrarily,

TABLE X

SUMMATION OF PARAMETERS FOR THE CALCULATION OF MOST LIKELY POSITION OF RARE GASES IN THE CAVITY FOR OUR 3A ZEOLITE DIFFUSION STUDIES

Parameter	Neon	Argon	Krypton	Xenon
r_1, A	2.63	2.42	2.20	1.78
r_2, A	4.33	4.08	3.97	3.72
ΔH_a, cal/mole	980	2300	2920	3320
λ, A	2.06	1.99	2.20	2.40
A_a, A^2/atom	8.4	12.6	14.1	17.9
$4\pi r_2^2/A_a$, atoms	27.8	16.4	13.9	9.70
$\frac{4}{3}\pi r_1^3$, A^3	76.1	59.3	44.5	23.6
$4\pi r_2^2$, A^2	235	209	197	173
Mean temp., °K	409	668	690	780
ν, sec^{-1}	1.54×10^{12}	1.74×10^{12}	1.22×10^{12}	9.58×10^{11}
Q_ν	6.06	8.51	12.0	17.2
Q_2	6.37×10^3	18.3×10^3	37.5×10^3	58.4×10^3
Q_3	10.7×10^3	48.6×10^3	116.1×10^3	145.4×10^3
ζ	32	9	7	8

since there is no region of exactly constant potential energy in the center of the cavity. Roughly, r_1 has been taken at a value of potential energy such that ΔH_a is ca. 85 per cent of the total difference in potential energy between the bottom of the trough and the middle of the cavity. Such an approximation will result in values which are too low. It is seen from Table X that the ζ values are considerably in excess of one for all the rare gases. Thus, to a good approximation, it is concluded that the most likely position of the rare gases in the cavity of the 3A zeolite is in the potential-energy minimum along the wall.

e. Potential Energies for Approach to Aperture Plane in 3A Zeolite. Potential-energy diagrams and activation energies for rare gases diffusing from the center of a cavity to an aperture plane in the 3A zeolite can be considered. This calculation will be divided into three parts. First, energies will be calculated for the interaction of the rare gases with the oxygens forming the aperture ring; but in this case, as we shall see, the gas will be approaching the ring at a point off its center. Second,

energies will be calculated for the interaction of the rare gases with the potassium ion sitting somewhere in the aperture. Third, the energy of interaction of the gases with the surface of the cavity, with the oxygens forming the aperture and the potassium ion removed, will be necessary. This calculation has already been made in the case of the 5A zeolite (Fig. 30). These three sets of potential-energy diagrams will then be added together to give the potential energy for the gases diffusing from the center of the cavity to the aperture plane.

Before making these calculations, it is necessary to fix a position for the potassium ion relative to the eight oxygens in the aperture. As discussed in Section II, it has not been possible to fix the exact position of the exchangeable cations from X-ray-diffraction studies. Let us consider the three positions shown in Fig. 34. In position (a), the potassium ion is not protruding into the aperture opening. Simple calculations show that the potential-energy levels for the rare gases passing through the aperture would be essentially unchanged from those shown in Fig. 29. Since experimental E for diffusion of the rare gases (except helium) through the 3A zeolite are substantial, this location is not reasonable. At the other extreme, the potassium ion can be sitting with its center in the plane of the aperture, as shown in Fig. 34(b). In this case, we can imagine a molecule (say helium) passing through the restricted aperture at a point midway between the potassium and an oxygen. Using the method of summation, the interaction energy of helium with the eight oxygens is 3.6 kcal/mole. The interaction energy with the potassium ion is 1.3 kcal/mole, giving a net repulsive energy of 4.9 kcal/mole. It is recalled that, expermentally, the diffusion of helium in the 3A zeolite was found not to be activated. Thus it is concluded that this extreme position is not reasonable for the location of the potassium ion.

Figure 34(c) depicts the apparent location of the potassium ion relative to the oxygen ring at some position intermediate between positions (a) and (b). Our first approach is to calculate potential energies for different locations of the potassium ion for neon diffusion and to compare the resultant theoretical E with that found experimentally for neon (7.0 kcal/mole). It is, of course, very laborious to calculate potential-energy patterns for all possible paths, in three dimensions, which a molecule might take in passing through the aperture. It is reasonable to assume, however, that point P', which lies midway between the potassium ion and oxygen on a line connecting their centers, as shown in Fig. 34(c), would be the location of maximum repulsive energy. The exact nature of the remainder of the path is then somewhat academic.

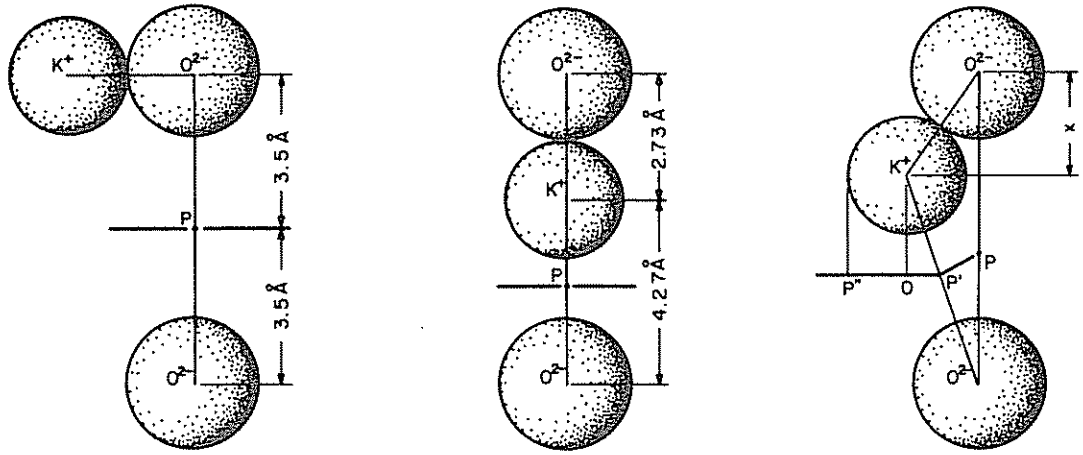

Fig. 34. Some possible positions for the location of the exchangeable potassium ion in the aperture, formed by eight oxygens, in type 3A zeolite.

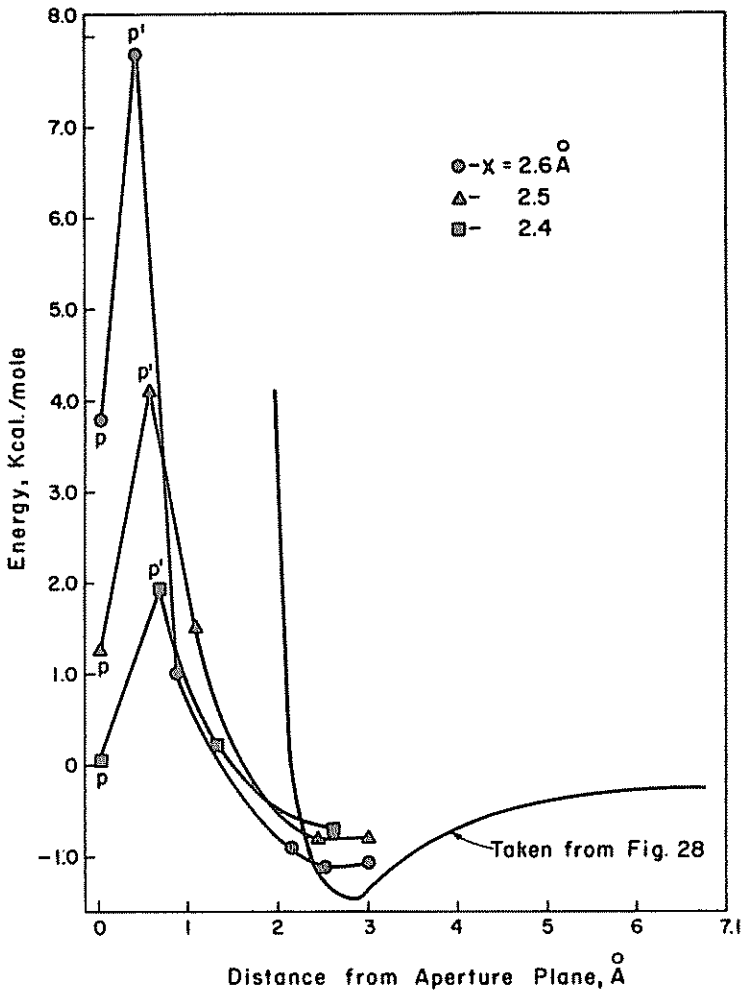

Fig. 35. Potential-energy plots for neon interacting with an aperture in type 3A zeolite, for the exchangeable potassium ion protruding different distances into the aperture opening. The potential-energy plot for neon interacting with the cavity surface, taken from Fig. 28, is superimposed.

For simplicity, we have calculated potential energies along the path $P''OP'P$, where P' and P are equidistant from the center of the potassium ion.

Figure 35 shows the potential-energy diagrams for neon diffusing from

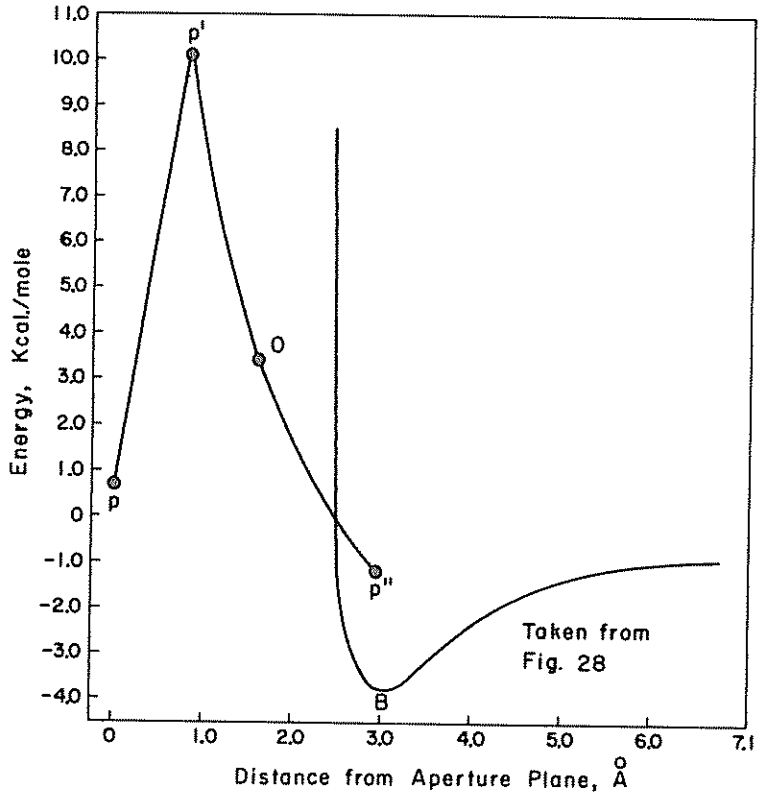

Fig. 36. Potential-energy plot for argon interacting with an aperture in type 3A zeolite. The exchangeable potassium ion protrudes into the aperture opening an (x) distance of 2.2 A. The potential-energy plot for argon interacting with the cavity surface, taken from Fig. 28, is superimposed.

point P in the aperture plane toward the center of the cavity for three different locations of the potassium ion. To obtain Fig. 35, the interaction energies of neon with the oxygen ring and the potassium were added to the interaction energy of neon with the remainder of the cavity, as given in Fig. 30.

If we again assume that the diffusing species after leaving the aperture reaches and travels in the potential-energy minimum along the wall of the cavity, an estimate of the total potential-energy difference which must be overcome in passing through the 3A zeolite can be obtained. The potential-energy profile for neon, taken from Fig. 28, has been

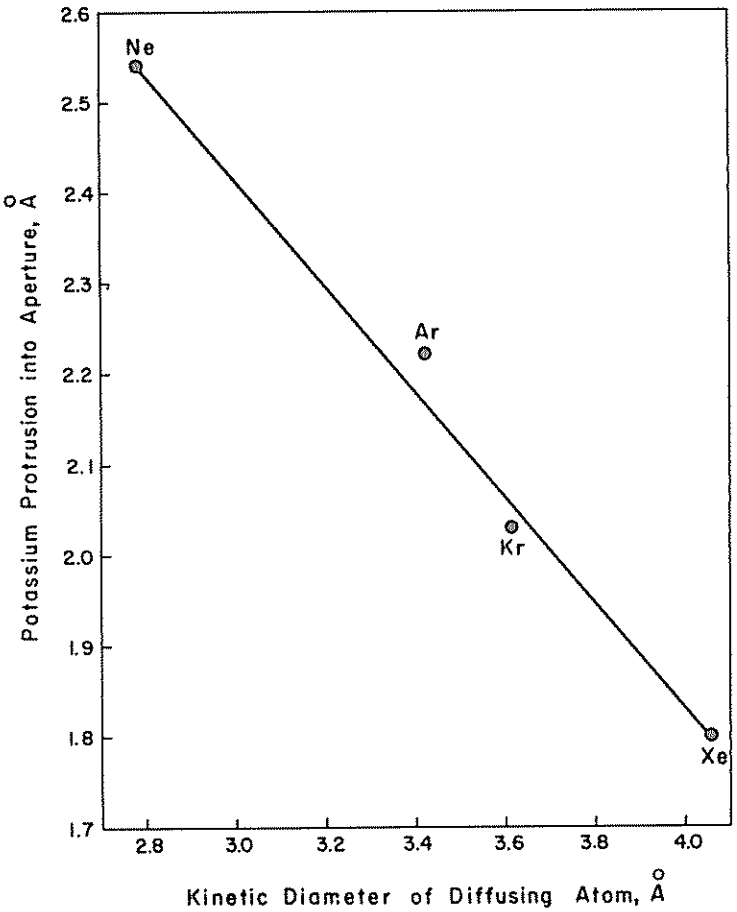

Fig. 37. The estimated extent of protrusion of the potassium ion into the aperature opening during passage of rare gases of different kinetic diameters through the aperture in type 3A zeolite.

superimposed on Fig. 35 for this purpose. For the potassium ion located at values of (x) of 2.4, 2.5, and 2.6 A, the E for passage are estimated as 3.4, 5.6, and 9.3 kcal/mole, respectively. These values bracket the experimental E for neon.

It is of interest now to calculate what the repulsive potential energy at point P' will be for argon diffusion, taking (x) = 2.5 A. The repulsive energy is found to equal 48 kcal/mole. Since the experimental E for

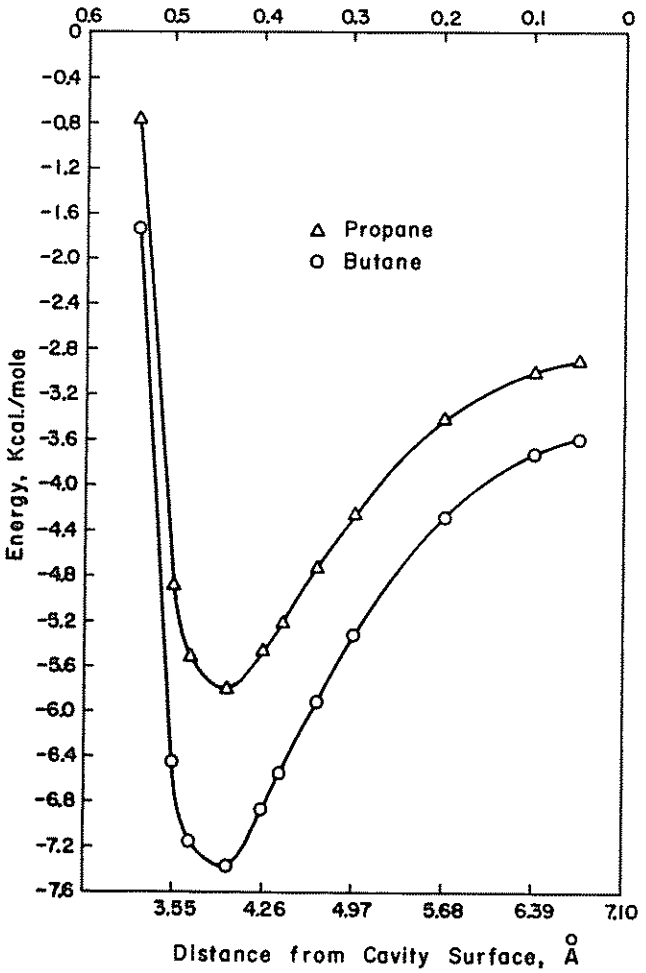

Fig. 38. Potential-energy plots for propane and *n*-butane interacting with the surface of a cavity in a type A zeolite.

argon diffusion in the 3A zeolite is only 12.6 kcal/mole, these calculations strongly suggest that the position of the potassium ion is variable and depends upon the size of the diffusing species passing through the aperture. In Fig. 36 the potential-energy diagram for argon is shown, when (x) is taken as 2.2 A. The potential-energy difference between points P' and B of 13.9 kcal/mole is in reasonable agreement with the experimental E of 12.6 kcal/mole. If we now calculate the potential

energy at point P' for krypton diffusion, taking $(x) = 2.2$ A, we obtain a value of 28.9 kcal/mole, which is much larger than the experimental E. Thus, again the value of (x) must decrease to give a reasonable E for krypton diffusion. A still further decrease in (x) will be necessary to give a reasonable E for xenon diffusion. A plot of the apparent extent of protrusion of the diameter of the potassium into the aperture (that is, x) versus the kinetic diameter of the diffusing rare-gas molecule is given in Fig. 37. Smith (*44*), who studied the structure of chabazite by X-ray diffraction, recognized that sorbate-aperture interaction can change the apparent size of the aperture opening.

3. Potential Energies for Hydrocarbons in Zeolite Cavity. Potential-energy diagrams for propane and n-butane diffusing radially from the center of a cavity toward the cavity surface can be considered. The potentials $\phi_D + \phi_R$ for the interaction of propane and n-butane with the lattice of the cavity in the type A zeolite have been calculated using (54). The results are shown in Fig. 38. The minima in these plots should correspond closely to the heats of sorption of the hydrocarbons on the type A zeolites. Burgess and co-workers report an experimental value of ca. 10 kcal/mole for the heat of sorption of n-butane at 350°C on the 5A sieve at low coverages (*121*). Since the heat of sorption q_1 equals the interaction energy at the equilibrium distance plus $\frac{1}{2}RT$ (*122*), it is predicted from Fig. 38 that q should equal 8.0 kcal/mole. Eberly (*20*) reports a value of 13.0 kcal/mole for the heat of sorption of n-hexane on type A zeolite over the temperature range 260 to 482°C. Extrapolation of the values for propane and n-butane in Fig. 38 to n-hexane give an approximate maximum net attractive energy of -10.6 kcal/mole fo. n-hexane. Thus it is predicted that q should equal 11.2 kcal/mole.

We have not calculated interaction energies for the normal hydrocarbons with the aperture for the 5A zeolites. However, Barrer and Peterson recently made such a calculation (*123*). They assumed that the potential energy in the aperture plane could be estimated from the interaction of three methylene groups with the ring of eight oxygens. In the center of the aperture plane, they estimate an interaction energy of -3.5 kcal/mole for all normal hydrocarbons.

B. Entropies of Rare-Gas Diffusion in the 3A Zeolite

To calculate entropies (or $\Delta\Phi^{\ddagger}$ values) from experimental values of diffusion coefficients, it is necessary to determine first which limiting physical case of activated diffusion is applicable to our results. As discussed in Section III, the two physical cases are (1) where there are a

number of diffusing molecules existing in each potential-energy valley or cavity, and (2) where there is only one (or no) molecule existing in each cavity.

As an example of the calculation which must be made to determine the operative physical case, we can consider the results for the diffusion of neon from 22 g of dried 3A zeolite at 84°C. For a charging pressure of 1230 torr, $V_c - V_0$ is found to equal 0.072 cc (STP)/g. Assuming Henry's law to hold from 1230 torr to zero pressure, it is estimated that at the start of this diffusion run the 3A zeolite held 0.18 cc/g of neon or 4.9×10^{18} atoms/g. The volume of the accessible cavities in the 3A zeolite is ca. 0.27 cc/g, or there are ca. 5×10^{19} cavities/g. This means that the second physical case exists for the neon-diffusion conditions. For the other rare gases, their concentration in the zeolite at diffusion conditions was even more dilute than was that for neon.

For the second physical case, the experimental diffusion coefficient can be written

$$D = (k_B T/h\gamma)(\delta^2) \exp(\Delta\Phi^{\ddagger}/R) \exp(-\Delta H_0^{0\ddagger}/RT) \qquad (65)$$

In (65), $\Delta H_0^{0\ddagger}$ is the zero-point enthalpy of activation; it is common practice to equate it with E. To calculate $\Delta\Phi^{\ddagger}_{(\exp)}$ values, experimental values of D_0, as given in Table VI, are set equal to $(k_B T/h\gamma)(\delta^2) \exp(\Delta\Phi^{\ddagger}/R)$. For the calculations, $\gamma = 6$ (that is, six apertures per cavity divided by one aperture per diffusion plane) and the distance between saddle points, $\delta = 14.2$ A. In Table XI, $\Delta\Phi^{\ddagger}_{\exp}$ values are summarized. The results are given in entropy units, or calories per degree Kelvin-mole. It is seen that $\Delta\Phi^{\ddagger}_{\exp}$ becomes more negative in going from neon to argon and then decreases in absolute value.

TABLE XI

VALUES OF $\Delta\Phi^{\ddagger}$ FOR RARE-GAS DIFFUSION IN 3A ZEOLITES

Gas	Av. diffusion temp., °K	$\Delta\Phi^{\ddagger}_{\exp}$, eu	$\Delta\Phi^{\ddagger}_{(\text{theor})}$, eu
Neon	413	−26.9	−17.5
Argon	688	−28.1	−20.3
Krypton	693	−22.6	−22.5
Xenon	782	−21.4	−24.1

Partition functions of the various rare gases in the cavity of the type A zeolite, at temperatures at which the diffusion experiments in the 3A

zeolite were conducted, were given in Table X. From these partition functions, $\Delta\Phi^{\ddagger}_{\text{theor}}$ can be estimated. That is,

$$\exp\left(\Delta\Phi^{\ddagger}/R\right)_{\text{theor}} = \gamma Q^{\ddagger}/Q_{\text{cavity}} \tag{66}$$

where $Q^{\ddagger}$ is the partition function of the activated species in the aperture and Q_{cavity} is the partition function of the species in the cavity (with the ground state factorized out, of course). It was previously concluded that the probability is high that the rare-gas atoms are located in the potential-energy trough while in the cavity, or Q_{cavity} equals the product of two degrees of translational freedom plus one degree of vibrational freedom in the trough. Values for Q_2 and Q_v are given in Table X.

Values of $Q^{\ddagger}$ can be obtained as follows. The entropy of vibration along the top of the energy barrier has already been factorized out in deriving the rate equation; therefore, only vibrations perpendicular to this axis need be considered. The high energies involved as the atoms approach the walls of the aperture mean that the vibrational frequency will be high and the partition functions close to unity. The equilibrium between activated complexes in the apertures and atoms in the cavities was considered in the derivation of (22); since there are more holes than one in equilibrium with each cavity, the number γ has to be included in (66). [If the equilibrium between only the apertures in the diffusing plane and the cavity atoms is considered, as in the derivation of (17), the γ term is not present either in $\exp\left(\Delta\Phi^{\ddagger}/R\right)$ or in the expression for the D_0 value.] Therefore,

$$\Delta\Phi^{\ddagger}_{\text{theor}} = 2.3R \log\left(6/Q_{\text{cavity}}\right) \tag{67}$$

Table XI shows the calculated values of $\Delta\Phi^{\ddagger}_{\text{theor}}$ compared with the experimental values.

Agreement between the experimental and theoretical values of $\Delta\Phi^{\ddagger}$ is not good. Theoretically, $\Delta\Phi^{\ddagger}$ should increase monotonically in absolute value with increasing size of the diffusing rare gas. Instead, $\Delta\Phi^{\ddagger}_{\text{exp}}$ is seen to undergo an over-all decrease in absolute value with increase in size of the diffusing rare gas. Of course, $\Delta\Phi^{\ddagger}_{\text{exp}}$ is found to undergo an over-all decrease because the D_0 values, from which $\Delta\Phi^{\ddagger}$'s are calculated, show an over-all increase with increasing size of the diffusing species. That is, D_0 or preexponential values are found to increase (over-all) as the E values for diffusion increase. Frequently, in studies on the kinetics of heterogeneous reactions the experimental results show the preexponential factor to increase as the activation energy increases (*124*). This phenomenon has been termed the *compensation effect*. The initial inter-

pretation of this effect in heterogeneous reactions is due to Constable (*125*), who assumed that reaction takes place on many different sites of varying energy, that is, an energetically heterogeneous surface. On this basis, Constable derived a rate equation in which the activation energy also appears in the numerator of the preexponential term. Hence his expression implies that for an energetically heterogeneous system, as the energy of activation is changed, the preexponential factor will compensate for the change. It is not obvious how such a phenomenon would be operative in the case of these diffusion studies.

In the theoretical calculations in Section V, the oxygen atoms forming the apertures and the potassium ions partially blocking the apertures have been taken as rigid spheres. As Kington and Laing (*9*) and Breck and Smith (*19*) point out, these atoms, in fact, are vibrating around equilibrium positions. This, in effect, can mean that the diffusing species upon reaching the aperture opening encounters a situation which is dynamic or continuously changing. The important question is how dynamic. At one instant, are the oxygen atoms, which form an aperture, all at a position of maximum distance from the center of the aperture? Is the potassium at this instant at its minimum value of x, or protrusion into the aperture? At another instant are all the oxygen atoms at a position of minimum distance from the center of the aperture and the potassium at maximum protrusion into the aperture? Or is the situation, in effect, not dynamic in a macroscopic sense? That is, at each instant are half the oxygens moving from the center of the aperture while the ther half are moving toward the center?

A dynamic situation would increase the over-all ease of a species getting through an aperture and increase the time-average diffusion coefficient. Let us take as an example, the diffusion of neon through the 3A zeolite. For the potassium ion located at values of (x) of 2.4, 2.5, and 2.6 A, the E for passage were estimated as 3.4, 5.6, and 9.3 kcal/mole. The preexponential term D_0 in the diffusion coefficient would be expected to change to a negligible extent with the above changes in (x). Therefore, the relative values of D can be estimated from the values of $\exp(-E/RT)$. In the rigid case of (x) fixed at 2.5 A, $\exp(-E/RT)$ equals 0.017 for a temperature of 680°K. If instead, (x) equals 2.4 A half the time and 2.6 A half the time, $\exp(-E/RT)_{av}$ equals 0.042. Of course, in the dynamic case (x) would assume all values between 2.4 and 2.6, but qualitatively the result would be the same.

The dynamic situation is further complicated, since the root-mean-square amplitude of vibration of atoms around their equilibrium position

increases with increasing temperature. Thus, for example, at some temperature above 680°K, the extreme values of (x), in the above example, might be 2.3 and 2.7 A. This would have the effect of further increasing the time-average diffusion coefficient. This means that the experimental D's would increase more rapidly with temperature in the dynamic case than in the rigid case. Thus in the dynamic case the E's would only be apparent E's and would have higher values than those for the rigid-atom case. Obviously, comparison of E_a with E calculated theoretically, based on rigid atoms, would not be valid. The dynamic situation is further complicated because the interaction energy of each diffusing gas is more or less sensitive to changes in the effective aperture opening. Clearly, this problem should be explored in much more detail.

VI. THEORETICAL CALCULATIONS OF POTENTIAL ENERGIES OF RARE GASES INTERACTING WITH CARBON SURFACES

A. Above the Infinite-Layer Plane

It is of interest to concern ourselves with the interaction of rare gases with the carbon surface. As we discussed in Section II, carbons are composed of material in the form of graphite-like layers plus material in an amorphous form. The amorphous material is thought to be primarily functional groups attached to and sometimes cross-linking layer planes. For these calculations, we shall be concerned only with the interaction of the rare gases with the layer plane. For simplicity, we assume a perfect layer plane, free of point defects, dislocations, and impurities. As also discussed in Section II, the voids in many molecular-sieve carbons appear to be slit-like. It is not unreasonable that the long sides of the slits are formed by layer planes of carbon. Therefore, calculations of interaction energies with the layer planes, from which we shall estimate potential energies for gases diffusing between layer planes at different distances apart, are of considerable interest.

In Fig. 39 we are looking down upon a perfect layer plane in carbon. At each position β, a carbon atom is located. (The significance of the other letters will become clear shortly.) Within the layer planes, the carbon atoms are 1.415 A apart, a spacing which is indicative of a one-third double-bond character. Each carbon atom has four valence electrons. Three of these electrons (usually called σ electrons) are engaged in forming regular covalent bonds with neighboring carbon atoms. The fourth electron (usually called a π electron) resonates between many

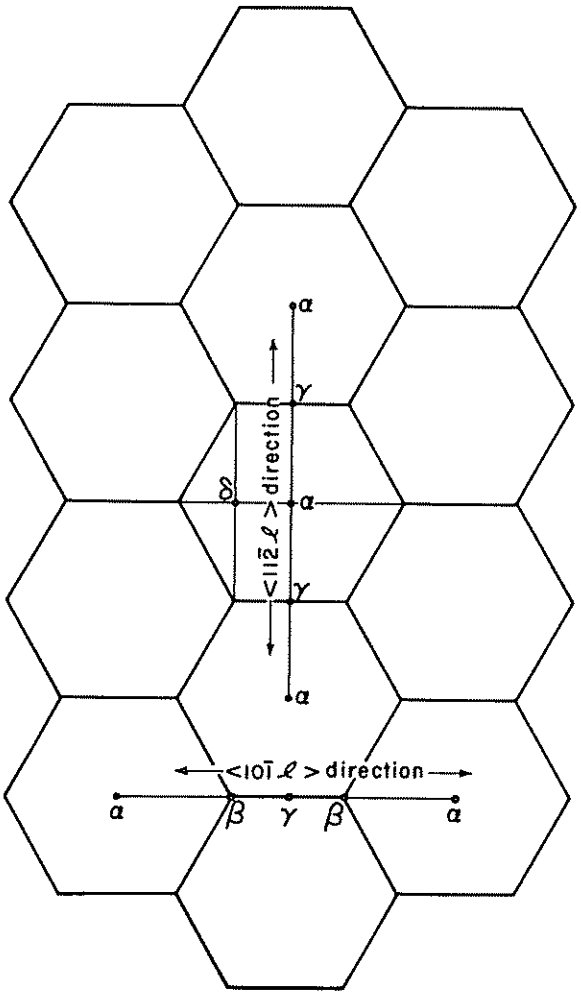

Fig. 39. Small segment of a perfect layer plane in carbon.

valence-bond structures, effectively giving each carbon-carbon bond a one-third double-bond character.

Workers have found that the layer-plane surface can be obtained to a very substantial extent in highly graphitized carbon blacks, such as P-33. Graham estimates that at least 99.9 per cent of the surface of graphitized P-33 is composed of basal planes (*126*). Hence workers have

experimentally measured isotherms of rare gases on graphitized carbon blacks and from their isotherms calculated isosteric heats of adsorption. These isosteric heats of adsorption can be used in conjunction with a potential-energy model to estimate interaction energies as a function of distance from an infinite layer plane of carbon atoms.

Halsey and co-workers have measured the adsorption of rare gases on graphitized P-33 at coverages of less than 10 per cent of a monolayer at different temperatures (*127*). The isotherms in the low-coverage region were all straight lines, so that isosteres taken from the data all had the same slope. Thus, one can, in effect, compute the isosteric heat of adsorption, q_{st}, at zero coverage. From the definition of the isosteric heat of adsorption, Everett (*122*) has shown by a thermodynamic argument that q_{st} is $\frac{1}{2}RT$ greater than the maximum net attractive energy of gas-surface interaction (called ϕ_{is}^* by Halsey et al.) for nonlocalized adsorption, which appears to be operative for the rare gas–carbon system. Values of q_{st} and ϕ_{is}^* are given in Table XII. The temperature was taken in the middle of the range of experimental temperatures for each gas.

Halsey and co-workers now derive a theoretical expression for the interaction energy of a gas molecule with an infinite-layer plane of graphite. They employ a Lennard-Jones (6-12) potential function for the interaction of one gas atom with one surface atom in the solid. Integration of the function over a single infinite plane results in the following (4-10) potential law:

$$\phi_{is} = 3.06\phi_{is}^*[-(\sigma/r)^4 + (\sigma/r)^{10}] \tag{68}$$

where σ, as previously defined, is the distance between a gas atom and the surface at zero net interaction energy and r is the distance from the surface. Further, Halsey and co-workers show that the maximum net attractive energy of a gas atom over a single infinite-layer plane of graphite is

$$\phi_{is}^* = (1/3.06)(N_0 A/2\sigma^4) \tag{69}$$

where N_0 is the number of atoms per unit area of surface and A is as given in (51). Therefore, from experimental values of ϕ_{is}^* and theoretical values of A, σ values can be calculated.

As usual, there is difficulty in deciding what theory to accept in calculating A. Halsey and co-workers consider five possible theories—those due to Slater and Kirkwood (*118*), to Kirkwood (*117*), to London (*116*), to Bardeen (*128*), and to Margenau and Pollard (*129*). Halsey

TABLE XII

VALUES OF ISOTERIC HEATS OF ADSORPTION AND MAXIMUM INTERACTION ENERGY OF RARE GASES WITH THE BASAL PLANE OF CARBON AT ZERO COVERAGE (*127*)

Gas	q_{st}, cal/mole	ϕ^*_{is}, cal/mole
Neon	849	734
Argon	2355	2142
Krypton	2999	2806
Xenon	4059	3720

and co-workers find that the use of the London expression to calculate A yields the lower limit of σ values; the use of the Kirkwood-Muller expression yields the upper limit of σ values. Values of A calculated from both expressions are considered, so that interaction energies can be bracketed between a lower and upper limit. Equation (52) gives the London expression for A. The Kirkwood-Muller expression for A is

$$A = \frac{6mc^2\alpha_1\alpha_2}{(\alpha_1/\chi_1) + (\alpha_2/\chi_2)} \tag{70}$$

where m is the mass of an electron, c is the velocity of light, α's are (as in the London expression) polarizabilities, and χ's are diamagnetic susceptibilities. Values of the parameters used to calculate A are given in the paper by Halsey and co-workers.

Values of σ_L, based on the London expression for A, and σ_{KM}, based on the Kirkwood-Muller expression for A, are given in Table XIII. Values for helium have been estimated by extrapolation of plots of σ_L and σ_{KM} versus $\sigma_{rare\ gas}$. It is of interest to compare these values with those calculated from the kinetic diameters of the rare gases and a σ value for carbon. Following Pace (*130*), the equilibrium diameter for carbon is taken as the spacing between layer planes. This value can then be converted to the kinetic diameter by dividing by $2^{1/6}$, or, by using the graphite interlayer spacing of 3.35 A, we have $\sigma_C = 2.99$ A. These values are listed in Table XIII. Comparison of the σ values lead to two conclusions: Values calculated by averaging the σ values for the rare gases and carbon, that is, σ_{av}, fall intermediate between σ_L and σ_{KM}; further, these values increase more sharply with increasing size of the rare-gas atoms than do σ_L and σ_{KM}.

Using (68), values of ϕ_{is} can now be calculated as a function of r. These values are compiled in Tables XIV and XV, for the rare gases for

TABLE XIII

σ VALUES FOR THE RARE-GAS–CARBON-LAYER-PLANE SYSTEM

Gas	σ_L, A	σ_{KM}, A	$(\sigma_{rare\ gas} + \sigma_C)/2$, A
Helium	2.27	3.57	2.78
Neon	2.32	3.68	2.89
Argon	2.45	3.70	3.20
Krypton	2.49	3.78	3.30
Xenon	2.57	3.92	3.52

values of r ranging from 1.677 to 5.0 A, using the σ_L and σ_{KM} values. To calculate ϕ_{is} values for helium, ϕ_{is}^* was taken as 350 cal/mole (*131*). Clearly, when σ_{KM} is used, the repulsive interaction term becomes dominant at smaller values of r. Even when ϕ_{is} is calculated using σ_L values, the repulsive interaction is very high for a distance from the layer plane of 1.677 A, or one-half the interlayer spacing in graphite. This means that the activation energy for the rare gases getting in between the layer planes of graphite is certainly very high. This is in line with the conclusion from X-ray-diffraction studies that argon does

TABLE XIV

INTERACTION ENERGIES OF RARE GASES WITH AN INFINITE CARBON-LAYER PLANE, USING σ VALUES BASED ON THE LONDON EXPRESSION

⊥ Distance from layer plane, A	Energy, cal/mole				
	Helium	Neon	Argon	Krypton	Xenon
1.677	18570	49300	vh[a]	vh	vh
2.0	2024	5850	35080	58060	vh
2.2	143	1030	9030	15550	32650
2.4	−244	−360	940	2400	7620
2.5	−320	−600	−690	−200	2260
2.6	−344	−700	−1550	−1670	−750
2.7	−346	−730	−1970	−2390	−2390
2.8	−321	−710	−2120	−2720	−3260
2.9	−309	−680	−2120	−2800	−3600
3.0	−287	−600	−2050	−2740	−3710
3.2	−236	−530	−1800	−2450	−3460
3.4	−194	−440	−1520	−2080	−3020
3.6	−158	−360	−1270	−1750	−2560
3.8	−130	−290	−1050	−1450	−2150
4.0	−107	−240	−870	−1210	−1800

[a] vh = very high, that is, >100,000 cal/mole.

TABLE XV

INTERACTION ENERGIES OF RARE GASES WITH AN INFINITE-CARBON-LAYER PLANE, USING σ VALUES BASED ON THE KIRKWOOD-MULLER EXPRESSION

⊥ Distance from layer plane, A	Energy, cal/mole				
	Helium	Neon	Argon	Krypton	Xenon
1.677	vh	vh	vh	vh	vh
2.0	vh	vh	vh	vh	vh
3.0	3946	12250	49800	64920	vh
3.4	443	1859	6069	11680	27120
3.6	−50	341	1304	3546	10720
3.7	−179	−69	0	1305	5872
3.8	−261	−342	−873	−263	2572
3.9	−310	−523	−1440	−1297	341
4.0	−336	−633	−1794	−1972	−1204
4.2	−348	−724	−2102	−2641	−2929
4.4	−332	−731	−2118	−2796	−3587
4.6	−303	−679	−2000	−2709	−3703
5.0	−240	−554	−1642	−2280	−3300

not penetrate between the layer planes of graphite at temperatures at least up to 1118°C (*132*). It is further consistent with the fact that the density of graphite, as measured by helium displacement at room temperature, agrees well with the density calculated from unit cell parameters.

Above Particular Positions in the Layer Plane

It is of interest to calculate interaction energies of the rare gases as they approach perpendicularly toward the layer plane of carbon at particular positions. Positions of primary interest have been designated in Fig. 39 as α, β, γ, and δ. Interaction energies have been calculated using (51) and the London expression for A in a manner analogous to that used for the zeolite–rare-gas calculations. In the summation method, interaction energies have only been considered for carbon atoms within a distance of 3.0 A from α, β, γ, or δ. Values used for the polarizabilities and ionization potentials of the rare gases are given in Table IX. The atomic polarizability of carbon is taken as 1.02×10^{-24} cc (*133*); the ionization potential of carbon is taken as 11.2 eV (*134*). Values of A calculated from the London expression for helium, neon, argon, krypton, and xenon are (5.8, 10.9, 39.4, 55.4, and 82.7) $\times 10^{-44}$ cal-cm^6/mole, respectively. Calculations have been performed for two different values

of the equilibrium separation of the interacting species, that is r_0 [see Eq. (53)]. As a lower limit, r_0 has been taken equal to $2^{1/6}\sigma_L$, where σ_L values are given in Table XIII. As an upper limit, r_0 has been taken as equal to $2^{1/6}\sigma_{av}$, where σ_{av} values are also given in Table XIII.

Values of the interaction energies for the rare gases approaching positions α, β, γ, and δ are given in Tables XVI to XIX for various distances from the carbon layer plane.

C. Between Two Layer Planes

Using the values in Tables XVI to XIX, we can estimate potential energies for rare-gas atoms between two carbon-layer planes having the graphite hexagonal (*ababab*) stacking (*135*). It is of interest to consider the potential energies encountered as the rare gases travel in the $\langle 10\bar{1}\ell\rangle$ and $\langle 11\bar{2}\ell\rangle$ directions, along paths shown in Fig. 39. Along the designated $\langle 10\bar{1}\ell\rangle$ path of travel, the atoms will see the maximum possible differences in potential energy; along the designated $\langle 11\bar{2}\ell\rangle$ path of travel, the atoms will see the minimum possible differences in potential energy. Therefore, potential-energy differences encountered during the diffusion of rare-gas atoms between carbon layer planes in random orientation [turbostratic carbons (*135*)] will be intermediate between the values which will be given.

Consider travel along the $\langle 10\bar{1}\ell\rangle$ direction in Fig. 39. For an atom directly above an α position in the layer plane shown, the atom will be directly below a β position in the plane above. The vertical location of the atom will be that at which its potential energy is a minimum. The potential-energy minimum will occur where the interaction energy resulting from the α position equals the interaction energy from the β position. By interpolating interaction-energy values given in Tables XVI and XVII as a function of distance from the layer plane, potential energies for the rare gases can be estimated. Values are given in Tables XX and XXI for the potential energies (called P) resulting from interaction with the α and β positions.

Resuming travel in the $\langle 10\bar{1}\ell\rangle$ direction, an atom directly above the β position can be in one of two potential-energy situations. In one case an atom directly above a β position will be directly below an α position in the plane above. The potential energy will again be P. In the second case an atom directly above a β position will be directly below another β position in the plane above. The potential energies resulting from the interaction of two β positions has been designated R in Tables XX and XXI.

TABLE XVI

INTERACTION ENERGIES OF THE RARE GASES AS THEY APPROACH PERPENDICULARLY TOWARD POSITION α IN THE CARBON LAYER PLANE

⊥ Distance from layer plane, A	Energy, cal/mole									
	r_0, helium		r_0, neon		r_0, argon		r_0, krypton		r_0, xenon	
	2.54	3.12	2.60	3.24	2.75	3.59	2.80	3.71	2.89	3.95
1.677	365	9580	1690	23700	17700	vh	32100	vh	66900	vh
1.8	−406	5130	−116	13100	6570	vh	13500	vh	31600	vh
2.0	−808	1660	−1210	4710	−1260	42000	164	75600	5340	vh
2.2	−791	348	−1330	1390	−3390	16500	−3870	30800	−3430	75200
2.4	−661	−122	−1160	126	−3520	5900	−4530	11900	−4820	32300
2.5	−590	−216	−1050	−155	−3330	3220	−4380	7050	−5770	20100
2.6	−525	−271	−946	−336	−3090	1350	−4140	3600	−5660	11800
2.7	−459	−273	−831	−384	−2760	497	−3730	1950	−5200	7660
2.8	−406	−283	−739	−444	−2510	−357	−3430	326	−4870	3630
3.0	−307	−238	−561	−396	−1930	−724	−2660	−556	−3840	936
3.2	−234	−197	−430	−341	−1500	−853	−2080	−949	−3030	−469
3.4	−179	−158	−330	−281	−1160	−809	−1620	−1000	−2380	−969
3.6	−139	−129	−256	−233	−912	−734	−1270	−962	−1880	−1170
3.8	−108	−102	−199	−185	−712	−611	−995	−819	−1470	−1070
4.0	−84	−80	−156	−146	−559	−500	−781	−679	−1160	−928
4.6	−53	−52	−98	−95	−351	−330	−492	−455	−732	−650
5.0	−27	−27	−51	−50	−184	−179	−258	−249	−384	−364

TABLE XVII

INTERACTION ENERGIES OF THE RARE GASES AS THEY APPROACH PERPENDICULARLY TOWARD POSITION β IN THE CARBON LAYER PLANE

⊥ Distance from layer plane, A	Energy, cal/mole									
	r_0, helium		r_0, neon		r_0, argon		r_0, krypton		r_0, xenon	
	2.54	3.12	2.60	3.24	2.75	3.59	2.80	3.71	2.89	3.95
1.677	13100	56900	29400	vh	vh	vh	vh	vh	vh	vh
1.8	4520	24100	10600	57600	63200	vh	vh	vh	vh	vh
2.0	297	6340	1250	15700	12100	vh	21700	vh	44900	vh
2.2	−542	1600	−757	4400	58	47600	1660	67400	6930	vh
2.4	−632	218	−1050	955	−2750	11900	−3210	22400	−3070	54900
2.6	−495	−135	−878	−17	−2720	3570	−3530	7440	−4580	20200
2.8	−413	−248	−749	−352	−2490	401	−3370	1670	−4690	6730
3.0	−319	−239	−583	−389	−2000	−586	−2740	−279	−3930	1640
3.2	−244	−203	−449	−350	−1560	−842	−2160	−904	−3150	−293
3.4	−187	−165	−346	−293	−1210	−832	−1690	−1020	−2480	−957
3.6	−145	−133	−268	−238	−950	−735	−1320	−949	−1950	−1105
3.8	−112	−105	−208	−191	−744	−621	−1030	−824	−1530	−1051
4.0	−88	−84	−163	−154	−585	−514	−819	−694	−1210	−933
4.2	−70	−68	−129	−123	−466	−421	−649	−575	−964	−796
4.6	−45	−44	−82	−80	−297	−281	−417	−389	−619	−556

TABLE XVIII

INTERACTION ENERGIES OF THE RARE GASES AS THEY APPROACH PERPENDICULARLY TOWARD POSITION γ IN THE CARBON LAYER PLANE

⊥ Distance from layer plane, A	Energy, cal/mole									
	r_0, helium		r_0, neor		r_0, argon		r_0, krypton		r_0, xenon	
	2.54	3.12	2.60	3.24	2.75	3.59	2.80	3.71	2.89	3.95
1.677	7800	38000	17800	90300	vh	vh	vh	vh	vh	vh
1.8	2500	17600	6810	42500	43400	vh	72600	vh	vh	vh
2.0	−40	5060	513	12700	8290	97500	15600	vh	33500	vh
2.2	−622	1300	−934	3670	−940	32700	186	58900	4240	vh
2.4	−642	135	−1100	760	−2990	10500	−3600	20100	−3770	49800
2.6	−536	−190	−955	−124	−3000	3050	−3950	6610	−5190	18700
2.7	−477	−262	−858	−296	−2800	1300	−3740	3410	−5110	11100
2.8	−420	−259	−762	−375	−2540	276	−3440	1470	−4810	6320
2.9	−369	−257	−673	−403	−2280	−315	−3120	316	−4420	3340
3.0	−324	−244	−591	−401	−2030	−646	−2790	−371	−4010	1470
3.2	−248	−207	−457	−358	−1590	−877	−2210	−954	−3210	−372
3.4	−191	−169	−353	−300	−1240	−857	−1730	−1050	−2600	−1080
3.6	−148	−136	−273	−244	−971	−756	−1350	−979	−1990	−1140
3.8	−115	−108	−212	−196	−758	−637	−1050	−848	−1560	−1090
4.0	−90	−86	−167	−157	−601	−528	−840	−713	−1240	−958

TABLE XIX

INTERACTION ENERGIES OF THE RARE GASES AS THEY APPROACH PERPENDICULARLY TOWARD POSITION δ IN THE CARBON LAYER PLANE

⊥ Distance from layer plane	Energy, cal/mole									
	r_0, helium		r_0, neon		r_0, argon		r_0, krypton		r_0, xenon	
A	2.54	3.12	2.60	3.24	2.75	3.59	2.80	3.71	2.89	3.95
1.677	4870	26000	11400	62300	68200	vh	vh	vh	vh	vh
1.8	1620	12500	4260	30300	29100	vh	49400	vh	96200	vh
2.0	−178	3800	129	9670	5490	75200	10800	vh	24300	vh
2.2	−542	1040	−823	2960	− 976	26600	−136	48000	3050	vh
2.4	−525	142	−900	701	−2400	9280	−2850	17500	−2890	43200
2.6	−427	−125	−760	−35	−2360	2920	−3070	6140	−3970	16800
2.8	−329	−186	−593	−250	−1960	545	−2640	1720	−3640	6240
3.0	−246	−176	−449	−279	−1530	−292	−2090	67	−3250	1900
3.4	−142	−102	−228	−185	−723	−602	−1110	−780	−2520	−822
4.0	−56	−51	−127	−118	−425	−302	−780	−672	−1100	−797

TABLE XX

POTENTIAL ENERGIES (CAL/MOLE) OF RARE GASES BETWEEN TWO CARBON LAYER PLANES HAVING THE GRAPHITE HEXAGONAL STACKING (CALCULATIONS BASED ON σ_L VALUES)

Spacing between layer planes, A	Energy between α and β points, P	Energy between γ and δ points, Q	Energy between two β points, R	$\lvert P - Q \rvert$	$\lvert R - P \rvert$	$\lvert R - Q \rvert$
Helium						
3.4	11700	10500	23000	1200	11300	12500
3.6	4400	4000	9000	400	4600	5000
4.0	−500	−240	600	260	1100	840
4.4	−1200	−1180	−1080	20	120	100
4.8	−1280	−1170	−1260	110	20	90
5.2	−1020	−980	−1000	40	20	20
6.0	−600	−570	−600	30	0	30
6.8	−360	−360	−370	30	0	30
Neon						
3.7	2600	6600	15000	4000	12400	8400
4.0	−800	640	2500	1440	3300	1860
4.4	−2040	−1680	−1500	360	540	180
4.8	−2160	−1750	−2100	410	60	350
5.2	−1860	−1660	−1750	160	70	90
5.6	−1480	−1360	−1500	120	20	140
6.0	−1140	−1040	−1150	100	10	110
6.8	−670	−580	−700	90	30	120
Argon						
4.0	6000	13800	24000	7800	18000	10200
4.2	−1000	3000	8200	4000	9200	5200
4.4	−4100	−1900	−100	2100	4000	1800
4.8	−5470	−4800	−5500	670	30	700
5.2	−5500	−4800	−5400	700	100	600
5.6	−5000	−4500	−5000	500	0	500
6.0	−3940	−3600	−4000	340	60	400
6.8	−2380	−2440	−2400	60	20	40
7.6	−1460	−1500	−1500	40	40	0
8.0	−1100	−1050	−1130	50	30	80
Krypton						
4.0	14600	26000	43000	11400	28400	17000
4.2	2000	9600	20000	7600	18000	10400
4.4	−3500	50	3300	3540	6800	3250
4.8	−7000	−5700	−6430	1300	570	730
5.2	−6850	−6200	−7060	650	210	860
5.6	−6800	−6000	−6750	800	50	750
6.0	−5440	−4900	−5500	640	60	600

(continued)

TABLE XX (continued)

Spacing between layer planes, A	Energy between α and β points, P	Energy between γ and δ points, Q	Energy between two β points, R	$\lvert P - Q \rvert$	$\lvert R - P \rvert$	$\lvert R - Q \rvert$
Krypton						
6.8	−3300	−2800	−3400	500	100	600
7.6	−2000	−2100	−2080	100	80	20
8.0	−1600	−1620	−1640	20	40	20
Xenon						
4.4	−2500	7000	13800	9500	16300	6800
4.8	−8000	−6000	−6140	2000	1860	140
5.2	−9100	−7600	−9170	1500	70	1570
5.6	−9400	−8000	−9400	1600	0	1400
6.0	−7800	−7200	−7860	600	60	680
6.8	−4800	−5000	−4970	200	170	30
7.6	−3000	−3000	−3100	0	100	100
8.0	−2370	−2340	−2400	40	30	60

Resuming travel in the $\langle 10\bar{1}\ell \rangle$ direction, the last position of interest is γ. An atom directly above γ in the layer plane shown will be directly below a δ position in the plane above. The potential energies resulting from the interaction of the rare gases with γ and δ positions, called Q, are also shown in Tables XX and XXI.

Travelling in the $\langle 10\bar{1}\ell \rangle$ direction, we are concerned with potential-energy differences of $|P - Q|$, $|R - P|$, and $|R - Q|$. Values are given in Tables XX and XXI.

Consider travel along the $\langle 11\bar{2}\ell \rangle$ direction. There are two unique positions to be considered. An atom above the α position will always be below a β position in the plane above, or a potential energy P will result. An atom above the γ position will always be below a δ position in the plane above, or a potential energy Q will result. Therefore, in the $\langle 11\bar{2}\ell \rangle$ direction, the potential-energy difference of concern will be $|P - Q|$.

The minimum value of layer-plane spacing at which the potential energy of the rare gases is attractive at all positions between the planes depends upon whether the calculated values have been based on σ_L or σ_{av}. For values based on σ_L, potential energies for all the rare gases are attractive at spacings greater than 4.8 A. A negligible E should be required for initial penetration of the gases between layer planes having this spacing. Further, potential-energy differences for travel of the rare

TABLE XXI

POTENTIAL ENERGIES (CAL/MOLE) OF RARE GASES BETWEEN TWO CARBON LAYER PLANES HAVING THE GRAPHITE HEXAGONAL STACKING (CALCULATIONS BASED ON σ_{av} VALUES)

Spacing between layer planes, A	Energy between α and β points, P	Energy between γ and δ points, Q	Energy between two β points, R	$\lvert P - Q \rvert$	$\lvert R - P \rvert$	$\lvert R - Q \rvert$
Helium						
3.8	11400	16000	25000	5600	13600	9000
4.0	6800	8800	12600	2000	5800	3800
4.4	2100	2300	3200	200	1100	900
4.8	150	280	440	130	290	160
5.2	−400	−300	−280	100	120	20
6.0	−480	−420	−480	60	0	60
6.8	−320	−280	−330	40	10	50
Neon						
4.0	16600	22200	31200	5600	14600	9000
4.4	5200	6600	8900	1400	3700	2300
4.8	1050	1450	1900	400	850	450
5.2	−340	−120	−40	220	300	80
5.6	−760	−600	−700	160	60	100
6.0	−780	−680	−780	100	0	100
6.8	−570	−480	−570	90	0	90
Argon						
4.6	28000	32000	45000	4000	17000	13000
4.8	16700	19600	23800	2900	7100	4200
5.2	4800	6000	7200	1200	2400	1200
5.4	2000	2800	3700	800	1700	900
5.6	200	900	800	700	600	100
6.0	−1300	−900	−1160	400	140	260
6.8	−1650	−1440	−1650	210	0	210
8.0	−1020	−800	−1020	220	0	220
Krypton						
4.8	33000	37000	44800	4000	11800	7800
5.2	10600	12700	14800	2100	4200	2100
5.6	2200	3100	3250	900	1050	150
6.0	−800	−200	−560	600	240	360
6.8	−2020	−1800	−2040	220	20	240
7.6	−1640	−1540	−1640	100	0	100
8.0	−1370	−1400	−1380	30	10	20
Xenon						
5.2	31600	36000	40400	4500	8800	4400
5.4	18800	21400	25000	2600	6200	3600
5.6	10300	12600	13500	2300	3200	900
6.0	2500	3300	2900	800	400	400
6.8	−1900	−1800	−1900	100	0	100
7.6	−2120	−1800	−2100	320	20	300
8.0	−1860	−1760	−1860	100	0	100

gases between planes, 4.8 A apart, are small. Diffusion should be non-activated. The value of layer-plane spacing at which the repulsive interaction becomes important and potential-energy differences large depends upon the particular rare gas. For values based on σ_L, it is seen that helium should require a negligible E to penetrate and travel between planes at a distance 4.0 A or greater apart.

For energy values based on σ_{av}, it is seen that potential energies for all the rare gases are attractive at spacings of 6.8 A or greater. Helium should require a negligible E to penetrate and travel between planes at a distance 4.8 A or greater apart. At present, it does not appear possible to decide which σ values are most reasonable to use to calculate potential energies in the rare-gas–carbon system.

APPENDIX

A. Interaction of Gas Atoms with Idealized Type A Zeolite Cavity

The potential energy $\phi(r)$ between two nuclei separated by a distance r can be represented by the Lennard-Jones (6-12) potential

$$\phi(r) = -A/r^6 + B/r^{12} \tag{A1}$$

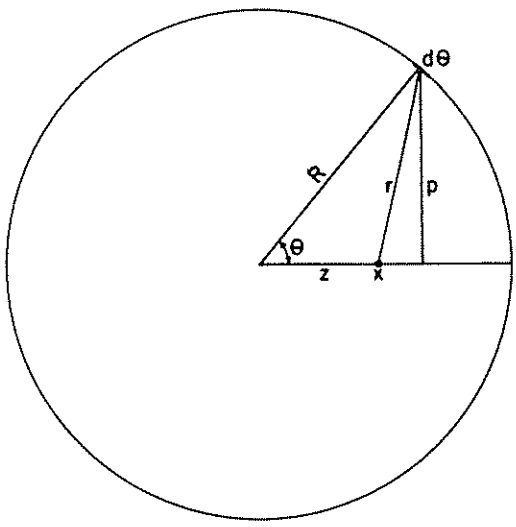

Fig. A1. Section of a zeolite cavity.

Figure A1 represents a section of the zeolite cavity. For the purpose of calculation, only the oxygen atoms on the surface of the cavity are considered. It is further assumed that the oxygen atoms are uniformly distributed. Consider N atoms of oxygen on the surface of the sphere. The atoms in a unit area of the surface are

$$dN/dA = N/4\pi R^2 \tag{A2}$$

or

$$dN = (N/4\pi R^2)\, dA \tag{A3}$$

The area of the circumferential ring subtended by a differential angle $d\theta$ at θ, is given by

$$dA = 2R\pi p\, d\theta \tag{A4}$$

Now, $p/R = \sin\theta$. Therefore,

$$dA = 2\pi R^2 \sin\theta\, d\theta \tag{A5}$$

The interaction energy of this element of oxygen atoms with an atom situated at x is given by

$$dE = dN\left(-\frac{A}{r^6} + \frac{B}{r^{12}}\right) \tag{A6}$$

We have $r^2 = R^2 + Z^2 - 2RZ\cos\theta$. Therefore,

$$dE = \left(\frac{N}{4\pi R^2}\right) 2\pi R^2 \sin\theta\, d\theta \left(-\frac{A}{r^6} + \frac{B}{r^{12}}\right) \tag{A7}$$

The interaction of the total number of oxygen atoms with the atom situated at x is

$$E = \frac{N}{2}\left[-A\int_0^\pi \frac{\sin\theta\, d\theta}{(R^2 + Z^2 - 2RZ\cos\theta)^3} + B\int_0^\pi \frac{\sin\theta\, d\theta}{(R^2 + Z^2 - 2RZ\cos\theta)^6}\right] \tag{A8}$$

or, letting $Z/R = a$, we have

$$E = \frac{N}{2}\left[-\frac{A}{R^6}\int_0^\pi \frac{-d(\cos\theta)}{(1 + a^2 - 2a\cos\theta)^3} + \frac{B}{R^{12}}\int_0^\pi \frac{-d(\cos\theta)}{(1 + a^2 - 2a\cos\theta)^6}\right] \tag{A9}$$

$$E = \frac{N}{2}\left\{-\frac{A}{R^6}\frac{1}{4a}\left[\frac{1}{(1-a)^4}-\frac{1}{(1+a)^4}\right] + \frac{B}{R^{12}}\frac{1}{10a}\left[\frac{1}{(1-a)^{10}}-\frac{1}{(1+a)^{10}}\right]\right\} \quad \text{(A10)}$$

B. Interaction of Gas Atoms Approaching a 4.2-A Free-Diameter Hole in the Type A Zeolite

In this case the gas atom is travelling toward the aperture formed by the eight oxygen atoms (Fig. B1). The cavity oxygens can be divided

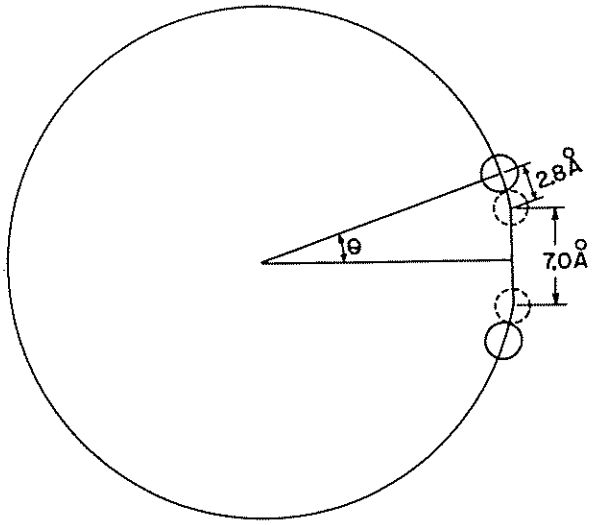

Fig. B1. Section of a zeolite cavity.

into two parts. One part is made up of the eight oxygen atoms constituting the hole and the other part is made up of the remaining 64 oxygen atoms. For the latter part, the interaction energy is calculated by the integration approach outlined in Appendix A.

From the geometry, θ in Fig. B1 is 52°; therefore, the integration is carried out from 52 to 180°. The interaction energy for this part, therefore, is given by

$$E = \frac{N'}{2}\left[-\frac{A}{R^6}\int_{52°}^{180°}\frac{-d(\cos\theta)}{(1+a^2-2a\cos\theta)^3} + \frac{B}{R^{12}}\int_{52°}^{180°}\frac{-d(\cos\theta)}{(1+a^2-2a\cos\theta)^6}\right] \quad \text{(B1)}$$

$$E = \frac{N'}{2}\left\{\frac{-A}{R^6}\frac{1}{4a}\left[\frac{1}{(1+a^2-1.23a)^2}-\frac{1}{(1+a)^4}\right] + \frac{B}{R^{12}}\frac{1}{10a}\left[\frac{1}{(1+a^2-1.23a)^5}-\frac{1}{(1+a)^{10}}\right]\right\} \quad \text{(B2)}$$

ACKNOWLEDGMENTS

Our interest in activated diffusion in molecular-sieve materials was prompted primarily by concern about diffusion in coals and carbons derived from polymers. The groups primarily responsible for this chapter, through their continuing financial help, are the United States Atomic Energy Commission on Contract AT(30-1)-1710 and the Commonwealth of Pennsylvania.

LIST OF SYMBOLS

A	constant in Lennard-Jones potential
A_a	area occupied by an atom
a	fractional distance between center of cavity and center of aperture plane
B	constant in Lennard-Jones potential
C, C_1, C_2	concentrations in appropriate units
C_s	concentration at saturation
C_T	total concentration
C_0	standard state of concentration
D	diffusion coefficient
$\bar{D}$	apparent diffusion coefficient
D_B	bulk diffusion coefficient
D_K	Knudsen diffusion coefficient
D_0	pre-exponential factor in the activated diffusion equation
E	activation energy from Arrhenius plot
E_a	apparent activation energy
E_1, E_2	characteristic energies of atoms or molecules (ionization potentials)
F_0	standard-state free energy
$\Delta F_0^{\ddagger}$	standard-state free energy of activation
$\Delta F_r^{\ddagger}$	free energy of activation (corresponding to ΔH_r shown in Fig. 15)
ΔF_a	free energy of adsorption for the particular mode of travel, as shown in Fig. 33
H_0	standard-state enthalpy
H_0^g	ground-state enthalpy
$\Delta H_0^{\ddagger}$	standard-state enthalpy of activation
$\Delta H_0^{g\ddagger}$	ground-state enthalpy of activation
ΔH_r	enthalpy of reaction (refer to Fig. 15)
ΔH_a	enthalpy of adsorption for the particular mode of travel, as shown in Fig. 33
h	Planck's constant

K	equilibrium constant
K_p	equilibrium constant at constant pressure
k	rate constant
k_B	Boltzmann's constant
$\bar{L}$	average layer diameter
M	number of occupied cavities per unit area
m	mass of a molecule or atom
N	number of holes per unit area
$N^\ddagger$	number of occupied holes per unit area
N'	$\gamma N^\ddagger$
$\bar{N}$	average number of carbon atoms per layer
N_A	Avogradro's number
N_0	number of carbon atoms per unit area of graphite basal plane
n	integers
P	potential energy resulting from the interaction of a species with α and β positions of two graphite basal planes (refer to Fig. 39)
p_a	atmospheric pressure in appropriate units
p_0	pressure at $t = 0$
Q	potential energy resulting from the interaction of a species with two β positions of two graphite basal planes (refer to Fig. 39)
Q_θ	partition functions of θ [refer to (39)]
Q_C	partition function defined by (40)
$Q^\ddagger$	partition function of the activated species in an aperture
Q_{cavity}	partition function of the species in cavity
Q_2	partition function defined by (61)
Q_3	partition function defined by (60)
Q_r	partition function defined by (64)
q	heat of adsorption
q_{st}	isosteric heat of adsorption at zero coverage
R	gas constant
R	radius of zeolite cavity [refer to (54)]
R	potential energy resulting from the interaction of a species with γ and δ positions of two graphite basal planes (refer to Fig. 39)
r	variable length denoting internuclear separation [refer to (51)]
r	pore radius or radial length [refer to (3)]
r_0	diffusion path length [refer to (10)]
r_0	equilibrium separation between interacting species
r_1	length (refer to Fig. 15)
r_1, r_2	length (refer to Fig. 33)
r_1	van der Waals diameter of oxygen or potassium ion in zeolite framework
r_0'	equilibrium separation between the nuclei of two diffusing molecules
S	surface area
S_0	standard-state entropy
$\Delta S_0^\ddagger$	standard-state entropy of activation
ΔS_0	standard-state entropy of adsorption
T	temperature, °K
T_a	ambient temperature, °K
t	time

$\bar{u}$	mean velocity of travel of an atom along the path indicated in Fig. 15
V	volume in appropriate units
V_e	volume of gas desorbed (adsorbed) at equilibrium or $t = \infty$
V_0	volume of gas desorbed (adsorbed) at $t = 0$
V_t	volume of gas desorbed (adsorbed) at $t = t$
$\bar{v}$	average molecular velocity
W	weight of sample
x	protrusion of cation into aperture (refer to Fig. 34)
$\alpha, \beta, \gamma, \delta$	denotes different positions on the perfect graphite basal plane (refer to Fig. 39)
α_1, α_2	atomic or molecular polarizabilities
γ	number of holes per cavity divided by the number in diffusion plane
δ	distance between two saddle points (refer to Fig. 15)
ϵ	open porosity
θ	Bragg angle (refer to Fig. 3)
θ	fractional coverage
$\theta^\ddagger$	fraction of holes occupied by activated molecules or atoms
λ	mean free path of a molecule or atom [refer to (1)]
λ	wavelength of radiation (refer to Fig. 3)
$\lambda/2$	maximum displacement in vibration (refer to Fig. 33)
ν	net rate of reaction [refer to (17)]
ν	frequency of vibration [refer to (62)]
ζ	a ratio of concentrations defined by (59)
ρ	density of the sample
σ	kinetic diameter of a molecule or atom
σ_{gas}	kinetic diameter of a free gas molecule or atom
σ_C	kinetic diameter of carbon atom in graphite lattice
σ_{av}	$(\sigma_{gas} + \sigma_C)/2$
σ_L	kinetic diameter from London expression of A
σ_{KM}	kinetic diameter from Kirkwood-Muller expression of A
$\Delta\Phi^\ddagger$	$\Delta S_0^\ddagger - (\Delta H_0^\ddagger - \Delta H_0^{0\ddagger})/T$
$\Delta\Phi^\ddagger_{exp}$	$\Delta\Phi^\ddagger$ calculated from experimental D_0
$\Delta\Phi_{theor}$	$\Delta\Phi^\ddagger$ calculated from partition functions
ϕ	net-interaction potential
ϕ_D	dispersion-interaction potential
ϕ_P	polarization-interaction potential
ϕ_Q	quadrupole-interaction potential
ϕ_R	repulsion-interaction potential
ϕ^*_{is}	maximum net attractive energy of gas-surface interaction
χ_1, χ_2	atomic or molecular diamagnetic susceptibilities

REFERENCES

1. R. M. Barrer, *Diffusion in and through Solids,* Cambridge University Press, New York, 1951.
2. P. C. Carman, *Flow of Gases through Porous Media,* Academic Press, New York, 1956.

3. A. Wheeler, in *Advan. Catalysis*, **3**, 249–327 (1951).
4. E. H. Kennard, *Kinetic Theory of Gases*, McGraw-Hill, New York, 1938.
5. R. B. Evans, III, J. Truitt, and G. M. Watson, *J. Chem. Eng. Data*, **6**, 522 (1961).
6. E. Wicke and R. Kallenbach, *Kolloid-Z.*, **97**, 135 (1941).
7. E. S. Golovina, *Dokl. Akad. Nauk SSSR*, **85**, 141 (1952).
8. C. Pierce, *J. Phys. Chem.*, **57**, 149 (1953).
9. G. L. Kington and W. Laing, *Trans. Faraday Soc.*, **51**, 287 (1955).
10. T. L. Thomas and R. L. Mays in *Physical Methods in Chemical Analysis* (W. G. Berl, ed.), Vol. 4, Academic Press, New York, 1961, pp. 45–97.
11. R. M. Milton, U.S. Patent 2,882,243, 1959.
12. V. J. Frilette, P. B. Weisz, and R. L. Golden, *J. Catalysis*, **1**, 301 (1962).
13. P. B. Weisz, V. J. Frilette, R. W. Maatman, and E. B. Mower, *J. Catalysis*, **1**, 307 (1962).
14. R. B. Anderson, W. K. Hall, J. A. Leeky, and K. C. Stein, *J. Phys. Chem.*, **60**, 1548 (1956).
15. T. Graham, *Phil. Mag.*, **32**, 401 (1866).
16. L. Cailletet, *Comp. Rend.*, **48**, 327 (1864).
17. R. W. Lee, R. C. Frank, and D. E. Swets, *J. Chem. Phys.*, **36**, 1062 (1962).
18. R. W. Lee, *J. Chem. Phys.*, **38**, 448 (1963).
19. D. W. Breck and J. V. Smith, *Sci. Am.*, **200**(1), 85 (1959).
20. P. E. Eberly, *J. Phys. Chem.*, **66**, 812 (1962).
21. R. M. Barrer, *Proc. Roy. Soc. (London)*, **A167**, 392 (1938).
22. R. M. Barrer, *Trans. Faraday Soc.*, **35**, 644 (1939).
23. R. M. Barrer and D. A. Ibbitson, *Trans. Faraday Soc.*, **40**, 195 (1944).
24. R. M. Barrer, *Chem. & Ind. (London)*, **1945**, 130.
25. R. M. Barrer, *J. Chem. Soc.*, **1948**, 2158.
26. R. M. Barrer, *Trans. Faraday Soc.*, **45**, 358 (1949).
27. R. M. Barrer, *J. Chem. Soc.*, **1950**, 2342.
28. R. M. Barrer and D. W. Riley, *J. Chem. Soc.*, **1951**, 127.
29. R. M. Barrer, *J. Chem. Soc.*, **1952**, 1561.
30. R. M. Barrer, *Chem. Soc.*, **1953**, 4035.
31. R. M. Barrer and A. B. Robins, *Trans. Faraday Soc.*, **49**, 807 (1953).
32. R. M. Barrer and D. W. Brook, *Trans. Faraday Soc.*, **50**, 1049 (1954).
33. R. M. Barrer, W. F. Grutter, and W. Buser, *Helv. Chim. Acta*, **39**, 518 (1956).
34. R. M. Barrer and W. I. Stuart, *Proc. Roy. Soc. (London)*, **A249**, 464 (1959).
35. R. M. Barrer and R. M. Gibbons, *Trans. Faraday Soc.*, **59**, 2569 (1963).
36. R. M. Milton, U.S. Patent, 2,882,244, 1959.
37. T. B. Reed and D. W. Breck, *J. Am. Chem. Soc.*, **78**, 5972 (1956).
38. L. Broussard and D. P. Shoemaker, *J. Am. Chem. Soc.*, **82**, 1041 (1960).
39. R. M. Barrer, "Physical Chemistry of Some Non-Stoichiometric Phases," report to the Xth Solvay Council, Brussels, 1956.
40. W. L. Bragg, *Atomic Structure of Minerals*, Cornell University Press, Ithaca, N.Y., 1937.
41. H. W. Habgood, *Can. J. Chem.*, **36**, 1384 (1958).
42. A. Tiselius, *Z. Physik. Chem. (Leipzig)*, **169A**, 425 (1934).
43. P. H. Emmett and T. W. DeWitt, *J. Am. Chem. Soc.*, **65**, 1253 (1943).

44. J. V. Smith, *Acta Cryst.*, **15**, 835 (1962).
45. G. A. Cook, (ed.), *Argon, Helium, and the Rare Gases*, Vol. 1, Wiley-Interscience, New York, 1961, p. 228.
46. D. W. Breck, W. G. Eversole, R. M. Milton, T. B. Reed, and T. L. Thomas, *J. Am. Chem. Soc.*, **78**, 5963 (1956).
47. J. O. Hirschfelder, C. F. Curtiss, and R. B. Bird, *Molecular Theory of Gases and Liquids*, Wiley, New York, 1954, p. 1111.
48. T. Kihara, *J. Phys. Soc. Japan*, **6**, 289 (1951).
49. T. G. Lamond and H. Marsh, *Carbon*, **1**, 281 (1964).
50. D. W. Breck, private communication, 1963.
51. J. J. Kipling and R. B. Wilson, *Trans. Faraday Soc.*, **56**, 557 (1960).
52. D. W. Van Krevelen and J. Schuyer, *Coal Science*, Elsevier, Amsterdam, 1957.
53. J. J. Kipling, J. N. Sherwood, P. V. Shooter, and N. R. Thompson, *Carbon*, **1**, 321 (1964).
54. S. P. Nandi, V. Ramadass, and P. L. Walker, Jr., *Carbon*, **2**, 199 (1964).
55. P. B. Hirsch, *Proc. Roy. Soc.* (*London*), **A226**, 143 (1954).
56. P. B. Hirsch, *Proc. Conf. on Science in the Use of Coal. Sheffield, 1958*, p. 294.
57. L. Cartz, R. Diamond, P. B. Hirsch, *Nature*, **177**, 500 (1956).
58. R. Diamond, Phil. *Trans. Roy. Soc.* (*London*), **A252**, 193 (1960).
59. L. Cartz and P. B. Hirsch, *Trans. Roy. Soc.* (*London*), **A252**, 557 (1960).
60. A. Guinier, G. Fournet, C. B. Walker, and K. L. Yudowitch, *Small-Angle Scattering of X-Rays*, Wiley, New York, 1955.
61. M. A. Short and P. L. Walker, Jr., *Carbon*, **1**, 3 (1963).
62. J. K. Brown, *J. Chem. Soc.*, **1955**, 744.
63. F. H. Winslow, W. O. Baker, and W. A. Yager. *Proc. 2nd Carbon Conf., Buffalo, 1955*, pp. 93–102.
64. F. H. Winslow, W. O. Baker, N. R. Pape, and W. Matreyek, *J. Polymer Sci.*, **16**, 101 (1955).
65. R. E. Franklin, *Proc. Roy. Soc.* (*London*), **A209**, 196 (1951).
66. D. H. Everett, E. Redman, A. J. Miles, and D. H. Davies, *Fuel*, **42**, 219 (1963).
67. R. E. Franklin, *Acta Cryst.*, **3**, 107 (1950).
68. R. E. Franklin, *Acta Cryst.*, **4**, 253 (1951).
69. M. Griffith and W. Hirst, *Proc. Conf. Ultrafine Structure of Coals and Cokes, 1943*, p. 80.
70. N. Brekowitz, *Can. J. Technol.*, **33**, 169 (1955).
71. P. Malherbe, *Fuel*, **30**, 97 (1951).
72. J. A. Lecky, W. K. Hall, and R. B. Anderson, *Nature*, **168**, 124 (1951).
73. P. Zwietering, A. P. Oele, and D. W. Van Krevelen, *Fuel*, **30**, 203 (1951).
74. S. Brunauer, P. H. Emmett, and E. Teller, *J. Am. Chem. Soc.*, **60**, 309 (1938).
75. S. P. Nandi and P. L. Walker, Jr., *Fuel*, **43**, 385 (1964).
76. F. A. P. Maggs, *Research* (*London*), **6**, 13S, 1953.
77. K. A. Kini, *Reports of the 27th International Congress on Industrial Chemistry, Brussels, 1954*, Vol. 2, Edition Den Presses, Documentaries, Paris, 1954, p. 110.
78. P. L. Walker, Jr., and I. Geller, *Nature*, **178**, 1001 (1956).

79. R. B. Anderson, L. J. E. Hofer, and J. Bayer, *Fuel,* **41,** 559 (1962).
80. K. A. Kini, *Fuel,* **43,** 173 (1964).
81. K. A. Kini, *Fuel,* **42,** 103 (1963).
82. K. A. Kini and P. L. Walker, Jr., *Fuel,* **44,** 453 (1965).
83. J. E. Metcalfe, III, M. Kawahata, and P. L. Walker, Jr., *Fuel,* **42,** 233 (1963).
84. C. Pierce, J. W. Wiley, and R. N. Smith, *J. Phys. Chem.,* **53,** 669 (1949).
85. B. R. Puri and R. C. Bansal, *Abstr. Symp. Carbon, Tokyo, 1964,* Paper VIII-3.
86. C. Pierce, R. N. Smith, J. W. Wiley, and H. Cordes, *J. Am. Chem. Soc.,* **73,** 4551 (1951).
87. J. R. Dacey and D. G. Thomas, *Trans. Faraday Soc.,* **50,** 740 (1954).
88. J. J. Kipling and R. B. Wilson, *Trans. Faraday Soc.,* **56,** 562 (1960).
89. T. G. Lamond, J. E. Metcalfe, III, and P. L. Walker, Jr., *Carbon,* **3,** 59 (1965).
90. M. M. Dubinin, *Proc. 5th Carbon Conference, Penn State, 1961,* Vol. 1, p. 81.
91. R. M. Barrer, *Proc. 10th Symp. Colston Res. Soc.,* p. 50.
92. P. L. Walker, Jr., T. G. Lamond, and J. E. Metcalfe, III, *Proc. 2nd Industrial Carbon and Graphite Conf.,* in press.
93. J. E. Metcalfe, III, Ph.D Thesis, Pennsylvania State University, University Park, Pa., 1965.
94. E. T. Nelson and P. L. Walker, Jr., *J. Appl. Chem.,* **11,** 358 (1961).
95. J. Crank, *Mathematics of Diffusion,* Clarendon Press, Oxford, 1956.
96. S. Glasstone, K. Laidler, and H. Eyring, *The Theory of Rate Processes,* McGraw-Hill, New York, 1941.
97. A. Stearn and H. Eyring, *J. Phys. Chem.,* **44,** 955 (1940).
98. A. Tiselius, *Z. Physik. Chem. (Leipzig),* **174A,** 401 (1935).
99. R. M. Barrer and D. A. Ibbitson, *Trans. Faraday Soc.,* **40,** 206 (1944).
100. R. M. Barrer and L. V. C. Rees, *Trans. Faraday Soc.,* **56,** 714 (1960).
101. R. M. Barrer and I. S. Kerr, *Trans. Faraday Soc.,* **55,** 1915 (1959).
102. R. M. Barrer and D. L. Peterson, *Proc. Roy. Soc. (London),* **A280,** 466 (1964).
103. R. M. Carr, D.I.C. Thesis, Imperial College of Science and Technology, London, 1962.
104. R. M. Barrer and E. A. Saxon-Napier, *Trans. Faraday Soc.,* **58,** 145 (1962).
105. E. T. Nelson, Ph.D. Thesis, Pennsylvania State University, University Park, Pa., 1961.
106. P. Zwietering, J. Overeem, and D. W. Van Krevelen, *Fuel,* **35,** 66 (1956).
107. A. S. Joy, *Proc. Conf. on Science in the Use of Coal, Sheffield, 1958,* p. A-67.
108. W. Pruss, *2nd Intern. Conf. Coal Science, 1958,* p. 535.
109. B. A. Bolt and J. A. Innes, *Fuel,* **38,** 333 (1959).
110. P. G. Sevenster, *Fuel,* **38,** 403 (1959).
111. W. S. Young and R. C. Taylor, *Ind. Eng. Chem. (Anal.),* **19,** 133 (1947).
111a. B. M. W. Trapnell and D. O. Hayward, *Chemisorption,* Butterworth, London, 1955.
112. J. P. Redmond and P. L. Walker, Jr., *J. Phys. Chem.,* **64,** 1093 (1960).
113. P. H. Emmett and R. W. Harkness, *J. Am. Chem. Soc.,* **57,** 1631 (1935).
114. S. J. Gregg and M. I. Pope, *Fuel,* **38,** 501 (1959).

115. R. M. Barrer and D. J. Ruzicka, *Trans. Faraday Soc.,* **58,** 2253 (1962).
116. F. London, *Z. Phys. Chem.,* **B11,** 222 (1930).
117. J. G. Kirkwood, *Phys. Z.,* **33,** 57 (1932).
118. J. C. Slater and J. G. Kirkwood, *Phys. Rev.,* **37,** 682 (1931).
119. Landolt-Börnstein, *Zahlenwerte und Funktionen,* Vol. II, Pt. 2, Springer, Berlin, 1951, p. 4.
120. F. H. Field and J. L. Franklin, *Electron Impact Phenomena and the Properties of Gaseous Ions,* Academic Press, New York, 1957.
121. C. G. V. Burgess, R. H. E. Duffett, G. J. Minkoff, and R. G. Taylor, *J. Appl. Chem.,* **14,** 350 (1964).
122. D. H. Everett, *Trans. Faraday Soc.,* **46,** 453 (1950).
123. R. M. Barrer and D. L. Peterson, *J. Phys. Chem.,* **68,** 3427 (1964).
124. G. C. Bond, *Catalysis of Metals,* Academic Press, New York, 1962.
125. F. H. Constable, *Proc. Roy. Soc. (London),* **A108,** 355 (1925).
126. Donald Graham, *J. Phys. Chem.,* **61,** 49 (1957).
127. J. R. Sams, Jr., G. Constabaris, and G. D. Halsey, *J. Phys. Chem.,* **64,** 1689 (1960).
128. J. Bardeen, *Phys. Rev.,* **58,** 727 (1940).
129. H. Margenau and W. G. Pollard, *Phys. Rev.,* **60,** 128 (1941).
130. E. L. Pace, *J. Chem. Phys.,* **27,** 1341 (1957).
131. E. L. Pace and A. R. Siebert, *J. Phys. Chem.,* **64,** 961 (1960).
132. P. L. Walker, Jr., H. A. McKinstry, and C. C. Wright, *Ind. Eng. Chem.,* **45,** 1711 (1953).
133. International Critical Tables, Vols. I and IV, McGraw Hill, New York, 1926 and 1928.
134. Handbook of Chemistry and Physics, Chemical Rubber Publishing Co., Cleveland, Ohio, 1953.
135. P. L. Walker, Jr., *Am. Scientist,* **50,** 259 (1962).